 © 2014 Russian Academy of Sciences and Turpion Ltd

DOI 10.1070/RC2014v083n01ABEH004372

Nanobiohybrid structures based on the organized films of photosensitive membrane proteins

S Yu Zaitsev,[a, b] D O Solovyeva,[a, b] I R Nabiev [a, c]

[a] *National Research Nuclear University 'Moscow Engineering Physics Institute' Kashirskoe shosse 31, 115409 Moscow, Russian Federation*
[b] *K I Skryabin Moscow State Academy of Veterinary Medicine and Biotechnology ul. Akademika Skryabina 23, 109472 Moscow, Russian Federation*
[c] *European Technological Platform 'Semiconductor Nanocrystals', Institute of Molecular Medicine, Trinity College James's Street, Dublin-8, Ireland*

The fundamental principles and technologies for the design of stable film systems based on biomembranes, photosensitive membrane proteins and complexes (retinal-containing proteins, reaction centres of photosynthetic bacteria, light-harvesting complexes of photosystems I and II), including their associates with metal and metal oxide nanoparticles or quantum dots are described. The advantages of controlled incorporation of the semiconductor or plasmonic nanocrystals into the biohybrid film structures are analyzed, first of all, the increase in the wavelength range of solar light harvesting and effective transfer of collected energy to the biological chromophores. Particular attention is devoted to the production of ultrathin and highly organized films at interfaces as the key stage of the design of nanobiohybrid materials with particular properties for photovoltaics, optoelectronics and nanophotonics.
The bibliography includes 182 references.

Contents

I. Introduction 38
II. Planar systems based on purple membrane fragments and retinal proteins 39
III. Planar systems based on reaction centre proteins of photosynthetic bacteria 51
IV. Planar systems based on the proteins of photosystems I and II 64
V. Conclusion 77

I. Introduction

The design and structure – function investigation of supramolecular planar systems based on photosensitive membrane proteins form an actively developing interdisciplinary area, which combines approaches of organic and biological, physical and colloid, inorganic and analytical chemistry with advanced techniques of nano- and biotechnology. Although artificial membrane systems based on retinal proteins (RP), reaction centres of photosynthetic bacteria and plants, light-harvesting complexes and plant photosystems I and II (PSI and PSII) are in some cases ready for use in particular science and technology applications, the design of competitive materials requires new approaches, first of all, nanobiotechnology approaches. In particular, the efficiency of primary charge separation in PSI is 38% to 59% depending on the energy of an absorbed light quantum,[1] and the quantum yield is close to 1.0.[1, 2] For comparison, we give a few examples characterizing the efficiency of modern photovoltaic cells based on various materials:[3]

Material	Charge separation efficiency (%)
Crystalline Si	25.0 ± 0.5
Crystalline GaAs	26.4 ± 0.8
Amorphous Si	10.1 ± 0.3
Organic dyes (Grätzel cell)	9.2 ± 0.4

The recently proposed approaches to the design of hybrid nanobiomaterials allow the use of complexes of

S Yu Zaitsev Professor, Ph.D., D.Sci., head of the Department of MGAVMB, leading researcher of NRNU MEPhI,
Tel. (7-495) 377 95 39, e-mail: szaitsev@mail.ru
D O Solovyeva Junior researcher of NRNU MEPhI, Ph.D.-student of MGAVMB. E-mail: d.solovieva@mail.ru
I R Nabiev Professor, Ph.D., D.Sci., head of laboratory of NRNU MEPhI, director of European Technological Platform 'Semiconductor Nanocrystals'. E-mail: igor.nabiev@gmail.com
Current research interests: nanobiotechnology, biophysics.

Received 5 February 2013
Uspekhi Khimii **83** (1) 38 – 81 (2014); translated by Z P Svitanko

biomembranes (proteins) with colloidal metal or metal oxide nanoparticles or with quantum dots (QD), which can absorb a large amount of light energy and transfer it to biological systems in the desired spectral range to increase the operation efficiency of such systems in the specified direction.[2]

Despite the presence of numerous reviews and books describing the structure, properties and application prospects of photosensitive membrane proteins, surveying papers are few in number, even for simple film systems based on bacteriorhodopsin[4–7] and reaction centre proteins.[7–10] Also, the structure, properties and applications of QD have been described for a broad range of physicochemical areas (this can be exemplified by a review[11]) but only a few biomedical areas. For example, this is the use of QD for cell, protein and DNA visualization, in immunology and biotechnology.[12–15] However, these rapidly developing interdisciplinary areas lack modern integrating papers on the film systems with examples of both a broad range of developed and patented materials and new hybrid systems based on membrane photosensitive proteins and inorganic nanoparticles for the subsequent use in technology.

A key issue in the design of these supramolecular systems for fundamental studies and hybrid nanobiomaterials for practical applications is to prepare oriented ultrathin films at interfaces. The principles and procedures used to prepare mono- and multilayer films of traditional surfactants (fatty acid derivatives, alcohols, amines and so on) were described in detail in a great number of publications; therefore, only the most significant monographs of the last 20 years are included here in the list of references.[16–18] In the case of biologically active compounds (BAC) having much more complex structure (lipids, proteins, peptides and so on), modified processes for the formation of Langmuir films (first of all, monolayers) are used; in the general form, they are presented in Fig. 1.

In terms of the type of the deposited objects, the protein films can be divided into the following groups: (i) films of biological membrane fragments, (ii) films of membrane proteins, (iii) mixed lipid–protein films, (iv) films of protein or polypeptide fragments, (v) films of water-soluble proteins.[16,17] Out of these groups, only i to iii are considered in this review, as most industrially feasible. Study of surfactant or BAC monolayers is markedly facilitated if they are first transferred by either a vertical lift (by the Langmuir–Blodgett method, LB) (see Fig. 1 *c*) or a horizontal lift (Langmuir–Schaefer method, LS) (see Fig. 1 *d*) to special solid substrates (optically transparent quartz or glass, macro- or microelectrodes of various geometry, mica, graphite and so on).[16–18] This may produce mono-, bi- and multilayers of specified thickness, which can be studied by the whole diversity of modern physicochemical methods, used as models of biomembranes, utilized in biosensor devices, *etc*. In recent years, considerable attention has been devoted to the preparation of so-called self-assembled (SA) films, which are formed spontaneously on the surface of various particles or planar substrates when the latter are incubated in a surfactant or BAC suspension.[18] Although these films have some defects, protein monolayers can be readily adsorbed onto them; therefore, SA films are considered more and more often as technologically feasible methods for the manufacture of promising nanomaterials. Many of the above drawbacks are not inherent in ultrathin layers of charged polymers and proteins prepared by layer-by-layer (LBL) assembly.[20–22] All these methods and approaches are considered below in relation to particular examples of photosensitive membrane proteins from the standpoint of the formation of planar systems and hybrid nanobiomaterials with specified structures and properties.

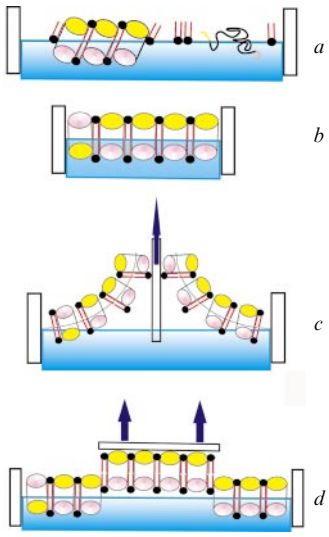


Figure 1. Schematic view of the monolayers and Langmuir films.[19]
(*a*) Liquid-expanded state of native and denatured membrane proteins and lipids; (*b*) liquid-condensed state of membrane proteins; (*c*) Langmuir–Blodgett monolayer transfer (vertical); (*d*) Langmuir–Schaefer monolayer transfer (horizontal).

II. Planar systems based on purple membrane fragments and retinal proteins

1. Structural and functional features of bacterial and visual rhodopsins

Retinal proteins are light-sensitive membrane biopolymers that provide, upon absorption of light quantum, for a number of highly important biological functions of animals and bacteria.[23–30] The molecular structures of important RP such as visual rhodopsin and bacteriorhodopsin (BR) are rather similar and have been determined at atomic resolution.[29,30] Due to the large bulk of published results, this review covers mainly data on the structure and function of BR, the more so, because the up-to-date knowledge on the structure of visual rhodopsin and the molecular physiology of vision was considered in detail in the review by Ostrovsky and Feldman.[23] Furthermore, among all RP, only BR is available in considerable amounts and has optimal properties for practical application.[3–6,10,24–28] The simplicity of isolation of BR is due to the fact that it is concentrated in the purple membrane (PM) domains (Fig. 2) of the well-studied halophilic bacterium *Halobacterium salinarum*.[24–28] The polypeptide chain of BR composed of 248 amino acids [molecular mass (MM) is ~26 500 Da] is bent and comprises seven transmembrane α-helices traversing the bilayer of plasmatic membranes of the bacteria. These seven α-helices

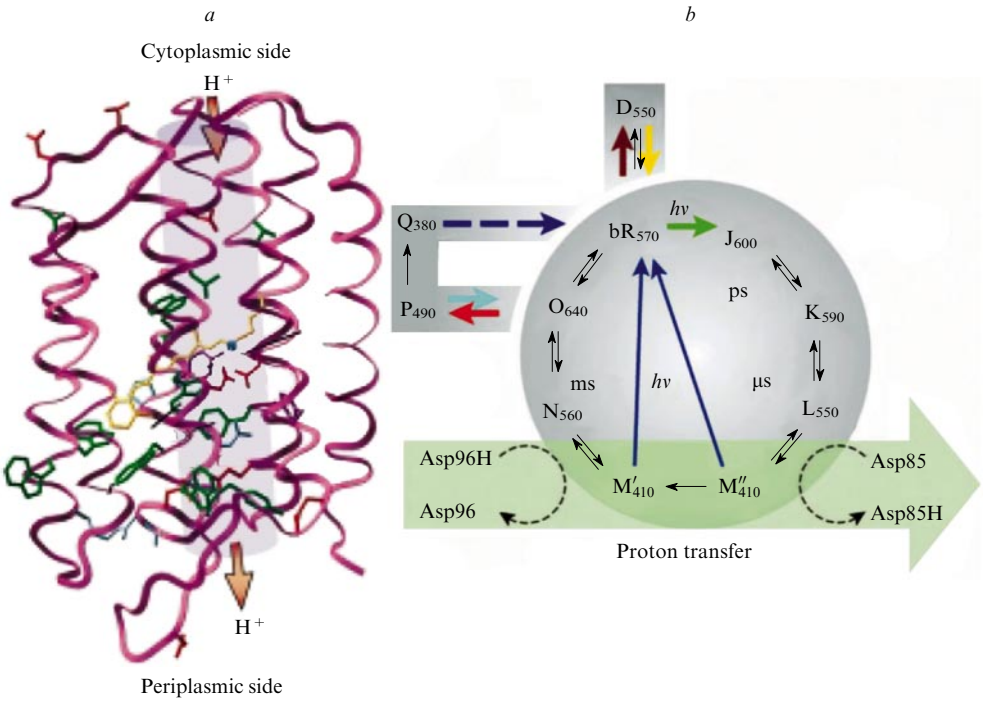


Figure 2. Schematic view of the structures of bacteriorhodopsin (*a*)[26] and key intermediates of its photocycle with absorption peaks (the ranges of characteristic times of the corresponding transitions are also indicated) (*b*).[4]

form two arcs: the outer one composed of helices E, F, G and A and the inner one made of helices B, C and D. The structure and the conformational changes of BR were studied by electron crystallography at 0.32 nm resolution in the membrane plane and 0.36 nm resolution in the perpendicular direction.[30] According to electron diffraction and X-ray diffraction data,[29,30] purple membranes represent hexagonal two-dimensional lattices with unit cell containing 3 protein molecules and 12–14 lipid molecules, and the membrane is asymmetric. A chromophore (retinal) is present in each protein molecule, being chemically bonded to Lys216 in helix G through formation of Schiff base. Upon absorption of a light quantum, retinal of BR isomerizes from the *trans*-configuration to the 13-*cis*-configuration, thus triggering a series of conformational transitions of the protein from the ground state with λ_{max} 570 nm (bR_{570}) to intermediate spectroscopically discernable forms (they are designated by Roman letters with digits indicating the absorption maximum of the given form) (see Fig. 2*b*). As regards the potential application, the M-form with $\lambda_{max} = 410$ nm (M_{410}) is among the most important forms; this is discussed in the subsequent sections. Here it is pertinent just to summarize the BR properties (induced by photoactivation) that are most important for applications in bionanotechnology: reversible change of the absorption maximum from 570 to 410 nm; generation of photocurrent and photopotential; pH change inside and outside the cells or model liposomes upon directed proton transfer; possible repetition of the above processes many times without protein denaturation; the accessibility and relative simplicity the preparation of specimens containing native BR. Thus, bacteriorhodopsin present as a part of the purple membranes is a membrane protein with unique properties and a promising component of functional planar systems.

2. Langmuir–Blodgett and Langmuir–Schaefer monolayers and films

Monolayers of purple membranes or purified proteins such as bacterial or visual rhodopsin are simple and well-described examples of model membrane systems.[7–10,24–28] Bacteriorhodopsin has remarkable physicochemical properties and combines three principal molecular functions that play the key role for fundamental research and for applications in technology, namely, photoelectric, photochromic and proton transfer functions.[24–28] For these purposes, PM are used more often than BR because the isolation of the latter from these 'crystal-like' membrane structures markedly decreases both the chemical and thermodynamic stability of the protein.[17] Purple membrane monolayers were first obtained by Stoeckenius' research group† by deposition onto a liquid–gas interface from a hexane solution; subsequently this procedure was modified for other organic solvents and solvent mixtures (a large body of such data are summarized in a monograph[7]). Several research groups[17,19,31] demonstrated that PM is partially denatured upon mixing of organic solvents with aqueous subphase, which may be related to both the loss of the hydrophobic interactions within the protein and exclusion of lipid molecules from the three-dimensional structure. More promising is the preparation of PM or BR by deposition from aqueous dispersions.[17,19] It was found that PM are mainly oriented in such a way that the cytoplasmic side is directed

† See, for example, S Hwang, J T Korenbrot, W Stoeckenius *J. Membr. Biol.* **36** 115 (1977); *ibid.*, p. 137.

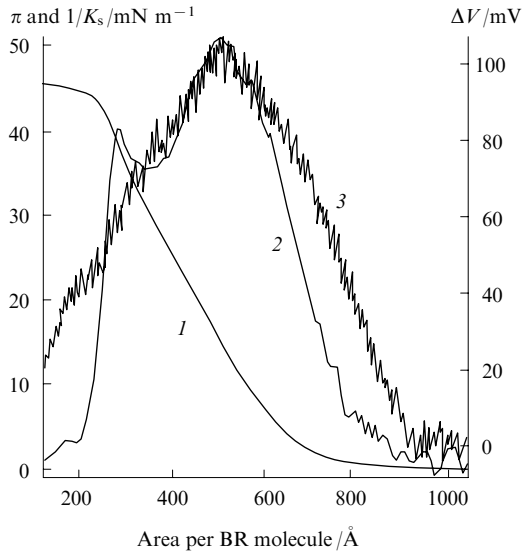


Figure 3. Surface pressure isotherm (*1*), inverse compressibility (*2*) and surface potential (*3*) of the monolayer of purple membranes on the surface of a 100 mM NaCl solution .[9, 33]

towards the aqueous subphase and, as PM monolayers are transferred to a hydrophilic substrate, about 85% of PM are directed to the glass surface by this side of the membrane.[32]

It is noteworthy that despite the large number of works on this subject matter, quantitative parameters of PM or BR were described only in several publications;[17, 31–33] the results of two studies [17, 33] being most trustworthy. It follows from the work of Méthot *et al.*[33] that the surface pressure isotherm (π) for a PM monolayer on a 100 mM NaCl solution (Fig. 3) shows a minor inflection at about 20 mN m^{-1} and the collapse at 46 mN m^{-1}. Both the surface potential (ΔV) and inverse compressibility ($1/K_s$) of a monolayer of purple membrane have maxima in the same region at an area of about 5 nm^2 per BR molecule ($\pi \approx 20$ mN m^{-1}).[33] In the authors' opinion, these parameters correspond to the closest packing of PM in a monolayer. This is also confirmed by measurements of the monolayer thickness, which was $\sim$3.8 nm [10, 33] (at surface pressures of <35 mN m^{-1}), which roughly corresponds to the size of hydrophobic α-helices of the PM.[30] At higher pressure, especially near the monolayer collapse region, the film thickness increases to 5.1 nm, which was attributed [10] to the gradual formation of a new layer above the already formed PM monolayer. In our opinion, this is due to transition of BR molecules into the fully vertical position with respect to the interface: schematically this transition may correspond to the transition of a three-dimensional structure shown in Fig. 1 *a*, into the structure shown in Fig. 1 *b*. The area per BR molecule in the monolayer (upon extrapolation to zero pressure) on the surface of a 100 mM KCl solution is $\sim$8 nm^2 (see Ref. 17), which is in good agreement with X-ray diffraction data for the protein in the membrane (a $2.5 \times 3.5 \times 4.5$ nm unit cell).[29] The sharp increase of the surface pressure–area (per protein molecule) isotherm and high pressure of the monolayer collapse (>45 mN m^{-1}) attest to the formation of fairly strong BR monolayers on concentrated salt subphases.[17]

On the other hand, the quantitative data on the surface area per BR molecule (about 4000–5000 Å^2) determined from the surface pressure isotherms for a PM monolayer [31] do not seem credible. The authors themselves think that these areas are more than 4 times larger than the possible areas for native BR in PM fragments and that they correspond most likely to an unfolded conformation of BR at an average area of 15 Å^2 per amino acid residue. The substantial denaturation of BR (defined as the unfolding of the polypeptide chain) can be related to both the use of a water–organic solvent mixture (for suspending BR and subsequent deposition to the surface of a 0.2 mM $CaCl_2$ solution) and long incubation time of a PM monolayer at the interface (30 min to 5 h).[31]

The effect of experimental conditions on the structure and orientation of a number of membrane proteins in monolayers at the water–air interface has been studied in many works, in particular, in some publications cited above.[17, 19, 31–33] These important effects were examined in most detail by the potent method of polarization modulation IR spectroscopy.[10, 34] By comparison of bands at 1655 (amide I band) and 1545 cm^{-1} (amide II band), it was shown that BR retains the native structure, while visual rhodopsin in the monolayer is partially denatured under above-indicated conditions at 20 °C.[34] An additional piece of evidence for this denaturation is the appearance of a shoulder at 1634 cm^{-1}, which corresponds to an increase in the number of β-sheets and a decrease in the intensity of the band at 1655 cm^{-1} responsible for the α-helical structures in rhodopsin.[10, 34] The minimum degree of denaturation of visual rhodopsin was observed when it was deposited in a large amount (150 μl) onto the above-noted salt subphase, which created an initial pressure of 5 mN m^{-1} at low temperatures (up to 4 °C).[10, 34] However, long-term maintenance of a visual or bacterial rhodopsin monolayer (30 or 50 min, respectively [34]) before beginning of the compression results rather in disruptions of the packing of membrane aggregates and even in partial unfolding of the three-dimensional BR structure instead of the formation of an adequate membrane layer (see Fig. 1 *a*, right-hand part). An important experimental fact corresponding to parameters of the natural environment for all types of proteins is the presence (in all cases) of 100–150 mM NaCl in the aqueous subphase for stabilization of the PM or protein monolayer, because in the absence of this salt, no isotherms could be recorded at the water–air interface even in the presence of a large amount of the protein.[17, 34] Thus, the main achievement of the cited publications [10, 34] is elucidating the conditions under which the native structure of membrane proteins is retained after formation of the monolayer. Generally, BR is most stable among the studied rhodopsins, denaturation of which at the interface is very difficult to prevent. For visualization of such structural transitions, a modern method called Brewster angle microscopy is used.[35] For example, it was possible [36] to demonstrate by this method that immediately after deposition to a 100 mM KCl aqueous solution, BR retains its domain structure in the monolayer rather than spreads over the surface even at low pressures (<0.1 mN m^{-1}). Soon after the beginning of compression of the monolayer (at pressures of >1.0 mN m^{-1}), these domains start to coalesce to form a continuous phase throughout the whole BR monolayer length.[36] The simultaneous atomic force microscopy (AFM) studies of the BR monolayers transferred onto a graphite substrate by the

Langmuir–Blodgett technique confirmed the domain structure of the BR monolayer with about 5 nm thickness.[5] Specified types of PM-based multilayer structures for purposes of science and technology are usually formed by LB transfer of the above-mentioned monolayers from the water–air interface to special solid substrates.[15–18] This procedure has been thoroughly elaborated for various surfactants and proteins, and the key results on the spectral photoelectric properties of the LB films of PM are most often obtained and discussed in the same studies in which the monolayers are considered.[8, 17, 19, 32, 35] The functionally native state of BR is also indicated by rather high photopotentials determined for BR-based multilayer structures upon illumination at wavelengths near the absorption maximum of this protein (~570 nm).[4–7]

Meanwhile, Japanese researchers from Fuji Photo Film[37] prepared PM monolayers by deposition from a water–hexane–DMF mixture in 10 : 10 : 2 ratio and transferred them by the LS technique (similarly to the picture in Fig. 1 *d*) at a constant surface pressure of 20 mN m^{-1} to the surface of an SnO_2 electrode. It is important that the intensity of the 560 nm band in the spectrum of the films thus formed (at the BR absorption maximum) is proportional to the number of transferred LS monolayers (from 2 to 10) with a proportionality factor of 0.002 per monolayer.[37] In the case of transfer of 6 PM monolayers to the SnO_2 electrode surface, the photocurrent was 50 (pH 4–5 or 8–10) to 200 nA cm^{-2} (pH 6–7),[37] which attests to high efficiency of this type of transfer for the generation of PM-based multilayer structures. Analogous LB and LS films of PM and BR monolayers were reported in other publications (see, for example, Ref. 19).

Thus, by considering all of the above data, one can distinguish two general types of structures of PM or BR mono- and multilayers (see Fig. 1 *c*,*d*) with parameters suitable for technological applications. These systems can be regarded as precursors of nanobiohybrid structures, since they are composed of fundamentally different components (organic layer on an inorganic material) and are nanosized, functional and molecularly integrated at an interface.

3. Purple membranes adsorbed on black lipid membranes and lipid bilayers of other types

A large number of papers deal with the preparation and investigation of PM films adsorbed on bilayer (black) lipid membranes (BLM) and membrane-like substrates.[38–42] This type of systems can be prepared by a variety of methods, the simplest one being the following two-stage method: (a) BLM self-assembly from a drop of a solution of a specified lipid mixture in a micron-sized hole in a Teflon septum between two electrolyte solutions [as a rule, 100 mM NaCl and 5 mM Tris-HCl at pH 7.0; Tris is tri(hydroxymethyl)aminomethane]; (b) the subsequent introduction of PM into one of the solutions by a microsyringe (50 μl from a suspension with an optical density of 4–5) with gradual adsorption for 20–40 min on the BLM (Fig. 4 *a*). It is considered that in this case, PM are adsorbed on the BLM by the periplasmic side to give a high degree of PM alignment with proton transfer from the medium to the BLM. However, none of the publications known in this field reports particular values for the degree of alignment of PM or other characteristics, which are key values for hybrid nanobiostructures. There are numerous earlier modifications of the above method for the preparation of a PM

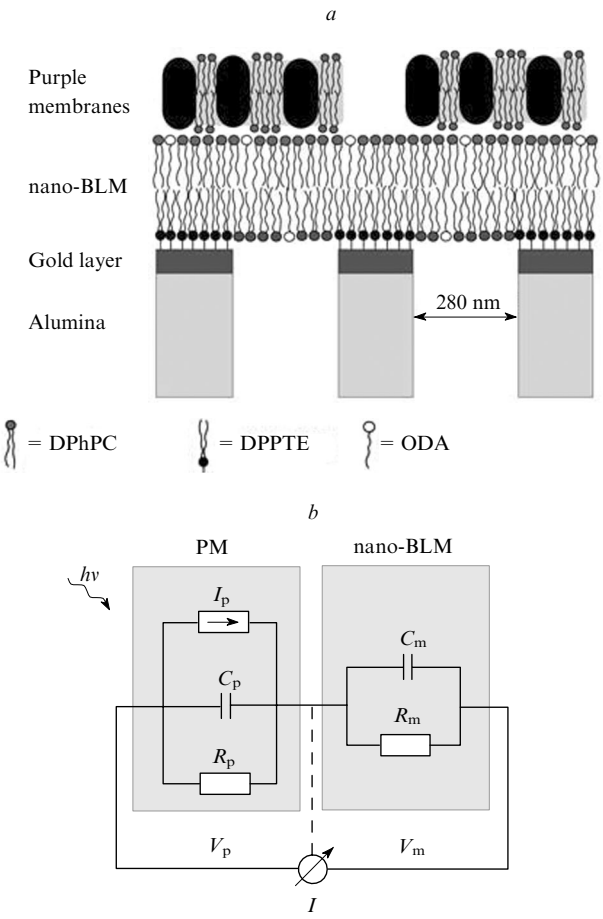


Figure 4. Schematic view of purple membranes adsorbed on nanobilayer lipid membranes (nano-BLM) (*a*) and the electric equivalent circuit of photoactivated bacteriorhodopsin adsorbed on nano-BLM (*b*).[40]
DPhPC is 1,2-diphytanoyl-*sn*-glycero-3-phosphocholine, DPPTE is the sodium salt of 1,2-dipalmitoyl-*sn*-glycero-3-phosphothioethanol, ODA is octadecylamine; C_m and R_m are the capacity and the resistance of nano-BLM; C_p and R_p are the capacity and the resistance of purple membranes; I_p is the photocontrolled proton current generated by bacteriorhodopsin. At short circuit, the voltage drop on the membrane (V_m) is equal to that on the purple membrane (V_p); I is the measurable current.

system on BLM, in particular, adsorption of PM (more rarely, vesicles of purified BR or its mutant strains) on lipid-impregnated filters or thin colloidal or Teflon films. Generally, the properties of such systems are characterized using traditional schemes for recording the changes in the current or potential (see Fig. 4 *b*) that arise upon film irradiation with visible light.

A number of contemporary studies in this field[40–42] develop the idea of PM adsorption on BLM, which are, in turn, adsorbed on porous metallic or polymeric substrates (so-called micro-BLM or nano-BLM). In these structures,[40] the photocurrent is >150 nA cm^{-2} (Fig. 5); however, the adsorption of PM on BLM requires about 40 min, which is not very convenient for technological applications.

One more example of rather simple hybrid systems based on PM is provided by mixed lipid and PM bilayers, which were reported by Dolfi *et al.*[41, 42] In this case, the first

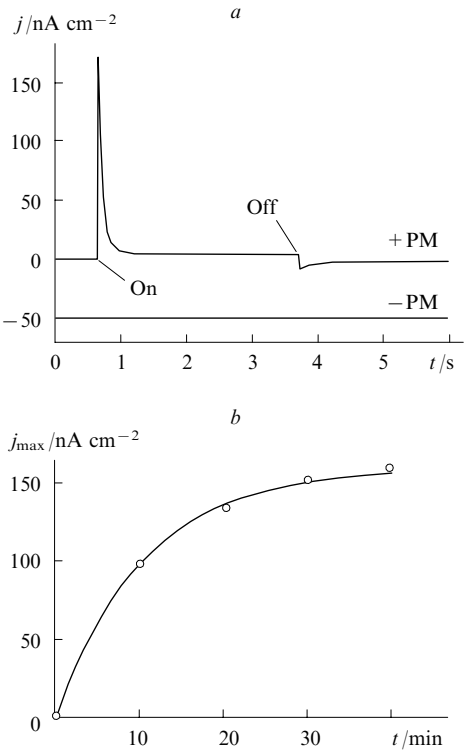


Figure 5. Photocurrent characteristics before and after the addition of purple membranes to bilayer lipid membranes.[40]
(*a*) Photocurrent density before (−PM) and after (+PM) the addition of PM to nano-BLM. +PM: the first and second transitions correspond to switching on and switching off of the light; the current was recorded 40 min after the addition of PM. −PM: the straight line in the plot corresponds to the current signal recorded before the addition of PM (shifted by −50 nA cm^2). No significant photo-artefacts were detected; (*b*) time dependence of the maximum current density after the addition of PM. The maximum current was observed after ~40 min (*b*).

stage was the modification of the surface of a mercury drop electrode by thiol surfactants and the second stage is the transfer of the phospholipid monolayer (dioleoylphosphatidylcholine or dioleoylphosphatidylserine) from a water–air interface to the thiol-modified surface of a mercury-drop electrode, and the third stage is the transfer of PM to the thus formed heterostructure. The photoactivation of this system gives rise to a negative current (up to −1.45 nA), whereas switching off the illumination induces a positive signal (up to 0.45 nA); in both cases, pH is 6.0. Much lower photocurrents are observed at very low (<2) and very high (>10) pH values.[42]

A more workable approach for the design of photocells based on the ITO/PM/Au system (ITO is indium tin oxide) is the use of conducting polymers, which was reported by Nicolini *et al.*[43] The PM orientation was attained by exposure of a PM layer on the subphase to an external electric field. The oriented PM layer was transferred by the LS method to a glass substrate with sputtered ITO. The ITO/PM/Au hybrid system was characterized by a photocurrent with a potential drop of ~5 mV for a 3×3 mm cell sample. Subsequently,[43] the conducting polymer, poly(*o*-anisidine), and the LB transfer of PM were used to fabricate a multilayer structure on an ITO electrode.[43]

Thus, it is important to distinguish between the PM (or BR) Langmuir films as monolayers of the same sort of molecularly integrated BR and adsorbed PM films on BLM as supramolecular structures.[43–45]

4. Self-assembly, layer-by-layer assembly and other types of organization of purple membranes in planar systems

The studies dealing with self-assembly or layer-by-layer assembly of BR or PM ultrathin films will be considered together, because these methods are similar[17] and are reported in the same publications.[46–52] Brizzolara[46] carried out a comparative study of parameters of PM structures obtained by self-assembly on the surface of a physically and chemically modified glass. On physically modified glass, various surfactants (~0.02 μg cm^{-2}) are adsorbed only by non-covalent forces, the contact angle being <10° and the amount of self-assembled PM being ~0.85 μg cm^{-2}. Conversely, surfactants are attached to chemically modified glass by covalent bonds, their amount varying from 0.05 to 0.09 μg cm^{-2}, and the contact angle is large (47–96°); the amount of self-assembled PM is ~0.57–0.09 μg cm^{-2} (see Ref. 46). These parameters vary substantially upon photoactivation of the structure, which is important, in the authors' opinion,[46] for the use of these systems for lithography.

The next step in the development of this line of research is the use of charged polymers (instead of surfactants). In a number of studies,[47–49] BR and PM ultrathin films were formed on glass substrates with ITO and an adsorbed layer of polycations, for example, polyallylamine hydrochloride or poly(dimethyldiallylammonium) chloride and gave a photocurrent of ~100–200 nA cm^{-2} (6 layers).[47] Analogous structures without polymers consisting of eight wild-type BR bilayers or six mutant D96N layers gave photocurrents of at most 52 or 80 nA cm^{-2}, respectively.[49] Other researchers[50–52] produced BR and PM ultrathin films on glass with a sputtered gold layer (100–200 nm thick) and a layer of 11-mercaptoundecanoic acid (11-MUA) preadsorbed for 24 h.[51] The 11-MUA layer was ~1.7±1 nm thick, which is close to the theoretically calculated range (1.8–1.9 nm) and is in good agreement with the data from ellipsometry and surface plasmon resonance (1.6–1.9 nm).[51] Then a ~1.2 nm-thick positively charged polylysine layer was obtained by self-assembly (during 2 h at pH 8.0); a layer of PM fragments was adsorbed by self-assembly on this layer (the PM fragments were negatively charged at pH 8.0, as the BR isoelectric point is pH 4.8–4.9).[3–7,51] Considering the surface topography of these hybrid structures determined by AFM, the conclusion was drawn[51,52] that the homogeneity and the degree of orientation of BR in these structures depend on the preparation method, while PM fragments are aligned parallel to the substrate surface. The general principle of layer-by-layer assembly of polylysine and BR or PM films by means of electrostatic attraction between polylysine and PM is depicted in Fig. 6.[52] In multilayer films, BR remains stable for a long period and retains the native structure, although according to the AFM data, the structures of some monolayers have defects (Fig. 7).[52] These multilayer hybrid nanobiostructures are used to enhance the photoelectric response of BR. For example, the photocurrent generated by polylysine/PM films linearly increases with an increase in the number of bilayers (maximum ~420 nA cm^{-2} for 8 polylysine/PM bilayers) (Fig. 8).[52]

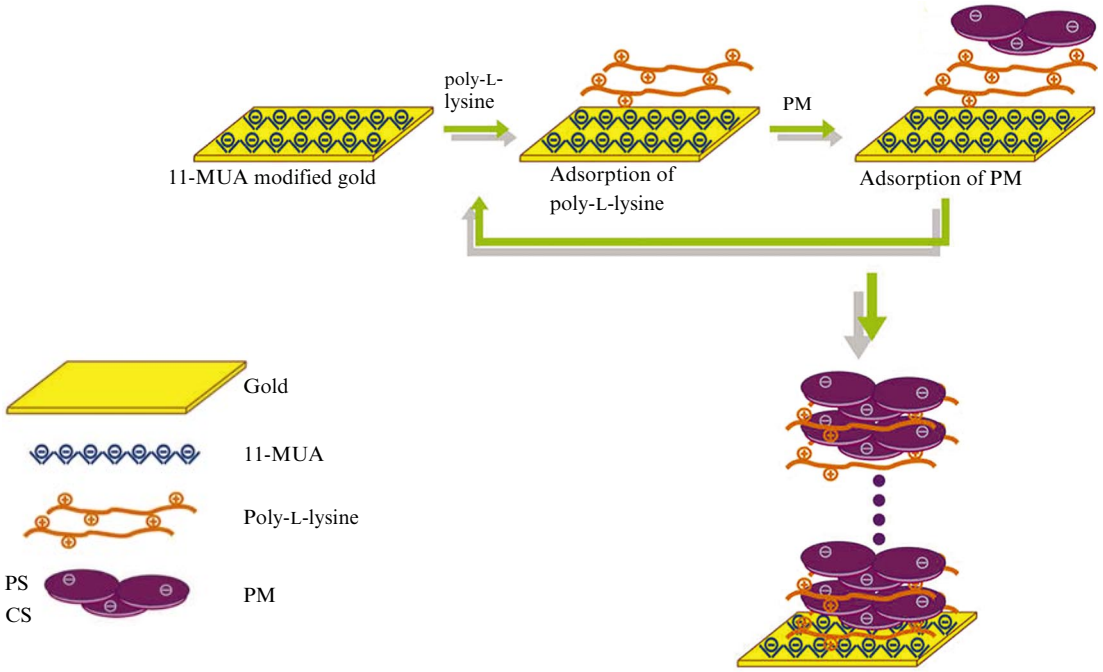


Figure 6. Schematic view of the assembly of poly-L-lysine/purple membrane layers on the negatively charged gold surface.[52] CS is the cytoplasmic side, PS is the periplasmic side.

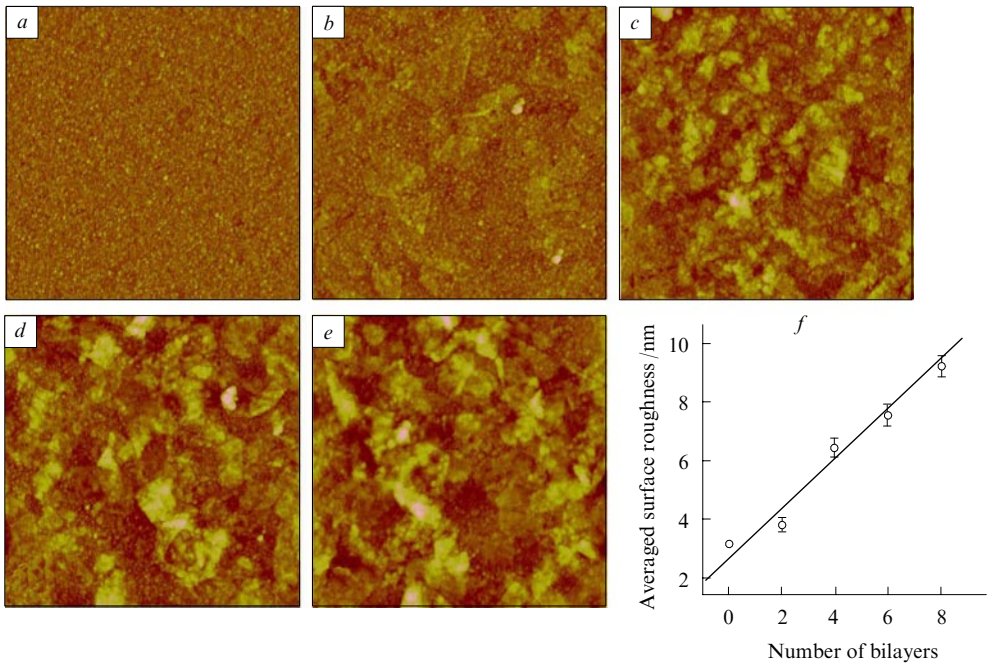


Figure 7. Atomic force microscopy images of poly-L-lysine/purple membrane layers adsorbed on the mercaptoundecanoic acid-modified gold surface (the outer layer of PM);[52]
(*a*–*e*) are images of 1, 2, 4, 6 and 8 poly-L-lysine/PM bilayers, respectively. The scale of this image is 5.0 × 5.0 μm; the maximum *z*-resolution is 80 nm; (*f*) relationship between surface roughness and the number of bilayers.

One of the most accessible methods for the preparation of oriented films containing large amounts of PM or BR is electrophoretic deposition (EPD) from their solutions (in particular, as mixtures with synthetic polymers) with gradual deposition and drying of the protein on the substrate. These works were started under the supervision of Prof. Keszthelyi in the Hungarian Academy of Sciences and are still continued.[53, 54] Among the optical parameters of these

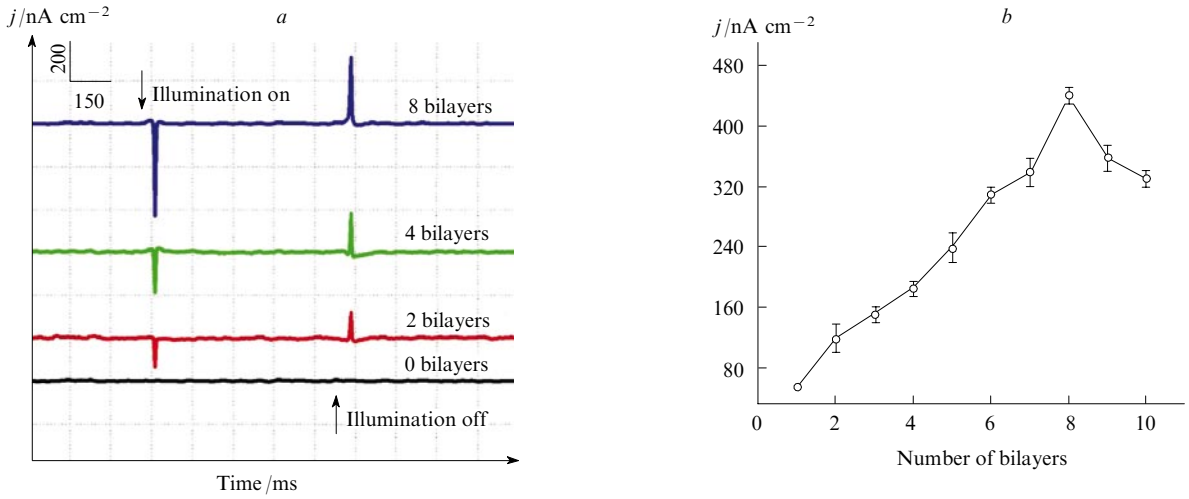


Figure 8. Photocurrent density for the poly-L-lysine/purple membrane structure.[52]
(*a*) Photocurrent generated by 2, 4 and 8 bilayers of poly-L-lysine/PM film formed under the optimal conditions; (*b*) maximum photocurrent upon photoactivation of different numbers of poly-L-lysine/PM bilayers.

films, most important are the lifetimes of the M-intermediate of the BR photocycle and the ability to generate photopotential after activation with light at >500 nm.[54] Takei *et al.*[55] described BR films with high technical characteristics: area of 1 cm^2, thickness of 25 μm, resistivity of 10^9-10^{10} Ω and optical density of $\sim$2.0 at 570 nm. A peculiarity of another study[56] is fabrication of a multilayer structure from two BR films separated by optical waveguides, the factor (quantum yield) of the photoinduced protein transformation from the initial form BR_{570} to M_{412} being 0.5–0.7 and decreasing to 0.2 over a period of 2–5 h. The use of glutaraldehyde (GA) as the cross-linking agent for BR films (BR : GA = 1 : 5) stabilized this factor at the level above 0.45 for a 120-day period.[56]

The breakthrough of publications by Zaitsev *et al.*[17,57] was in the development of technologically simple and cheap procedures for the preparation of photochromic materials (PCM) by immobilization of BR or PM in various polymer matrices: gelatine, polyacrylamide, polyvinyl alcohol, polystyrene or methylcellulose (Mc); methylcellulose proved to be most convenient and durable.[17] Testing of all resulting PM-based PCM demonstrated good parameters: high sensitivity (up to 10^{-3} J cm^{-2}) and reversibility ($>10^4$ record–erase cycles), narrow and non-overlapping absorption areas of the initial and photoinduced forms (570 and 412 nm), and high resolving power ($>10^3$ lines per mm).[17] A valuable feature of the resulting PCM is the possibility to adjust the half-transition time ($\tau_{1/2}$) of BR from the state (λ_{max} = 412 nm) to the ground non-excited state (λ_{max} = 570 nm): it was $\sim$40 ms in suspension and 0.5–1.0 s in acrylamide-based polymer films. With Mc (MM = 56 000) as the polymeric matrix, $\tau_{1/2}$ increased to 70–100 s, *i.e.*, by a factor of $\sim$2000. Among the most promising applications of these polymeric films based on BR is the application in photorefractive elements of holographic systems.[57]

It was demonstrated[17,58] that the inclusion of PM into polymer matrices, *e.g.*, polyvinyl alcohol (PVA), results in rather high degree of BR orientation, comparable with that for films obtained by EPD, the photoelectric signals were also found to be similar ($\sim$300 mV) at the film optical density of 0.13.[58] Moreover, comparison of the normalized signals of second harmonic generation in such films demonstrated that this signal is higher for PM–PVA films than for PM films prepared by EPD. This unusual fact was attributed[58] to inhomogeneities that appear in EPD PM films upon drying and considerably deteriorate their optical properties. In addition, the determined[58] non-linear susceptibility values for PM–PVA films are 4.7×10^{-10} (arb.u.) for the initial BR form (570 nm) and 5.0×10^{-11} (arb.u.) for the M-form (412 nm), *i.e.*, this parameter decreases 10-fold as the PM–PVA film is photoactivated in the visible region; therefore, the second harmonic generation signal can be used to read out the recorded images without erasing.[58]

Manoj *et al.*[59,60] described the following advanced system: (1) conducting polymer layer ($\sim$200 nm) of a poly(3,4-ethylenedioxythiophene)–poly(styrenesulfonate) (PEDOT–PSS) mixture deposited on an ITO electrode; (2) PM dispersion (10 mg ml^{-1}, pH 6.8), which was dried under external voltage of (0.1–10.0 V) to give a $\sim$500 nm-thick PM layer; (3) upper aluminium electrode. On exposure of this hybrid system, ITO/PEDOT–PSS/PM/Al, to light at 532 nm, a photoelectric response of $\sim$1.5 nA was recorded.[59]

Thus, for all of the indicative prospective applications of PM-based materials, a topical task is to prepare PM oriented ultrathin films.

Comparison of the preparation techniques of PM thin films and their structural and functional characteristics provides the conclusion that the homogeneity and the degree of PM orientation in these films depends on the preparation method, increasing in the series SA < LS (LB) < EPD.

5. Hybrid nanobiomaterials based on purple membranes

Currently, a highly promising approach is the design of hybrid systems from several functionally and structurally interrelated nano-sized components. However, due to the absence of clearly defined criteria, different research-

ers [11–15, 60–62] often assign various types of systems to the same hybrid nanobiostructures, which, in our opinion, does not interfere with discussing them together. Here the attention is focused on PM complexes with metal nanoparticles and especially QD. It is known that QD have a very broad absorption band and emit in a narrow range (the emission band half-width is ~30 nm), and they are 100–4000 times more photostable than the best organic fluorophores. The position of the QD fluorescence band depends on the size of nanocrystals, which makes it possible to synthesize QD that fluoresce in different colours. The quantum yield of QD can reach 70% and the absorption cross-section is more than 100 times as large as the absorption cross-section of organic fluorophores. Combination of these unique properties opens up the way to novel materials based on QD/BR or PM hybrid nanostructures.

Photosensitive proteins including BR are able to use only a minor portion of light energy in the visible range. The absorption of UV photons can induce destruction of the chromophore, the protein and the whole cell. The approach based on the inclusion of QD as a sort of converter antennas (like antennas of plant photosystems) allows the use of light that has not been absorbed by BR (from deep UV to the blue optical region), convert this energy to photons with wavelengths that can be absorbed by BR, effectively transfer the energy to BR in the FRET mode (Förster resonance energy transfer) and use this energy to improve its biological function. The use of BR is especially convenient also due to the fact that the chromophore in this protein (retinal) is located at a ~2.5 nm [24–30] distance from both surfaces of the purple membrane (Fig. 9 *a*).[61] This distance is much shorter than the average Förster radius (~5 nm) determined for many FRET systems.[13, 61–65] In addition, specially adjusted [61] QD have a broad absorption region, which overlaps with the BR absorption band in the 400–600 nm range, the absorption intensity of QD being several times higher than that of BR at 450–600 nm and almost an order of magnitude higher at 400 nm (see Fig. 9 *b*). Thus, there appear spectral conditions for effective energy transfer upon photoactivation from the donor (QD) to the acceptor (BR).

An equally important condition is adsorption of QD directly on the domains of purple membranes containing BR trimers; this was attained [61] by functionalization of the QD surface by cysteine or thioglycolic acid. The formation of high-quality structures of BR–QD conjugates of this sort was proven by AFM (Fig. 10).[61] The image in Fig. 10 *a* corresponds [61] to regularly packed BR trimers with ~6.2 nm distances between them and 0.4–0.5 nm height,

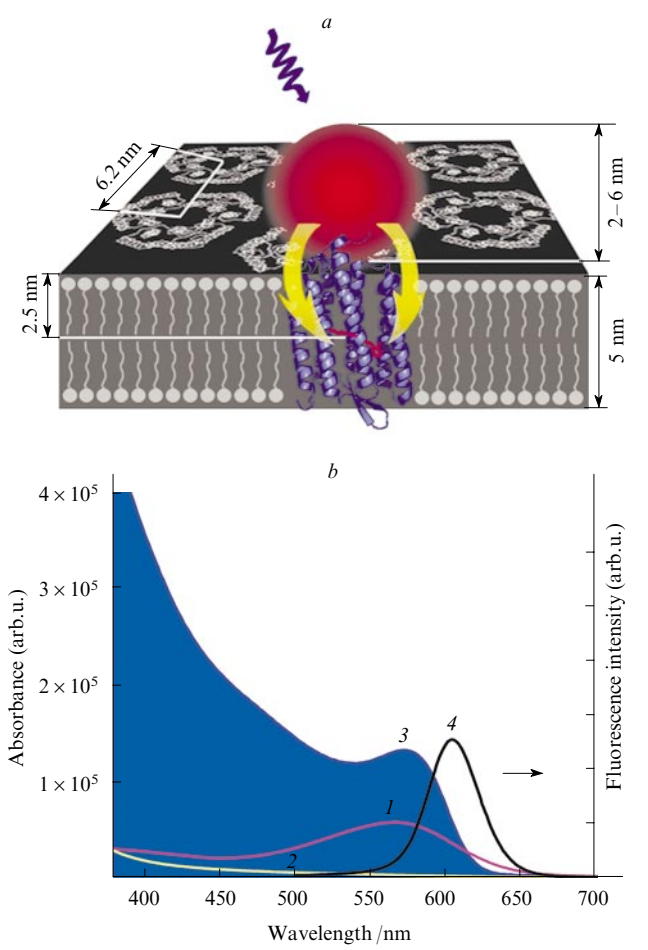


Figure 9. Structural organization of the hybrid material 'quantum dots–purple membrane' (*a*) and optical properties of bacteriorhodopsin (BR) and QD (*b*).[60]
All items in *a* are given on a scale. Photons are absorbed by quantum dots that are immobilized on a BR-containing PM surface. The exciton from the QD (donor) (shown by arched arrows) is transferred by FRET to the BR chromophore (retinal, the acceptor), thus initiating retinal photoisomerization, charge separation in the Schiff base, BR photocycle, and proton pump operation through PM. This energy transfer also results in pronounced QD fluorescence quenching.
Figure *b* shows the UV and visible absorption spectra of PM (*1*), white membranes (*2*) and one type of QD (*3*) used in the work; fluorescence spectrum of these QD (*4*).

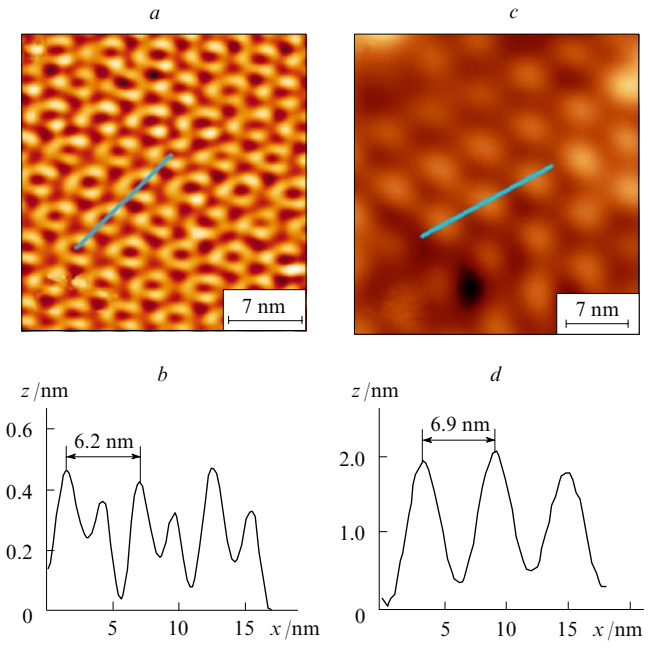


Figure 10. AFM images of bacteriorhodopsin, purple membranes (*a*) and PM associates with quantum dots (*c*).[60]
AFM profiles scanned along the blue lines in AFM images (*b*, *d*).

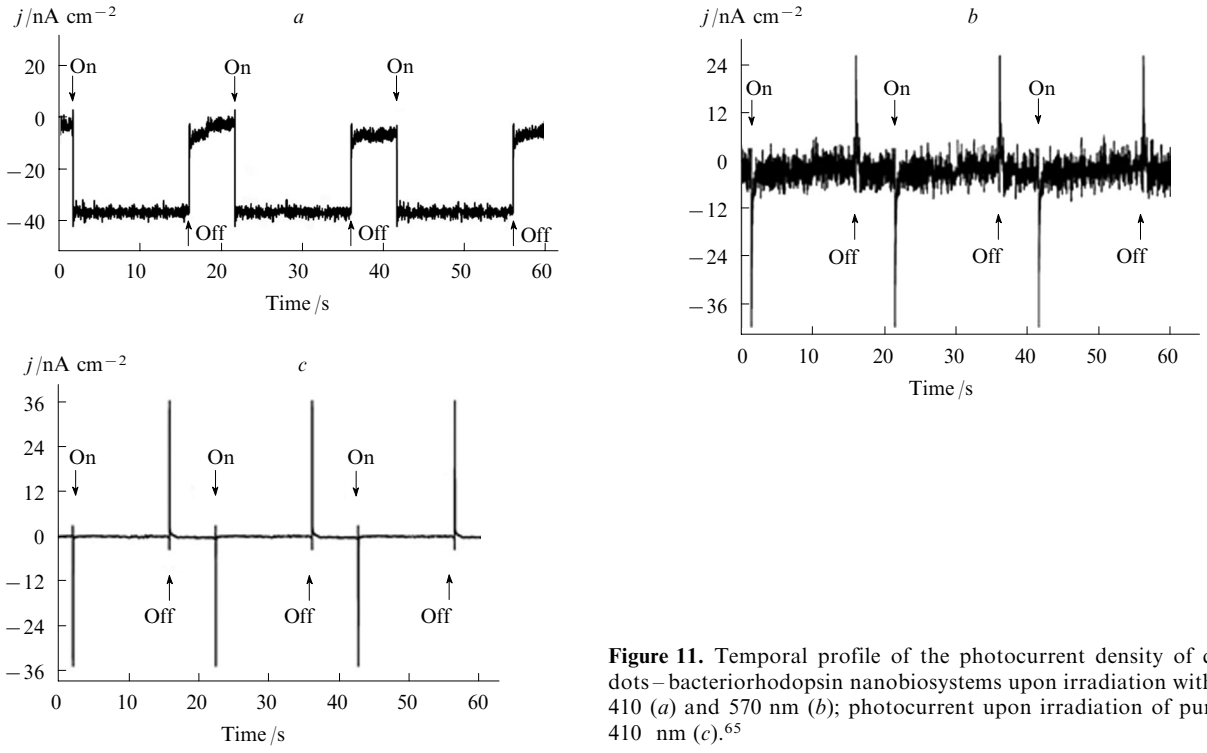


Figure 11. Temporal profile of the photocurrent density of quantum dots–bacteriorhodopsin nanobiosystems upon irradiation with light at 410 (*a*) and 570 nm (*b*); photocurrent upon irradiation of pure BR at 410 nm (*c*).[65]

as indicated by the profile of the AFM image (Fig. 10 *b*) along the blue line drawn in Fig. 10 *a* through several such trimers. The image in Fig. 10 *c* was obtained[61] after assembly of QD on the PM surface in QD : BR ratio of 1 : 2, which substantially increases the height of associates (up to 1.7–2.0 nm) and decreases the distance between the BR trimers approximately to 6.09 nm (see Fig. 10 *d*, the profile of the AFM image along the blue line drawn through several such trimers). These data attest to specific binding of QD to BR regions exposed on the PM surface. The regular structure of BR in the domains is retained at low QD : BR ratios, whereas above the equimolar ratio the regular structure of the QD–BR domains disappears and multilayer structures are formed.[60] The specific binding of small amounts of negatively charged QD to particularly accessible BR sites is caused by the presence of numerous positively charged lysine and arginine residues in the latter, whereas the membrane lipids surrounding the BR have a small negative charge due to the large number of phosphate groups on the PM surface.

This specific interaction of QD with BR results in pronounced quenching of QD fluorescence, which becomes almost complete for QD : BR ratios from 1 : 2 to 1 : 1 (in the case of QD-590)‡ or from 1 : 1.2 to 1 : 1 (in the case of QD-650).[61] Direct evidence for the FRET effect rather than other types of QD fluorescence quenching in these cases is the decrease in the QD fluorescence (by ~20%) in the presence of 'bleached' PM,[61] *i.e.*, membranes in which retinal has been thoroughly removed under mild conditions that do not damage the bilayer structures of the membrane and BR in these membranes. This detailed investigation[61] is the central one in a series of works[2, 13, 61–63] of this group of authors; another publication[63] reports a thorough study of the effect of the changes in the QD charge and size and the organic layer thickness on the specificity of the reaction of QD with BR.[65] From all the data described above, the authors conclude that the QD–BR functional elements operating in the FRET mode may give rise to a new trend in molecular electronics and in photogalvanic cells with more advantageous size, efficiency of light- and electrically controlled functions, structure persistence, stability and simplicity. For example, the existing nano-sized sensors use rather large light sources, whereas the size and properties of QD are perfectly suited for selective activation of separate protein molecules and, hence, they promote miniaturization of the sensor system with the simultaneous possibility of light-driven switching on/off of particular hybrid nanobiostructures among the large number of structures of this type on a common integral platform. These prospects of using hybrid structures attract much attention of researchers.[64–76]

In the publications[64, 65] dealing with the formation of film elements containing various proteins and QD, it was demonstrated that the influence of FRET on the properties of these composite materials is rather pronounced. For example, it was found[65] that immobilization of QD-537 (CdTe, diameter of 2–3 nm with a fluorescence maximum at 530–540 nm) on bovine serum albumin (in 1 : 9 ratio) upon electrophoretic sedimentation did not lead to changes in the QD-537 fluorescence parameters, whereas immobilization of QD-537 on BR (isolated from S9 strain of *Halobacterial halobium*) decreases the fluorescence of QD-537 by 95% with respect to the initial level. An achievement of the researchers[65] is the design of the QD–BR hybrid system able to generate direct current. Figure 11 shows reversible photoelectric changes in the QD–BR hybrid system upon laser excitation at 410 nm (power 7 mW cm^{-2}).[65] These signals crucially differ in the form

‡ In the QD designation, the numerals mean the fluorescence maximum wavelength in nm.

from the photocurrents that are generated in an identical system upon laser excitation at 570 nm (power of 6.5 mW cm^{-2}) (see Fig. 11 *b*) or in the system containing only BR (see Fig. 11 *c*) under the action of light at 410 nm, although the amplitude is $\sim$45 nA cm^{-2} in all cases.

According to Li *et al.*,[65] the phenomenon they detected is inherent in the QD–BR hybrid system on excitation at 410 nm. They proposed the following model to explain how QD can act as nano-sized 'light sources' incorporated in the BR films to produce stable photocurrents; this is the key feature distinct from the QD–BR hybrid systems reported earlier.[61–64] Since the initial BR state (B_{570}) and the M-form (M_{412}) have much longer lifetimes than other intermediates in the BR photocycle, only these two states are considered in this model (Fig. 12). In a series of experiments by these authors, not only illumination at 410 nm was taken into account but also the fluorescence of CdTe QD-537 induced by this illumination (blue light and green light), *i.e.*, BR irradiation in this system occurs simultaneously, which substantially affects the system parameters. The authors believe that QD fluorescence at 537 nm activates the nearby BR molecules and triggers the photocycle to give the M-form (M_{412}) and to release a proton. Meanwhile, stationary illumination at 410 nm accelerates the subsequent transformation of the M-form (M_{412}) to M_E (see the energy levels in Fig. 12) with fast proton capture. In this case (when blue light is applied together with green light), the proton has not enough time to reach the outer surface of the membrane, so that the BR molecule can rapidly take it back, *i.e.*, the proton pump is shunted. In the above-described experiment, two illumination wavelengths are superimposed onto each other throughout the whole process when the light source is switched on. Thus, the proton liberation and capture repeatedly and rapidly occur inside the membrane, *i.e.*, the protons do not escape into the intercellular spaces, which accounts for the generation of stationary photocurrent under these conditions.

It is noteworthy that the model proposed by the researchers cited[65] is not sufficiently substantiated, and other researchers[3, 6, 17, 26, 53] have already considered the simultaneous illumination of BR by two light sources at wavelengths of 570 and 412 nm. If the use of the QD–BR hybrid system in this chart actually results in the specific parameters indicated by the authors, which is still to be independently confirmed, this may provide the grounds for the design of new types of multifunctional systems.

However, Griep *et al.*[66] proposed an unusual method for the design of structures with alternating QD–BR layers, which gives a 23% increase in the BR signal with respect to the BR electrodes without QD. Two systems were obtained: I, non-modified BR and QD (575 nm) of the CdSe/ZnS structure; and II, biotinylated BR, which efficiently binds to the streptavidin shell of identical QD. It is well known that the biotin–streptavidin binding constant is 4×10^{14} mol $litre^{-1}$. System I in which QD are deposited on the surface of the PM film shows a 54.0% decrease in the QD fluorescence with respect to the standard QD layer on glass. For system II, fluorescence quenching is 43.8%, *i.e.*, a minor change in the distance between QD and BR (by 1–1.5 nm) caused by the QD shell induces pronounced changes in the QD fluorescence. This is attributable to the fact that FRET is very sensitive to the distance between the donor (QD) and the acceptor (BR) in the nanometre range. Fluorescence spectra[66] prove that only 'biotinylated' PM are able to bind 'streptavidin' QD to increase the distance between QD and BR to 6–8 nm. The highest photovoltaic parameters obtained on illumination of system II is 306 mV (as the light is switched on) and -200 mV (the light is switched off), whereas without QD these values are 249 and -158 mV, respectively.[66] The ratio of these values varies from 1.55 (PM–QD system) to 1.42 (only PM at the electrode), which coincides with the value (1.5) obtained previously for PM electrodes in other studies. Thus, the use of the streptavidin–biotin system results in specific interaction of QD with BR at a distance of about the Förster radius.[66]

The interest in commercial implementation of these systems is demonstrated by the patent application,[67] which describes a film multilayer structure based on BR and QD layers. This publication demonstrates the possibility of inducing an electrical response (potential step) of the hybrid system upon photoactivation. Griep *et al.*[68] reported a nanobiohybrid system containing QD (CdSe/ZnS) and BR. It was shown that at a distance of 3.5 nm between the donor and the acceptor, 88.2% of the QD energy is transferred,

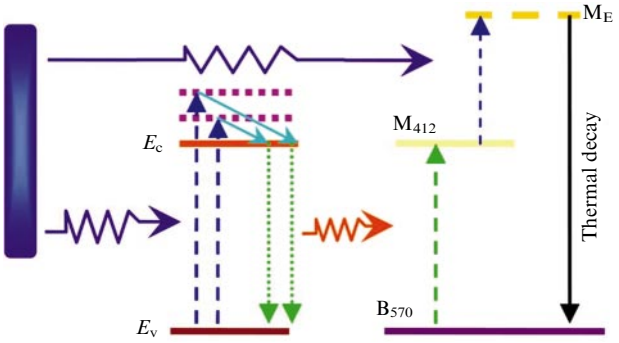


Figure 12. Equivalent energy level diagram of the photochemical cycle describing the current generation in the quantum dots–bacteriorhodopsin nanobiosystem.[65]
Subscripts v and c refer to the valence and conduction bands, respectively.

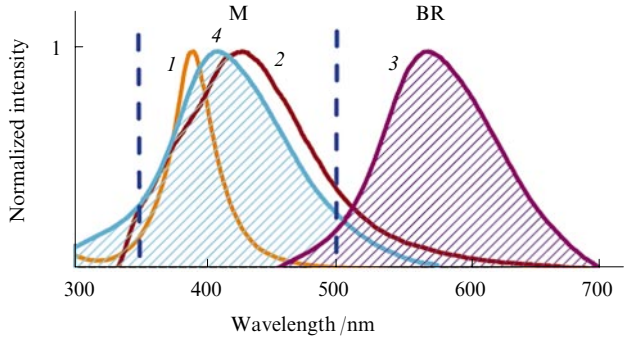


Figure 13. Normalized spectrum of the surface plasmon resonance of Ag nanoparticles of size 8 (*1*) and 40 nm (*2*); absorption spectra of bacteriorhodopsin (*3*) and its M-form (*4*) with peaks at 570 and 412 nm, respectively.[71]
The BR photocycle is initiated by a laser flash at 532 nm and continuous irradiation with blue light between 350 and 500 nm (marked by vertical dashed lines).

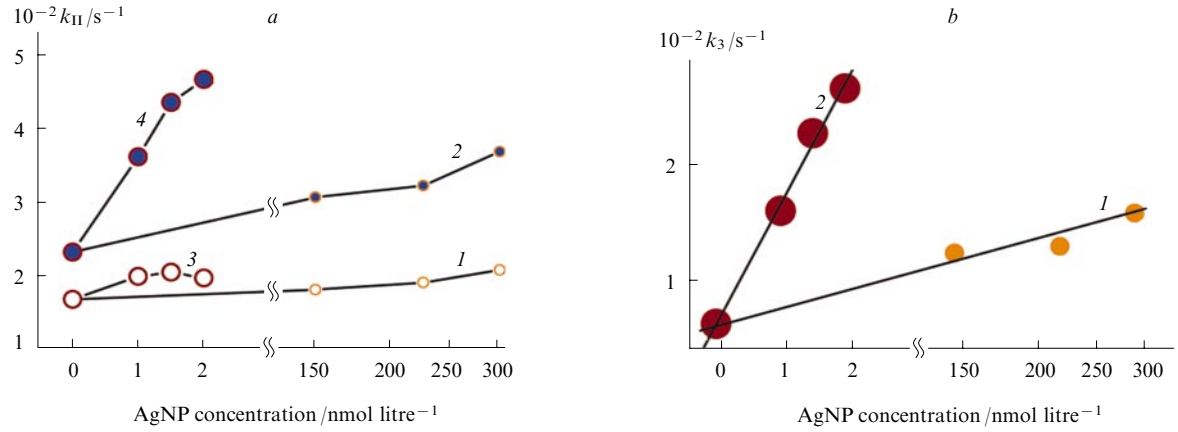


Figure 14. Influence of the electromagnetic field of Ag nanoparticles (AgNP) on the spectral parameters and kinetics of the bacteriorhodopsin photocycle.[71]
(*a*) Observed rate constant for the conversion of the M-form to B_{570} (k_{II}) *vs.* 8 (*1*, *2*) and 40 nm (*3*, *4*) Ag nanoparticle concentration on irradiation with blue light (*2*, *4*) and without irradiation (*1*, *3*); (*b*) difference between the k_{II} values with and without blue light irradiation equal to the rate constant of the bypass cycle (k_3). Silver nanoparticles of size 8 (*1*) and 40 nm (*2*).

while a 8.5 nm distance results in a 51.1% energy transfer. These data are close to the theoretically calculated Förster radius for the QD–BR system, which is 7.94 nm. The effective lifetime of QD in the excited state decreases from 18.0 to 13.3 ns. The authors discuss the possibility of application of QD–BR systems in solar batteries, biosensorics, optoelectronics and biocomputer and other technologies.[68]

For the development of an alternative system of QD and BR monolayers on a conducting surface of the ITO electrode, the use of ionic self-assembled monolayers (I-SAM) was proposed.[69] Poly(diallyldimethylammonium) (PDDA) served as the I-SAM material; it was deposited onto the ITO electrode by the Langmuir–Blodgett technique. This was followed by deposition of the following layers (the value in parentheses is the adsorption period): BR (5 min), QD (10 min) and PDDA (5 min). The same procedure was used to prepare bilayer (BR/PDDA and QD/PDDA) and trilayer (BR/PDDA/QD) structures.[69] It was shown that BR/PDDA bilayers have an absorption maximum at 570 nm the intensity of which linearly increases with the increase in the number of bilayers (the authors studied 2 to 12 bilayers).[69] However, the photovoltaic response of I-SAM film with adsorbed 12 BR/PDDA bilayers was nearly equal to that of the system comprising three such bilayers. A linear dependence of the intensity of the QD fluorescence maximum (at 570 nm) on the number of the QD/PDDA bilayers was obtained. Subsequently, the ternary system containing the sequence of layers ITO/PDDA/(BR/PDDA/QD)$_n$ ($n = 1-6$) was studied in

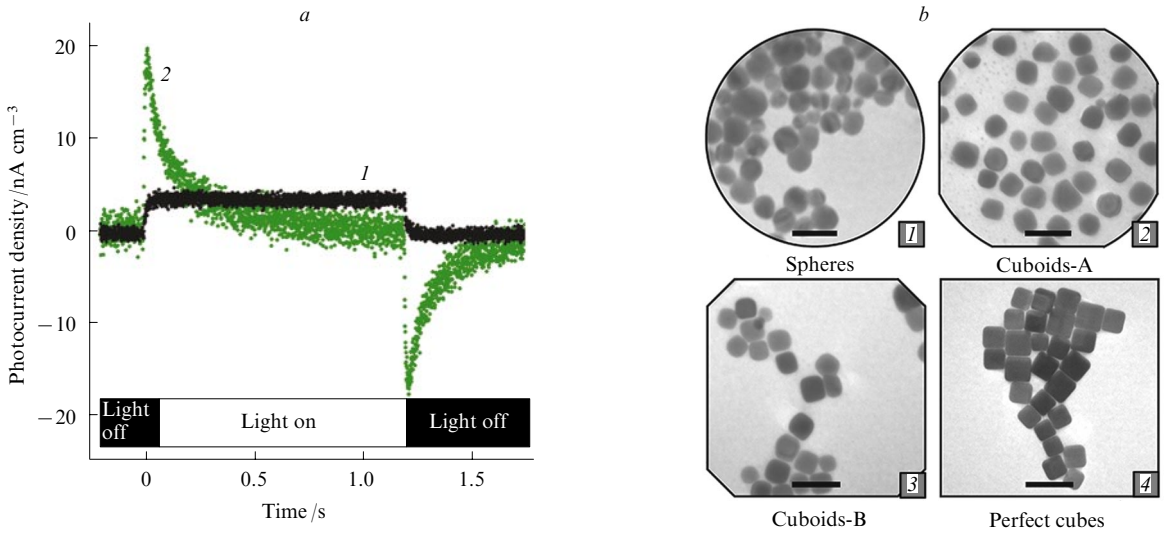


Figure 15. Characteristics of porous and proton-selective membranes and images of nanoparticles of different shape.[72]
(*a*) Photocurrent generated by native bacteriorhodopsin with the use of a Nafion membrane (*1*) and a porous membrane (*2*); (*b*) transmission electron microscopy images: spheres (*1*), cuboids-A with highly truncated corners (*2*), cuboids-B with slightly truncated corners (*3*), perfect cubes (*4*) (scale: 100 nm).

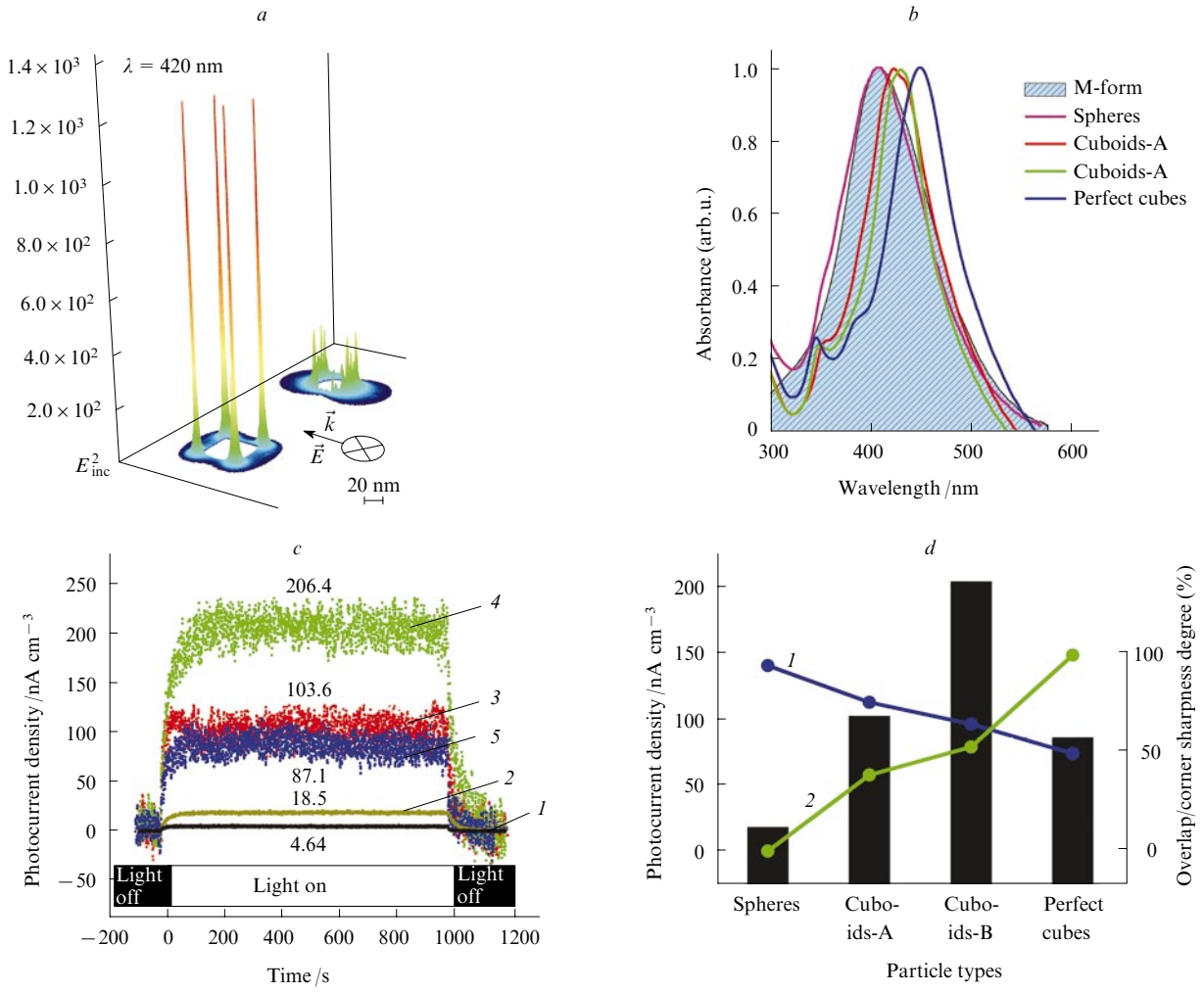


Figure 16. Plots of electromagnetic fields, absorption spectra of silver nanoparticles and 'photovoltaic properties' of bacteriorhodopsin.[72] (*a*) Graphical representation of electromagnetic fields of gold nanoparticles in the discrete dipole approximation: spheres 40 nm in diameter (on the right) and cubes with 40 nm edge (on the left) (E^2_{inc} is the electric field energy); (*b*) absorption spectra of silver nanoparticles as spheres, cuboids and cubes of 40 nm size coated by PVP (MM = 55 kDa); the hatched area is the absorption region of the M-form of BR; (*c*) BR photocurrent generation on exposure to blue light in the presence of PVP-coated (MM = 55 kDa) silver nanoparticles (40 nm): native BR (*1*) in the presence of spheres (*2*), cuboids-A with highly truncated corners (*3*), cuboids-B with slightly truncated corners (*4*) and perfect cubes (*5*); (*d*) BR photocurrent density for nanoparticles of different shape (column diagram); degree of overlap of the nanoparticle plasmon resonance band and absorption band of the BR M-form (*1*) and degree of silver particle corner integrity as a measure of the field strength (*2*).

the same way.[69] These results attest to a linear increase in the QD fluorescence when considering only the points corresponding to complete transfer of the trilayer, *i.e.*, integer *n*; the authors detected a 20% decrease in the QD fluorescence for every trilayer as compared with that for the QD/PDDA bilayer. This finding is confirmed by the fact that an equal 20% decrease in the QD fluorescence was also observed for 'incomplete' trilayers such as PDDA/BR on the surface of each complete trilayer.[69] This fluorescence quenching is attributable to the QD to BR energy transfer according to the FRET mechanism, which indicates the possibility of the designing of nanobiohybrid structures with controlled BR and QD multilayer architecture on the I-SAM surface.

Thavasi *et al.*[70] carried out an extensive comparative study of wild-type BR and its triple (3Glu) mutant (E9Q/E194Q/E204Q) combined with a wide-band-gap semiconductor TiO_2 and demonstrated the applicability of these structures as effective biosensitized solar batteries. In particular, differential scanning calorimetry measurements demonstrated the thermal stability of both the wild-type BR and the 3Glu mutant, while molecular modelling revealed the binding of BR and 3Glu mutant to the TiO_2 oxygen atoms favourable for electron transfer. From comparison of the obtained characteristics for different solar cells, it follows that the 3Glu mutant exhibits relatively low photoelectric performance, but it is still better than that of wild-type BR, the short-circuit photocurrent being $\sim$0.09 mA cm^{-2} and the photopotential being 0.35 V at a 40 mW cm^{-2} illumination intensity.[70]

Yet another important line of research in this area is investigation of influence on BR of the electromagnetic field of gold and silver nanoparticles,[71–75] the plasmon resonance bands of which overlap with the absorption band of the M-form (Fig. 13).[73] It was found that in these hybrid systems, the electromagnetic field changes appreciably both

the photocurrent and the proton pumping rate and also the effect of blue light acting on the slow metabolites of the photocycle (such as the M-form).

The influence of electromagnetic fields of Ag nanoparticles is vividly illustrated by the dependence of the BR photocycle kinetics on the size of these particles and on the system exposure to blue light (Fig. 14).[71]

Experiments showed that the joint action of blue light on Ag nanoparticles and short-pulse laser excitation (532 nm) on BR substantially accelerates both the restoration of the initial form (BR_{570}) and the proton pumping rate and also transformations of the M-form. Besides, in the presence of 40 nm Ag nanoparticles, the transformation rate of the M-form increased by a factor of 400 with respect to that for 8 nm Ag nanoparticles. This was caused by a much stronger electromagnetic field and wider overlap of the absorption bands of 40 nm Ag nanoparticles and the M-form (see Fig. 13).[71] This magnitude of the effect is in good agreement with the theoretical value (a 375-fold increase) calculated with the following assumptions: (i) the increase in the electromagnetic field is proportional to the nanoparticle size, the proportionality factor being 125; (ii) the increase in the efficiency of light quantum absorption by the M-form in the presence of 40 nm nanoparticles as compared with 8 nm nanoparticles with a factor of about 3. Further studies of this effect[72–75] demonstrated additional prospects for increasing the photocurrent, mainly by reducing the time of the BR photocycle. An achievement of the researchers cited[71] is the detection of three factors that improve the parameters of this process in a liquid electrochemical cell. First, the authors improved the separation of charge carriers upon photoactivation of the system in solution by replacing the conventional porous membrane by the proton-selective Nafion membrane (Fig. 15 *a*). Second, the authors preserved as fully as possible the electromagnetic field effect by using polyvinylpyrrolidone (PVP) with MM = 55 kDa to prepare an ultrathin polymer coating of nanoparticles, which decreases the electromagnetic field to a minimum extent and retains the high nanoparticle stability. Third, specially synthesized nanoparticles of a specified shape were used (Fig. 15 *b*); the best of them considerably increased the electromagnetic field strength (Fig. 16 *a*) and the width of spectral overlap of their absorption with that for the M-form (see Fig. 16 *b*). An elegant theoretical model was also developed to interpret the fact that the photocurrent reached a value of about 210 nA cm^{-3} in an electrochemical cell with a Nafion membrane containing BR and plasmon nanoparticles (of a specified shape and size) (see Fig. 16 *c*,*d*).[72] The authors claimed that this is almost 5000 times higher than the photocurrent observed earlier in electrochemical cells containing BR thin films; however, this seems somewhat doubtful.

Indeed, the photocurrent for non-oriented wild-type BR layers is much lower than that indicated above (usually it is 1–3 nA cm^{-2} but can be increased to 4–6 nA cm^{-2} after removal of lipids from BR samples[76]). The photocurrent for BR films can in principle be even higher than 20 nA cm^{-2} at relatively high voltage (500 mV) for some BR mutant strains. They were obtained, for example, by Patil *et al.*,[76] who replaced methionine (in position 163) by cysteine to provide the oriented binding of BR to the surface of a gold electrode. On the other hand, we have already cited a number of publications on electrochemical cells with LBL-fabricated films with a large number of polyelectrolyte layers alternating with BR (wild type or mutant) in which the photocurrents were from 100–200 nA cm^{-2} (Refs 47–49) to 420 nA cm^{-2} (Ref. 52). In PM LS films, this value varied from 50 to 200 nA cm^{-2} (Ref. 37), while in the case of PM BLM films it varied from 100 to 150 nA cm^{-2} (Ref. 40). Thus, these photocurrents are comparable[37,40,47–49] with the values reported by Yen *et al.*[72] or are even much higher.[52]

The effective film nanobiohybrid systems based on photosensitive membrane proteins with nanoparticles will not be soon placed on the market but the above examples demonstrate their high potential value and good prospects for application in technology. The approaches and techniques considered in this review serve as the basis for the design of new nanobiohybrid film systems with higher efficiency compared with currently available systems.

III. Planar systems based on reaction centre proteins of photosynthetic bacteria

1. Structural and functional features of reaction centre proteins

An example of photosensitive membrane proteins of a more complex structure is provided by the reaction centres (RC) of photosynthetic bacteria, which serve as key elements of the photosynthesis system.[77–85] The reaction centres of bacteria are integrated membrane protein–pigment complexes able to perform charge (electron) transfer and separation in photosynthetic membranes upon absorption of a light quantum (Fig. 17 *a*,*b*).[77] The protein part of the RC from the thermophilic bacteria *Chloroflexus aurantiacus* comprises two subunits called L and M; the RC from *Rhodobacter sphaeroides* have an additional H-subunit (see Fig. 17 *a*); and the RC from *Rhodopseudomonas viridis* has also the fourth subunit, a cytochrome.[77–81] These differences in the RC structure are related to evolution of bacteria: the homology of the like protein subunits of the RC of these purple and green bacteria is up to 40%. The best studied RC from *Rb. sphaeroides*, apart from three polypeptides (L, M and H with molecular masses of 28 000, 32 000 and 35 000), also contains a large number of cofactors (see Fig. 17 *b*): four bacteriochlorophyll *a* molecules (BChl), two bacteriopheophytin *a* molecules (BPhe), two ubiquinone molecules (Q_A and Q_B), a non-haem iron ion and a carotenoid molecule (Car).[77]

It is known[77–79] that each of L- and M-subunits of the complex contains five transmembrane α-helices (A, B, C, D, E), and they are roughly related to each other by a twofold symmetry axis; RC cofactors are non-covalently linked to polypeptides. On the periplasmic side of the membrane, two BChl form the special pair (P) the chromophores of which overlap, the macrocycles of these BChl of the P dimer being nearly parallel to each other and normal to the membrane surface. Due to this arrangement (the distance between the planes of P macrocycles is 0.34 nm), the electron density of the BChl pair merges, which changes the properties of tetrapyrroles (in particular, the spectral properties of the P dimer differ from the properties of other RC bacteriochlorins). The other cofactors — monomeric $BChl_A$ and $BChl_B$, $BPhe_A$ and $BPhe_B$, ubiquinones Q_A and Q_B — form two nearly symmetric branches A and B, which run from the P dimer to the Fe^{2+} ion on the cytoplasmic side of the membrane (see Fig. 17 *b*). The only carotenoid is linked to

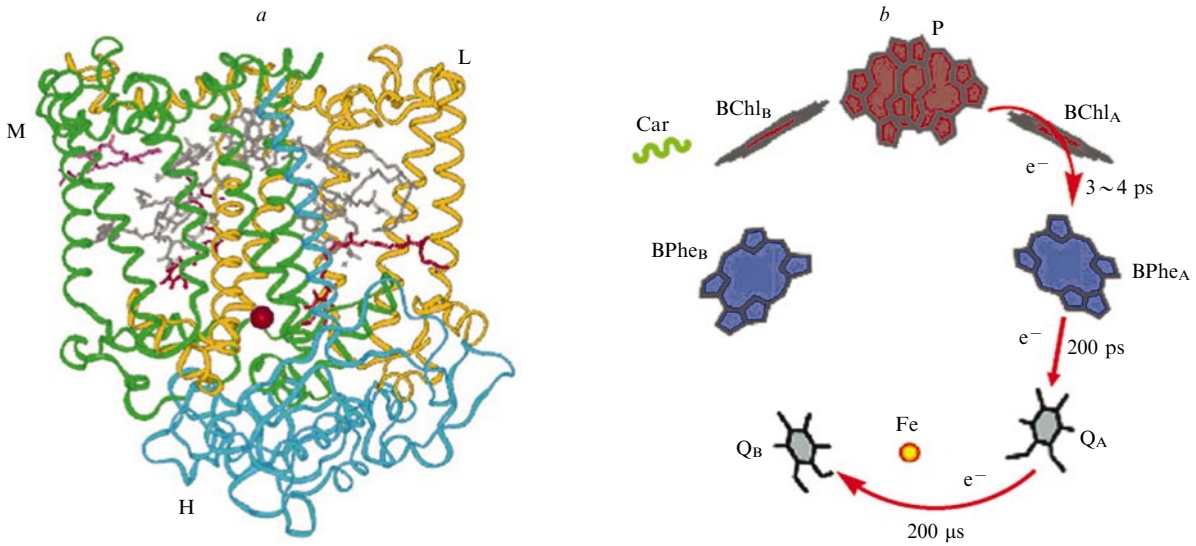


Figure 17. Three-dimensional structure of the reaction centre from *Rhodobacter sphaeroides* (*a*) and arrangement of cofactors and photoinduced electron transfer in the RC (*b*).[77]
Subunits L, M and H are indicated by yellow, green and blue helixes, respectively (for explanation, see the text).

the M-subunit in the close vicinity of $BChl_B$. The H-subunit comprises one transmembrane α-helix and the large cytoplasmic domain, which separates the quinone binding sites and protects the Fe^{2+} ion from the aqueous phase. Despite the hydrophobic environment, the RC structure incorporates water molecules which are important for complex functioning. In addition, several cardiolipin molecules involved in stabilization of the complex were determined by crystallography in many RC structures from *Rb. sphaeroides* known to date. Most of cofactors exhibit well-discernable bands in the absorption spectrum of the RC (located in near-infrared, visible and near-ultraviolet regions).[77–81]

In the RC from *Rb. sphaeroides*, the transmembrane electron transfer goes only along the A-branch starting with the transition of the BChl dimer (P) to the excited state (P*). The electron transfer from P* to a number of intermediate cofactors ends on the ubiquinone Q_A and takes a period somewhat longer than 200 ps under normal conditions. The charge-separated state ($P^+ Q_A^-$) recombines to the ground state (P) in 120 ms. The overall energy change upon the P to P* transition is 1380 meV.[81–84] As the P* state is formed, the absorption of P at 870 and 600 nm and the stimulated fluorescence at 920 nm decrease. As the electron is transferred from P* to bacteriochlorophyll *a*, the intensity of the 800 nm band decreases and an absorption band at 1020 nm appears.[81] Further electron transfer from Q_A^- to Q_B (to give ubisemiquinone) occurs within 200 μs, and after the transfer of the second electron from P*, Q_B is completely reduced to ubiquinol, which leaves the RC being replaced by another oxidized ubiquinone molecule from the intramembrane pool.[81] The oxidized dimer is reduced by either exogenous *c*-type cytochrome (as in *Rb. sphaeroides*) or by the cytochrome of the integrated C-subunit (as in *R. viridis*).[77–81]

Yet another important structural unit is the light-harvesting antenna, which absorbs light throughout the whole visible region and transfers the excitation energy to BChl of the reaction centre, which absorbs at 875 nm in *Rhodospirillaceae* and at 890 nm in *Chromatiaceae*. This complex contains two polypeptides, as well as bacteriochlorophyll and carotenoids in 1 : 1 ratio. The BChl : RC ratio remains constant being about 25 : 1. The reaction centre contains also minor amounts of carotenoids incorporated into the light-harvesting complex of the antenna. Some species, *e.g.*, *Rhodospirillum rubrum*, have only one light-harvesting complex, whereas other organisms, *e.g.*, *Rhodopseudomonas* sp., contain also one more such complex, which absorbs at shorter wavelengths (800 and 850 nm). It comprises two peptides, two bacteriochlorophyll forms (two BChl-850 molecules and one BChl-800 molecule) and one carotenoid molecule. The ratio of the number of these complexes to the number of reaction centres varies, depending on the environmental conditions, from 10 to 100 BChl-800(850) molecules per RC.[81–85] There are numerous photosynthetic bacteria, which are beyond the scope of this review, and the indicated RC will be considered in the following sections.

2. Langmuir – Blodgett and Langmuir – Schaefer monolayers and films

Large series of works dealing with the preparation and study of Langmuir monolayers and films from bacterial RC were performed nearly simultaneously by research groups from the USA,[86,87] Russia (USSR)[88–95] and Germany[96,97] at the border of the 1990s. These and many other works were considered in a number of reviews (see, for example[4,7,77]), so that we can concentrate on only some important issues in some of the publications. Most fundamental among the listed works are two papers of US scientists,[86,87] who described in detail the methods used to prepare Langmuir monolayers and films from bacterial RC and proved their native character by spectral and photoelectric measurements.

In some papers of Russian scientists, these objects were studied in more detail (in both structural and functional aspects).[89–91] In particular, it was discovered that the surface pressure (π) – area per molecule (A) isotherms for various types of RC (*C. aurantiacus*, *Rb. sphaeroides*, *R. viridis*) are qualitatively similar and have two regions

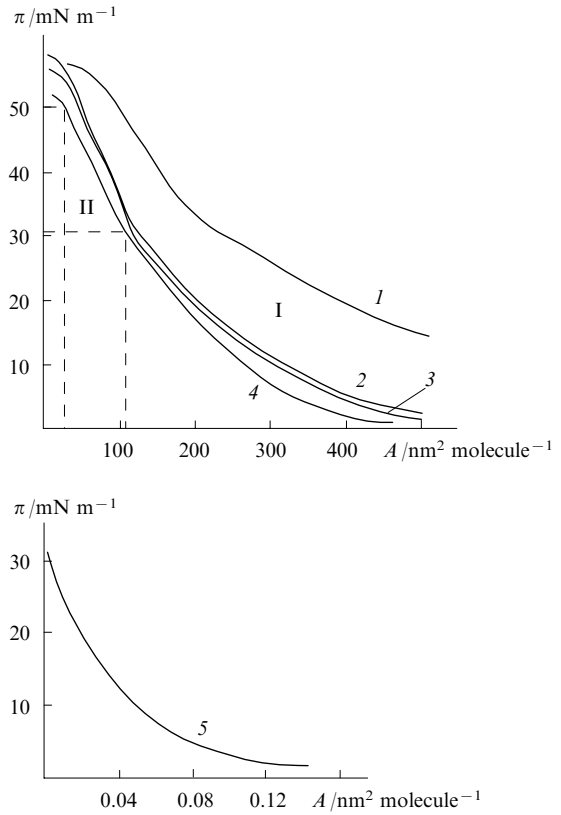


Figure 18. Surface pressure–area per molecule isotherms for the reaction centres isolated from *R. viridis* (*1*), R-26 strain of *Rb. sphaeroides* (*2*), *C. aurantiacus* (*3*), *Rb. sphaeroides* (wild type) (*4*) and for LDAO (*5*) in 10 mM phosphate buffer at pH 7.0 and 20 °C.[17]

with different slopes of the curves (Fig. 18),[17] each corresponding to a particular state of the monolayer. The pressure of transition between these regions is about 30–32 mN m^{-1}, which corresponds to the surface tension in liposomes and lipid membranes. At low pressures and large areas per molecule (region I, liquid-expanded state), the behaviour of RC monolayers is determined by the surfactant molecules [lauryldimethylamino oxide (LDAO), octyl-β-glycopyranoside, *etc.*], which are used in the isolation of RC from biomembranes; by enveloping the hydrophobic surface of protein globules, they prevent aggregation of RC in an aqueous suspension. This is why in the pressure region from 0 to 30 mN m^{-1}, the shape of $\pi-A$ isotherms for the monolayers of all RC is similar to that of individual surfactants. Since these surfactants cannot form stable monolayers and completely pass to the aqueous subphase at pressures of about 30 mN m^{-1},[90] the inflection in the $\pi-A$ isotherms of RC at pressures of 30–32 mN m^{-1} corresponds to the onset of compression of particularly the protein monolayer. Region II located at high pressures (up to the collapse pressure of the monolayers) corresponds to liquid-condensed state of the RC protein monolayer. The collapse pressure (π_c) of the monolayers of *C. aurantiacus* RC is 58 mN m^{-1}, which is 3 and 8 mN m^{-1} higher than that of *Rb. sphaeroides* RC (wild type and strain R-26, respectively) and 5 mN m^{-1} higher than for *R. viridis* RC. This attests to high strength of monolayers of RC, especially the RC from *C. aurantiacus*, which implies that they have only two hydrophobic protein subunits. The areas A_c corresponding to the maximum compression of the layer for the RC from *Rb. sphaeroides* and *C. aurantiacus* are about 35–45 nm^2 (see Fig. 18), which corresponds to the radius of 3.3–3.8 nm for the protein in the spherical approximation.[92] These results are in good agreement (to an accuracy of 0.3 nm) with the X-ray diffraction data obtained for the RC from *Rb. sphaeroides*.[77,82] It is of interest that these parameters coincide for all three RC having substantial structural differences: three protein subunits (L, M, H) in the RC from *Rb. sphaeroides* and only two membrane subunits (L, M) in the RC from *C. aurantiacus*. From this it follows that the hydrophilic H-subunit, which is strongly bonded to the RC from *Rb. sphaeroides* on the cytoplasmic side of the membrane, has virtually no influence on the size of the 'horizontal cross-section' of the RC in the monolayer. The A_c value for the RC from *R. viridis* is about 90 nm^2 (see Fig. 18), which corresponds to a protein sphere diameter of 10.7 nm. According to the crystallographic data,[77] the RC from *R. viridis* are substantially asymmetric (13.0 × 7.0 nm) due to the presence of two hydrophilic protein subunits (cytochrome and H-subunit) located on the periplasmic and cytoplasmic sides of the membrane, respectively, and strongly bonded to the membrane subunits (L, M). Thus, the A_c value for the RC from *R. viridis* in the monolayer is between the two indicated crystallographic sizes of the protein, which attests to the inclined position of the longer axis of this RC with respect to the interface.

A number of publications[90–94] present detailed studies of parameters of the monolayers of these RC under various conditions (composition of the medium, concentration, pH and temperature), which provided the determination of the optimal conditions for their formation: 10 mM phosphate buffer in aqueous subphase at pH 7.0 and a temperature not higher than 20 °C. Under these conditions, the RC monolayers were quantitatively transferred to various solid substrates (quartz, semitransparent and electrochemically etched silver electrodes). These experiments identified the optimal transfer procedure (with a 95% coefficient), namely, the LB method at a >30 mN m^{-1} pressure.[94,95]

Interesting results on RC films are related to photoinduced changes in the photoelectric parameters of RC multilayers.[94,95] It was found for LS multilayers of RC on SnO_2 electrodes coated by a liquid electrode (In–Ga paste) that the H-subunit is 80% directed towards the aqueous subphase. An opposite situation was found for films of the *R. viridis* RC (the SnO_2 electrode is negative) where a more hydrophilic subunit, cytochrome, was directed towards the aqueous subphase, while the H-subunit was oriented towards the air phase. In the case of *C. aurantiacus* RC films, the photopotential was relatively low; along with the retention of the functional activity of the protein (from spectral data), this attests to the absence of the predominant orientation of the protein at the interface. This may be attributed to the lack of substantial asymmetry in the structure of the RC from *C. aurantiacus*. In our opinion, films based on the RC from *R. viridis* and *Rb. sphaeroides* are promising materials for parts of bioelectronic devices.

To increase the stability of the RC Langmuir films and bring these systems closer to real biomembranes, a group of researchers[7] prepared mixed mono- and multilayers of RC with various lipids and polymers. Analysis of numerous data on the influence of the protein : lipid ratio on the

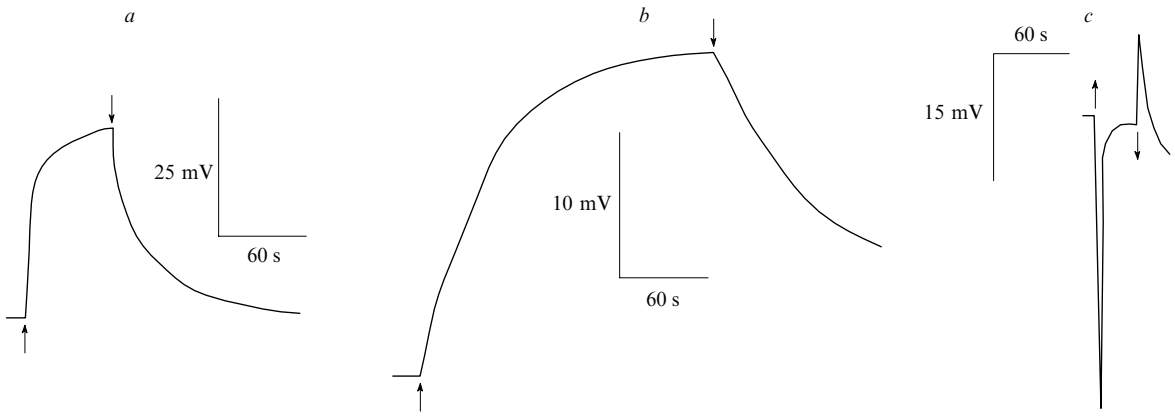


Figure 19. Photoinduced electrical response on continuous irradiation of a multilayer film consisting of 15 monolayers of *N*-acryloylphosphatidylethanolamine with the RC from *Rb. sphaeroides* (10 : 1, mol), 10 stearic acid monolayers at the top and at the bottom of the film and 10 ACPE–*Rb. sphaeroides* RC (10 : 1, mol.) monolayers (*a*), of 10 ACPE–*Rb. sphaeroides* RC (10 : 1, mol.) monolayers after polymerization (*b*), of 25 monolayers of tetracosa-11,13-diynoic acid with the RC from *Rb. sphaeroides* (100 : 1, mol.) and 10 stearic acid monolayers at the top and at the bottom of the film (*c*).[95]
Here and below ↑ is light switching on, ↓ is light switching off.

monolayer characteristics is beyond the scope of this review; however, it was noted that an increase in the lipid percentage (> 100 : 1) in the mixed lipid–RC monolayer makes the corresponding $\pi - A$ isotherms similar to those for a layer of pure lipid. In addition, in the case of the *Rb. sphaeroides* RC, the characteristics of the mixed monolayer are affected most appreciably by the overall charge of the lipid molecule, while in the case of the RC from *C. aurantiacus*, the key role is played by the hydrophilic-hydrophobic balance of the lipid molecule. Thus, the optimal conditions for the formation of mixed RC–lipid monolayers are 0.01 M phosphate buffer, pH 7.0, and a temperature not higher than 20 °C.[89–93]

A film composed of 15 monolayers of the *Rb. sphaeroides* RC–ACPE in 1 : 10 ratio (mol.) (ACPE is *N*-acryloylphosphatidylethanolamine) both before and after polymerization exhibited long-wavelength absorption peaks typical of proteins (700–900 nm). The use of lipid-like polymer is favourable for preserving most of the protein molecules in the native state and for increasing their stability compared with a neat protein film without lipids.[94, 95]

The sign of the photopotential on a semitransparent conducting SnO_2 substrate in these Langmuir films of the *Rb. sphaeroides* RC and ACPE was positive (Fig. 19 *a*).[94, 95] The predominant orientation of the RC from *Rb. sphaeroides* in the ACPE monolayer determined from the sign of the photopotential (the H-subunit is oriented to the aqueous subphase) is identical to that for neat protein monolayers. The same form and sign of the photopotential were found in a study of the RC–ACPE Langmuir films polymerized preliminarily at the interface (see Fig. 19 *b*). As another polymer matrix for RC immobilization, tetracosa-11,13-diynoic acid (TDA), which is distinguished by exceptionally high polymerization rate upon UV irradiation, was used. Langmuir films composed of 25 monolayers of RC from *Rb. sphaeroides* and TDA (1 : 100) and coated by 10 monolayers of stearic acid on each side have a negative photopotential on the SnO_2 substrate (see Fig. 19 *c*). In view of the Langmuir–Schaefer transfer of RC–TDA to the SnO_2 substrate, one can conclude that the H-subunit of RC in the TDA monolayer is directed towards the air rather than towards the aqueous subphase, as was shown for the mixed RC–ACPE monolayer. The faster generation of the photopotential for the RC–TDA film as compared with the RC–ACPE film is apparently related to the possibility of additional electron transfer along the conjugation chain of the diacetylenic acid. Thus, by using special polymerizable lipid-like monomers, it is possible to considerably affect the orientation of these RC in mixed monolayers and increase the stability of protein monolayers.

A scanning tunnelling microscopy (STM) study of LB monolayers of the *Rb. sphaeroides* RC demonstrated the following:[98] (i) the molecular structure of the RC monolayers obtained in the dark had a period of 6.4 and 3.0 nm, which corresponds to the sizes of the protein and its subunit found from X-ray diffraction data; (ii) conversely, on irradiation, no periodic structure was found in RC monolayers. A change in the voltammetric characteristics of LB monolayers of RC in the STM mode demonstrated charge separation in single protein molecules at the interface and their different behaviours in the dark and in the light.[98] By fixing the protein monolayer with glutaraldehyde, the researchers[98] were able to prevent the perturbing cantilever tip action and obtained a periodic molecular structure with a periodicity of 3.0 nm even in the light. The next publication of these authors[99] dealt with the structural changes of the RC in the monolayers on water and after deposition to a solid substrate and with the changes in the protein orientation depending on the surface pressure. At low surface pressure (15–25 mN m^{-1}), the protein structure substantially depends on the surface tension, as indicated by both the results of measurement of isotherms at the air–water interface and the optical spectroscopy data. At a surface pressure of 30–45 mN m^{-1}, the native structure of RC is almost completely retained, these films being characterized by not only higher surface density but also by enhanced anisotropy, as follows from the results of polarization

§ Z-Type films were deposited on a hydrophilic substrate by the vertical technique, while X-type films were deposited on a hydrophobic substrate by a horizontal technique.

absorption spectroscopy, microgravimetric analysis (piezoelectrical microweighing) and optical ellipsometry.[99]

In a series of works of Japanese scientists,[100–102] the RC orientation in various types[§] of LB films was evaluated for the first time by enzyme-linked immunosorbent assay (ELISA) to compare the antibody signal to the RC H- and C-subunits. In the LB films of Z-type RC from *R. viridis*, 80% of the H-subunits were directed towards the substrate, as was derived from the ratio of antibody signals to C- and H-subunits.[101] The same method was used to find out that in the LB films of X type RC from *R. viridis*, 65% of the C-subunits were directed towards the substrate.[101] It was assumed[102] that the RC orientation (by the H- or C-subunit towards the substrate) can be controlled by varying the sign of the applied bias voltage to the electrodes in the Langmuir bath or at the ITO-electrode with the transferred RC monolayer or by adding counter-ions into the aqueous subphase. In general, this forced orientation of protein molecules in the specified way in Langmuir monolayers and films opens up new prospects for the design of photosensitive materials and sensors based on them.

3. Self-assembled and other film systems from reaction centre proteins

Self-assembly of bacterial reaction centre proteins on the surface of modified electrodes is the most readily accessible and workable method for the preparation of materials for photoinduced energy transfer.[77, 103–106] In SA film systems, as in Langmuir films, the RC protein complexes can be aligned on the solid substrate (electrode) so that the longer axis of the complex (running from the donor to acceptor part of the electron transport chain of RC cofactors) is mainly normal to the substrate plane, although predominance of one of the two orientations of the RC is relatively low. This is apparently caused by the insignificant difference between the hydrophilic characteristics of the polar ends of the extended RC globule. Therefore, a priority challenge for all studies devoted to the possible application of these systems in technology is the design of highly oriented RC layers in film structures.

Katz and co-workers[103–106] used for this purpose SA layers of long-chain naphthoquinone derivatives, which were chemically immobilized (*via* aminosilanes or thiol groups) or physically adsorbed on platinum electrodes. These adsorbed quinones were recognized by RC at the binding site of the primary quinone in the RC molecule to form strong RC layers the cycloplasmic side of which faced the electrode.[103, 104] By adding reduced cytochrome (as a donor of electrons) and ubiquinone-2 (as the secondary quinone), the authors were able to obtain photocurrent using these modified 'biophotoelectrodes'.[103–105] Subsequently the use of an amalgamated platinum electrode modified with naphthoquinone with a disulfide group resulted in a considerable increase in the photoelectric activity of the adsorbed RC layer.[105] It should be emphasized that in all of the described cases, both naphthoquinones (chemically immobilized or physically adsorbed on the electrodes) and exogenous ubiquinones (added to the aqueous electrolyte) play the key role in the effective operation of such systems. These quinones were needed in the system in rather large concentrations (~ 50 μmol · litre^{-1}) in order to eliminate the diffusion restrictions and prevent the predominance of Q_B^- recombination with P^+, which occurs in solutions of RC with a rate constant of

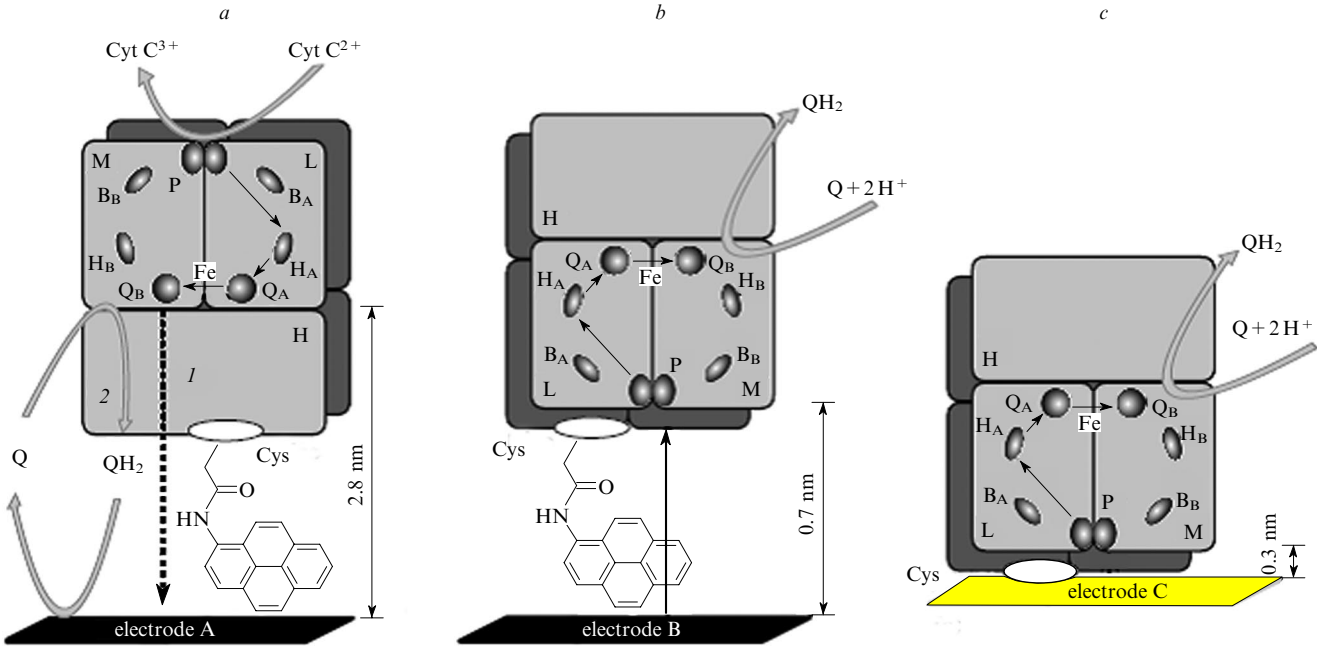


Figure 20. Scheme of binding of the reaction centres to electrodes.[107]
The black arrows show the electron transport path. (*a*) Wild-type RC linked by the H-subunit to the highly oriented pyrolytic graphite through a pyrene derivative. The large distance between the electron donor site and the electron reduces the probability of tunnelling (dashed arrow, process *1*); addition of quinone acting as the charge transfer mediator induces the process *2*; (*b*) RC L191C attached by the P-region through pyrene to highly oriented pyrolytic graphite; the electron-acceptor site (P) is located at a 7 Å distance from the electrode surface; (*c*) RC with TM mutation is attached to gold through the cysteine residue. H is bacteriopheophytin, B is bacteriochlorophyll.

about 1 s^{-1}. In order to further increase the photoinduced directed electron transfer between the layer immobilized on the electrode and the redox site of RC, the distance between them was to be decreased. This was achieved in a later publication [106] of the same research group by adsorption of special aromatic fused compounds (pyrene derivatives) at the electrode followed by the addition of RC to the amino acid residues located on the surface of the molecule: (i) to cysteine located in the vicinity of ubiquinone molecules (Q_A and Q_B) on the cytoplasmic surface of the RC or (ii) to lysine residues located around the special pair on the periplasmic surface of the RC. The fact that the photocurrent was higher upon RC immobilization at cycteine than upon immobilization at lysine was attributed to higher degree of RC orientation in the former case compared with the latter case.[106]

In some later studies [107–109] along this line, the authors compared three possible ways of orientation of the RC from purple bacteria (*Rb. sphaeroides*) on the electrode surface (highly oriented pyrolitic graphite), the resulting structures being called electrodes A, B and C (Fig. 20 *a*,*b*,*c*, respectively). For the preparation of electrode A, the wild-type RC from *Rb. sphaeroides* was grafted through cysteine present on the surface of the RC H-subunit to the pyrene derivative adsorbed on the electrode, *i.e.*, the H-subunit was directed towards the electrode (see Fig. 20 *a*). For the preparation of electrode B, the mutant RC with leucine-191 in the M-subunit being replaced by cysteine, (M)L191C, was attached *via* this cysteine located on the protein surface near the special pair to the pyrene derivative adsorbed directly on the electrode, *i.e.*, the RC were oriented by the P-region of M- and L-subunits towards the electrode (see Fig. 20 *b*). Electrode C was prepared using RC with three mutations (TM) involving one site of the M-subunit, (M)E100C, and two sites of the L-subunit, (L)E72C and (L)N274C. This RC was attached through the three indicated cysteine residues located on the surface of M- and L-subunits near the RC special pair directly to the gold electrode, *i.e.*, the RC was directed by the special pair to the electrode surface (see Fig. 20 *c*).[107] It is generally accepted now that the generation of photocurrent in the RC films occurs in the following way: (a) an absorbed photon excites the RC special pair (*i.e.*, transforms it from state P to P*); (b) an electron is transferred from P* through a chain of cofactors in the L-subunit to ubiquinones (electron acceptors) and finally completely reduces ubiquinone-10 (Q_B); (c) the process ends when the electrons migrate to the upper electrode after the reduced Q_B has moved from the RC to the medium being replaced by the oxidized quinone from the membrane pool of quinone mediators. For continuous operation of the system, electrons from the lower electrode (so-called cathodic current of the working electrode) should directly reduce P*, thus completing the chain. For electrode A, the reversible change of the basic photocurrent was positive and very small: $\sim$0.5 nA cm^{-2}, whereas the addition of quinone-10 (designated by Q in Fig. 20 *a*) induced a substantial increase in the photocurrent to the positive region by 20 nA cm^{-2} (Fig. 21 *a*). This confirms the known fact that the electron transfer from RC-bond quinone (Q_B) to the electrode is the rate-limiting step, as an increase in the distance between the electron-donor site of the RC and the electrode reduces the probability of electron tunnelling. Indeed, in the case of electrode A, the distance between Q_B and the electrode is 2.8 nm. It is the sum of the lengths of the RC H-subunit (2.4 nm) and the pyrene linker (0.4 nm) (see Fig. 20 *a*).

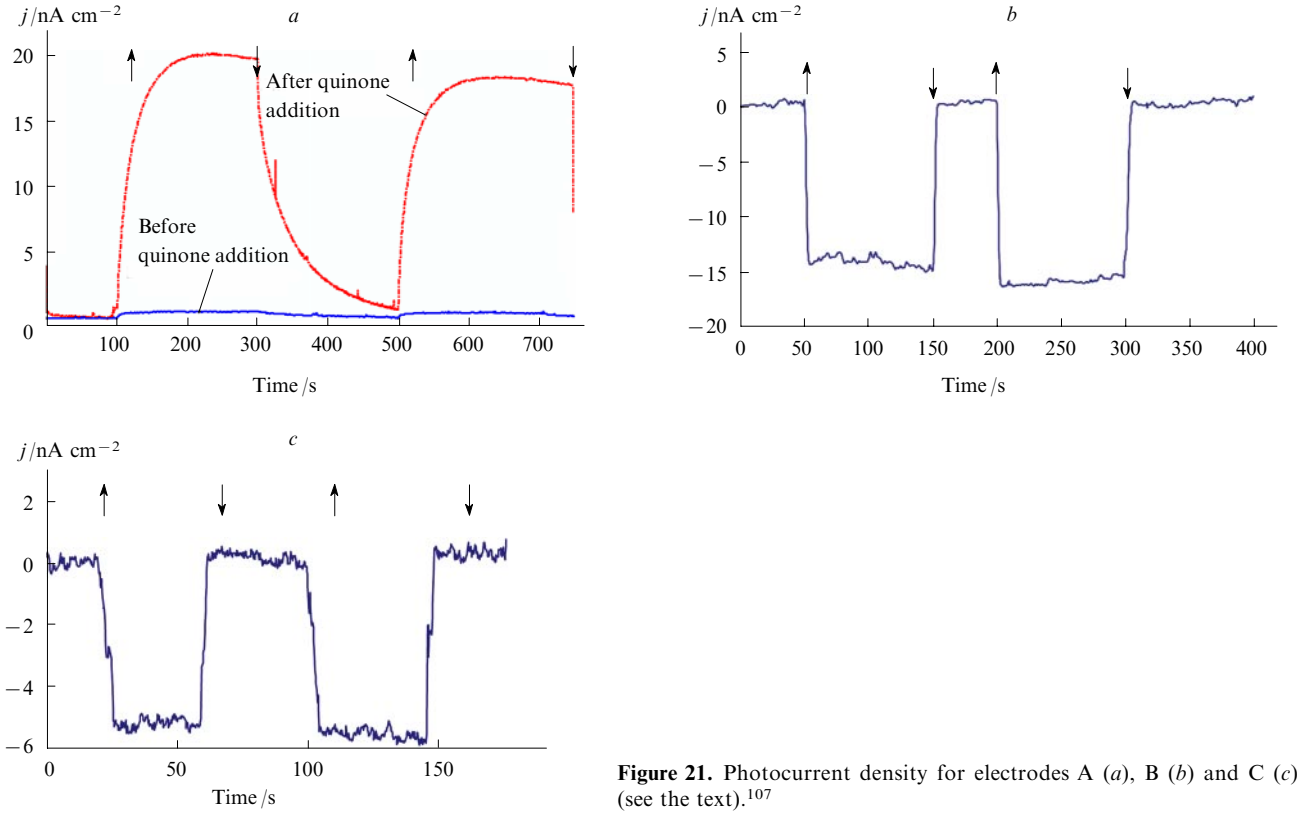


Figure 21. Photocurrent density for electrodes A (*a*), B (*b*) and C (*c*) (see the text).[107]

Upon photoirradiation of electrode B, the reversible change in the current was negative (about -15 nA cm^{-2}) (see Fig. 21 *b*), which was caused by the opposite orientation of the RC on this electrode with respect to electrode A (suffice is to compare Figs 20 *a*,*b*). In the case of electrode B, the distance between the RC special pair and the electrode was about 0.7 nm. This was the sum of the protein cofactor length (0.3 nm) and the pyrene linker length (0.4 nm) (see Fig. 20 *b*).

Upon photoirradiation of electrode C, the reversible change in the current was negative and about -5 nA cm^{-2} (see Fig. 21 *c*), which is much lower than that for electrode B, although Takashi and co-workers [107–109] expected higher values due to the very close positions (at a distance of only 0.3 nm) of the RC special pair and electrode C. The discouraging result may be attributed to lower coverage of the gold electrode surface by RC molecules, since proteins are non-specifically bound to the surface of this electrode. To verify this assumption, the cited researchers [107–109] obtained the RC mutant depleted in cysteine and detected, by surface plasmon resonance, nearly equal binding of this mutant and TM (mutations at three RC sites) to the gold electrode surface. From comparison of the photocurrents for electrodes B and C, it was concluded that only $\sim$33% of the mutant RC are arranged on the gold electrode surface as shown in Fig. 20 *c*. Thus, pyrene spacers proposed back in publications of Katz and co-workers [103–106] still represent a convenient way for orientation of any RC, in particular, without additional mutations.

A remarkable result obtained according to this approach by a large group of researchers headed by Trammel and Lebedev [110] was the photocurrent of 0.12 mA cm^{-2} upon excitation of mutant RC layers (adsorbed by the special pair to the surface of the modified Au electrode) with light at $\lambda = 808$ nm with intensity of 10 W cm^{-2} (Figs 22 and 23). By a series of intricate procedures of building-up different layers on the ITO electrode, the researchers [110] produced highly oriented films of mutant RC (SMpHis *Rb. sphaeroides* strain) containing a polyhistidine tag (a fragment of 6 histidine residues at the C-terminus of the M-subunit polypeptide chain). This tag interacted with self-assembled layers of the Ni^{2+} complex with the

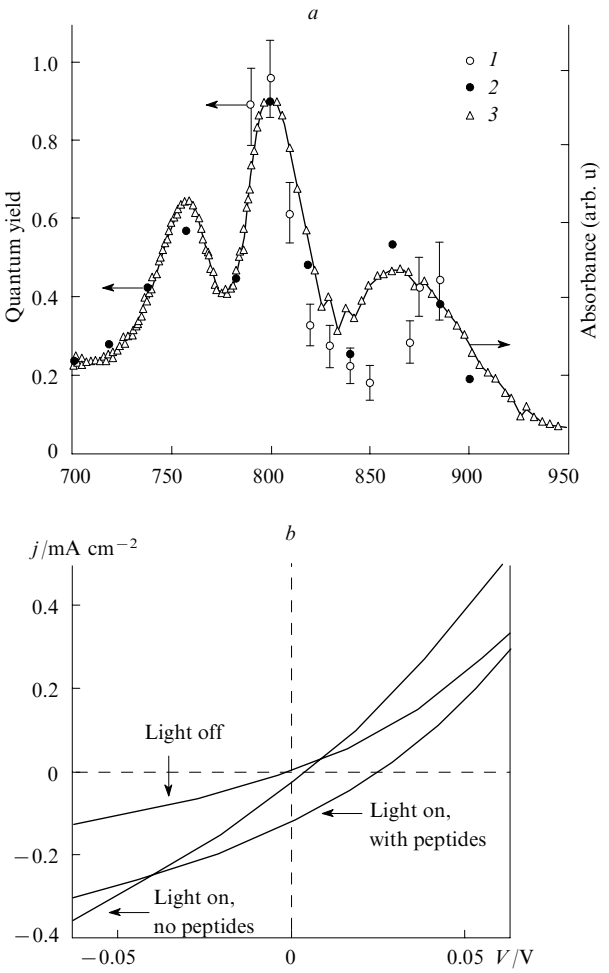


Figure 23. Photovoltaic characteristics of photoelectric devices based on bacterial reaction centres.[110]
(*a*) comparison of the photocurrent spectra of the solid (*1*) and liquid (*2*) electrochemical photocells and the absorption spectrum of solutions of bacterial RC (*3*) shows that the observed photocurrent arises in the RC; (*b*) effect of stabilization of RC complexes by peptides (A_6K or V_6D) on the voltammetric characteristics of the device (light: λ = 808 nm, intensity 10 W cm^{-2}).

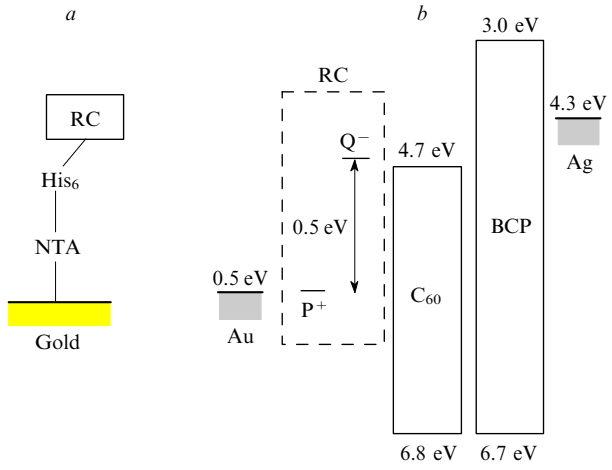
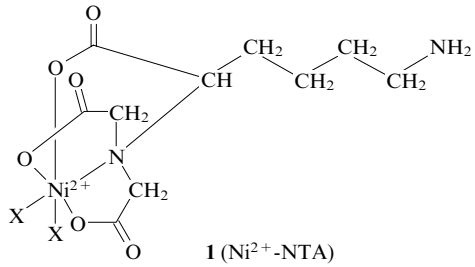


Figure 22. Schematic view of the bacterial reaction centres immobilized by the His_6 tag at the C-terminus of the M-subunit (*a*) and energy level diagram of the RC-based photoelectric cell (*b*).[110]

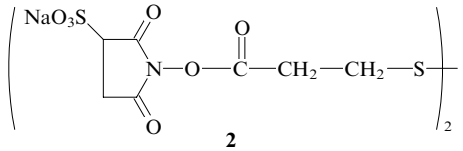
nitrilotriacetic acid (NTA) anion derivative (structure **1**), which was chemically immobilized on the 4 nm-thick gold layer on the ITO electrode *via* a bifunctional spacer, 3,3′-dithiobis(sulfosuccinimidylpropionate) (DTSSP, **2**) (the resulting electrode was designated by SMpHis-Au). This electrode was coated by a layer (60 nm) of electron-conducting fullerene C_{60} chosen for this purpose due to its relatively deep-lying lowest unoccupied molecular orbital with an energy of 4.7 eV (see Fig. 22 *b*), which considerably increased the probability of electron transfer from Q_B. The C_{60} layer was coated by a layer (12 nm) of 2,9-dimethyl-4,7-diphenyl-1,10-phenanthroline (BCP) having a relatively low-lying highest occupied molecular orbital, which efficiently prevented the inclusion of holes into the device and considerably improved the bias current parameters in the case considered by the authors.[110] Only after that, the 80 nm thick upper Ag electrode was sputtered on, and this completed the fabrication of a complex photovoltaic device; the diagram of the energy levels of this device is shown in Fig. 22 *b*. The self-assembly of photosystem I oriented in a

similar way is achieved when the native PsaD subunit is exchanged with the immobilized PsaD-His, which has been previously genetically modified with the His_6 tag. In some cases, layers of two polypeptide surfactants, cationic A_6K and anionic V_6D, were used; in the authors' opinion,[110] these layers improve some photovoltaic characteristics and stabilize the voltammetric parameters of the device.

Structures 1 and 2



1 (Ni^{2+}-NTA)



2

The same authors[110] calculated theoretically that the most closely packed layer of mutant RC with perfect orientation on the ITO electrode (3×10^{-12} mol cm^{-2}) would provide a photocurrent of up to 1 mA cm^{-2}. Thus, the quantum efficiency of this type of cell may amount to 12%,[110] which approaches the *in vivo* efficacy of natural bacterial and plant photosynthetic complexes. The fairly high photocurrents (0.12 mA cm^{-2}) and integral quantum efficiencies of this cell indicated by the authors are hardly believable not only due to general biophysical considerations but also due to the fact that during the eight years that have elapsed since the publication,[110] none of researchers from other groups confirmed these high values (neither for an identical device nor for some other devices of this type). Moreover, in some other publications[111–113] with the participation of the same authors, considerably (several orders of magnitude) lower photocurrents were reported for devices of this type. For example, in a publication[111] (of the same 2004 year as Ref. 110), the authors obtained the maximum photocurrent of about 30 nA cm^{-2} (upon photoactivation at $\lambda \geqslant 700$ nm with 0.06 W cm^{-2} intensity) for a structure with mutant RC containing a polyhistidine fragment at the C-terminus of the polypeptide chain of the M-subunit, *i.e.*, the P-regions of the M- and L-subunits of the RC were directed toward the self-assembled layer of the Ni^{2+}–NTA complex, which was chemically immobilized

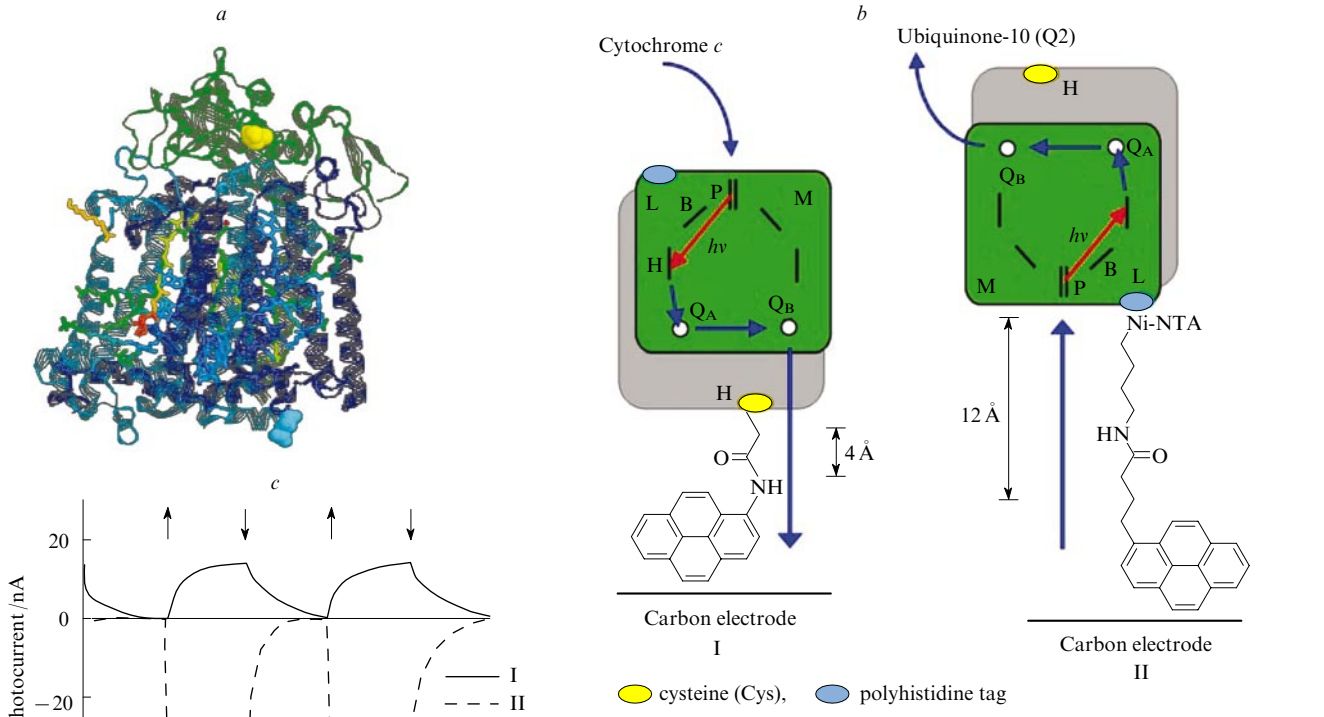


Figure 24. Molecular structure of the photosynthetic reaction centre from *Rb. sphaeroides*, which shows the position of the cysteine residue on the H-subunit surface (spheres at the top) and the tag of 7 histidine residues at the C-terminus of the M-subunit (spheres at the bottom) (*a*); two possible modes of RC binding and electron transport paths between the RC and the electrode (*b*) and photoinduced electric current in modified carbon electrodes of types I and II (*c*).[112]

P is the main electron donor (special pair), B is monomeric bacteriochlorophyll, H is bacteriopheophytin, Q_A and Q_B are the primary and secondary electron acceptors (quinones). The concentration of Q2 and the reduced cytochrome *c* is 40 μmol litre^{-1}; excitation wavelength > 700 nm.

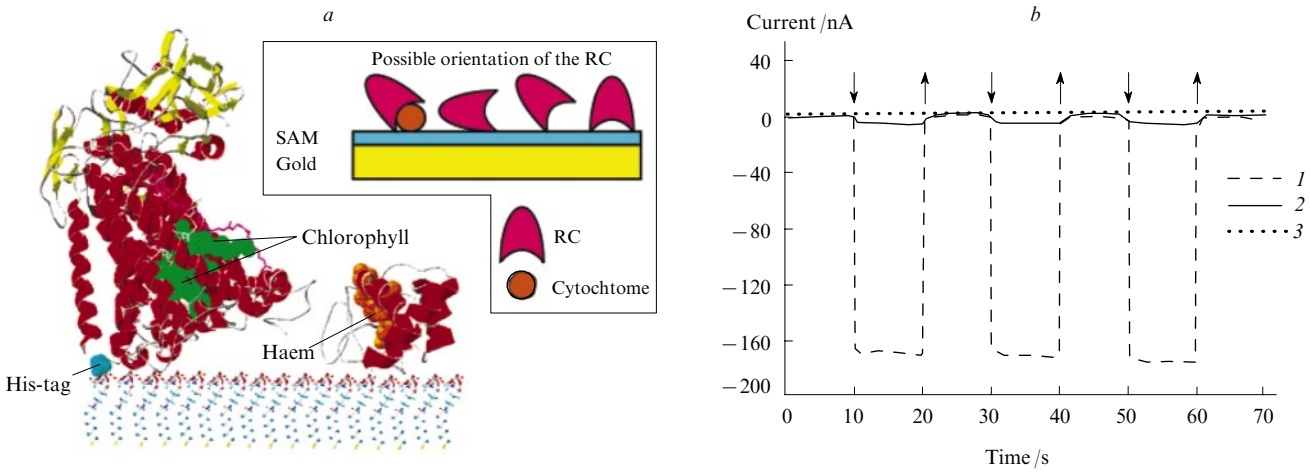


Figure 25. Scheme of the reaction centre and cytochrome *c* on a self-assembled monolayer of nitrilotriacetic acid (SAM) (the inset shows the possible orientation of RC with respect to the SAM surface) (*a*) and stationary photocurrent at the RC-NTA electrode under various conditions (*b*);[113]
(*a*) red are α-helixes, yellow are β-strands, green are chlorophylls and blue is his-tag;
(*b*) (*1*) in the presence of cytochrome *c* (1 μmol litre^{-1}), (*2*) in the absence of cytochrome *c*, (*3*) NTA electrode in the presence of cytochrome *c* without RC.

on the Au electrode. These results are of the same order of magnitude as the results of Katz and co-workers[103–106] for structures of this type. It is noteworthy that the addition of imidazole, which specifically cleaves the bond between the polyhistidine fragment and the Ni^{2+}–NTA complex, leads to a decrease in the photocurrent to 6 nA cm^{-2} (*i.e.*, by 80% with respect to the maximum value) over a period of 40 s, which additionally confirms the structural and functional integration of the system.[111] Moreover, in a study published two years later,[112] the same authors manufactured two types of structures with oppositely arranged RC from the purple bacteria *Rb. sphaeroides* (Fig. 24 *a*) in which the maximum photocurrents were +15 nA and −45 nA (see Fig. 24 *b*, structures I and II, respectively). The authors compared in detail two methods for RC alignment, namely, in structure I, the wild-type RC from the purple bacteria *Rb. sphaeroides* are linked through cysteine located on the surface of the RC H-subunit to the pyrene derivative adsorbed on the carbon electrode, *i.e.*, the RC H-subunit was directed towards the electrode (see Fig. 24 *b*); in structure II, the mutant RC contains the polyhistidine fragment at the C-terminus of the polypeptide chain of the M-subunit and is bonded *via* this fragment and the Ni–NTA complex to the pyrene derivative, *i.e.*, the P-region of the M- and L-subunits of the RC was directed to the electrode (see Fig. 24 *b*).[112]

Considering the whole set of data, Trammel *et al.*[112] concluded that structure II is more promising as it produces higher photocurrent and reaches the photochemical steady state an order of magnitude faster than structure I. The results are reliable and confirm both the possibility of opposite orientations of the RC in films on carbon electrodes and their native state. It is notable that in subsequent publications[113–115] of the same authors, various aspects of redox reactions of the components of these systems were studied in detail and cytochrome *c* was used additionally to improve the parameters of the structure containing mutant RC with a polyhistidine tag (Fig. 25 *a*). Indeed, the photocurrent in a new structure [113] analogous to structure II (Fig. 24) but without cytochrome was lower than −10 nA, whereas in a similar structure but containing only 1 μmol litre^{-1} of cytochrome in the electrolyte, the photocurrent increased almost 20-fold, *i.e.*, to −180 or −190 nA (see Fig. 25 *b*).[113] The cited researchers suggested three possible arrangements of the RC on the surface of the self-assembled layer of the nitrilotriacetic acid (SAM), which is directly grafted to the electrode and proved that the RC is arranged by the P-region at an angle to the electrode plane and forms a small cavity into which cytochrome is incorporated (see Fig. 25 *a*). This is also supported by a later publication of the same authors.[114] The advantages of using cytochrome include, according to the authors, the separation of the electron tunnelling process into two shorter segments (from the SAM layer to the haem and from the haem to the special pair) and the possibility to decrease the total tunnelling path (the formally calculated distance) due to electron delocalization in the porphyrin ring of the molecule.

Thus, according to Lebedev and co-workers,[113, 114] the use of cytochrome as a conducting fibre to the RC special pair is a great advantage, which indeed provides higher photocurrents. However, the indicated values of about 180–190 nA (see Fig. 25 *b*)[113, 114] cannot compete with the amazing value of 0.12 mA cm^{-2} (*i.e.*, 120 000 nA cm^{-2}!) achieved [110] for an earlier and simpler structure with similar component composition (see Fig. 23). The above-mentioned works occupy an important place in the series of studies [103–117] dealing with evaluation of the possibility to align the mutant RC with a polyhistidine tag and determination of alignment parameters. Some of these studies [106, 117] report important details about the manufacture and parameters of these systems; however, they are irrelevant here as the objective of these works was to produce sensors (microchips) for detecting signals from organic analytes (such as pesticides) by surface plasmon resonance technique rather than photovoltaic cells as such.

As regards the design of photovoltaic cells, noteworthy is the approach proposed by a group of Chinese researchers,[118–120] who formed multilayer films (Fig. 26) from

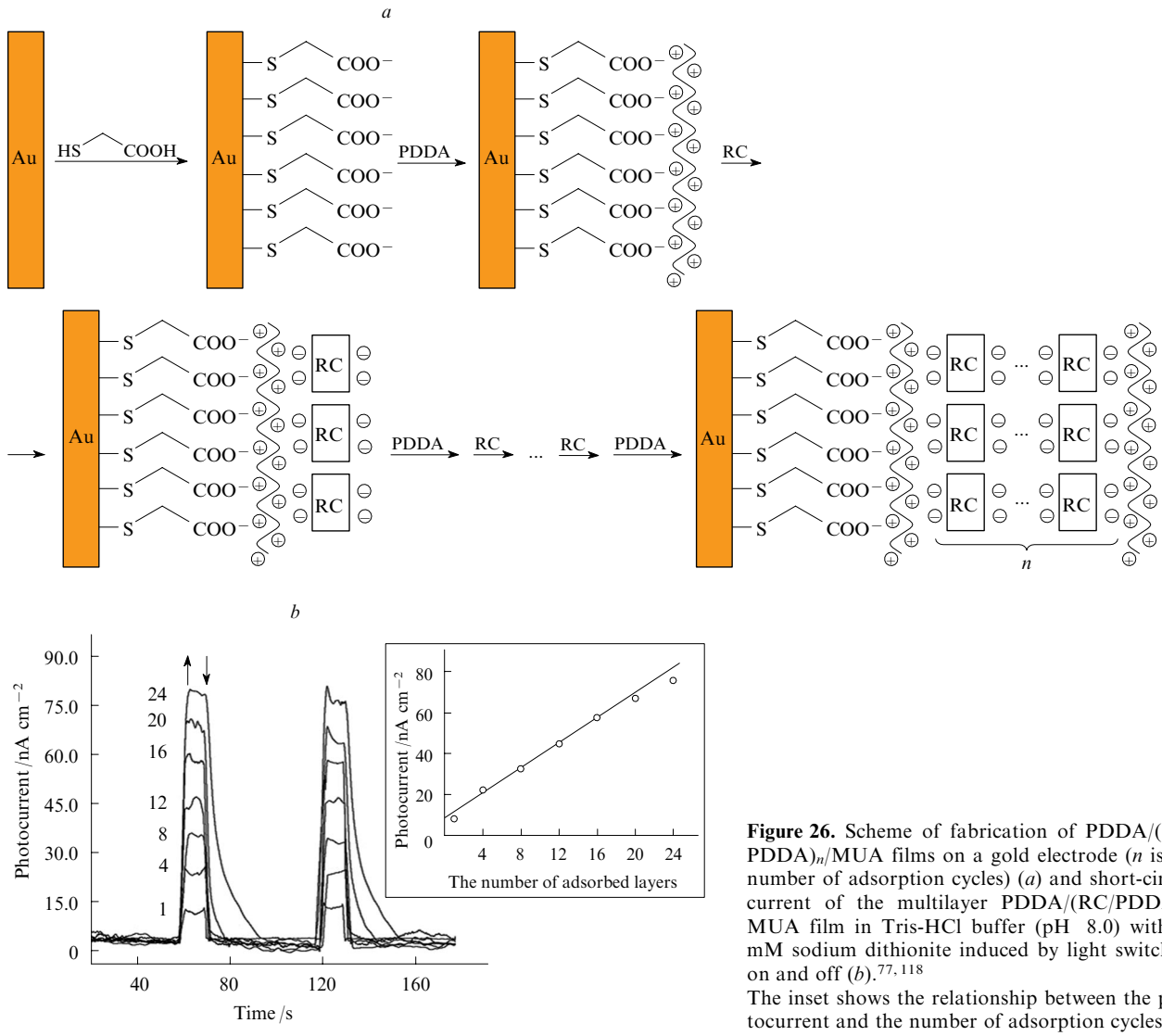


Figure 26. Scheme of fabrication of PDDA/(RC/PDDA)$_n$/MUA films on a gold electrode (n is the number of adsorption cycles) (*a*) and short-circuit current of the multilayer PDDA/(RC/PDDA)$_n$/MUA film in Tris-HCl buffer (pH 8.0) with 10 mM sodium dithionite induced by light switching on and off (*b*).[77,118]
The inset shows the relationship between the photocurrent and the number of adsorption cycles.

alternating layers of RC and polymers such as poly(dimethyldiallylammonium) chloride on the gold electrode surface modified by a mercaptoacetic acid (MAA) monolayer. Zhao *et al.*[118–120] used the excessive negative charge present on the RC surface for oriented adsorption of the RC on the positively charged PDDA and thus obtained structures comprising up to 24 RC/PDDA layers (see Fig. 26 *a*) and exhibiting almost linear dependence of absorption at 802 nm on the number of layers, which is indicative of good quality of the resulting layers. The photoelectric properties of these systems regularly change as the number of layers increases. For example, the photocurrent increases from 8.5 to 77.0 nA cm^{-2} as the number of adsorbed layers grows from 1 to 24 (see Fig. 26 *b*); these changes appear in the beginning of photoactivation (↑) and reversibly diminish as photoactivation ends (↓). The highest photocurrents were attained by using the electrode potential of about −0.3 V at pH of 7 to 9.[118–120] These results directly indicate that it is possible to manufacture photovoltaic cells based on oriented films of RC proteins for particular technological applications.

One more option for the manufacture of engineering materials based on RC proteins is the immobilization in polymer gels and films. For example, parameters of the system were markedly improved upon RC immobilization in a three-dimensional structure of the mixed titanium vanadium oxide (WO_3-TiO_2), which was deposited on the ITO electrode (Fig. 27 *a*).[121,122] These mesoporous WO_3-TiO_2 films exhibit unique properties because they have narrow pore size distribution; moreover, the oxide film pore size matches the RC size, and, hence, the RC are incorporated in the pores with retention of the protein activity. Also, close energy levels of WO_3-TiO_2 and RC induce pronounced enhancement of the photoelectric properties of these nanostructures (see Fig. 27 *b*), especially in the far- and near-infrared regions as compared with these properties for TiO_2–RC films with simpler composition. For example, the photocurrent in the (WO_3-TiO_2)/RC system is about 30 μA cm^{-2} and that for TiO_2–RC is only 6.4 μA cm^{-2}.[121,122] This approach to the design of biophotovoltaic nano-sized structures is an alternative to RC systems with quantum dots, which are discussed below.

4. Hybrid nanobiomaterials based on reaction centre proteins and quantum dots

Development of artificial photosynthetic systems based on inorganic semiconductor nanocrystals or quantum dots for more efficient utilization of solar energy is a new trend in

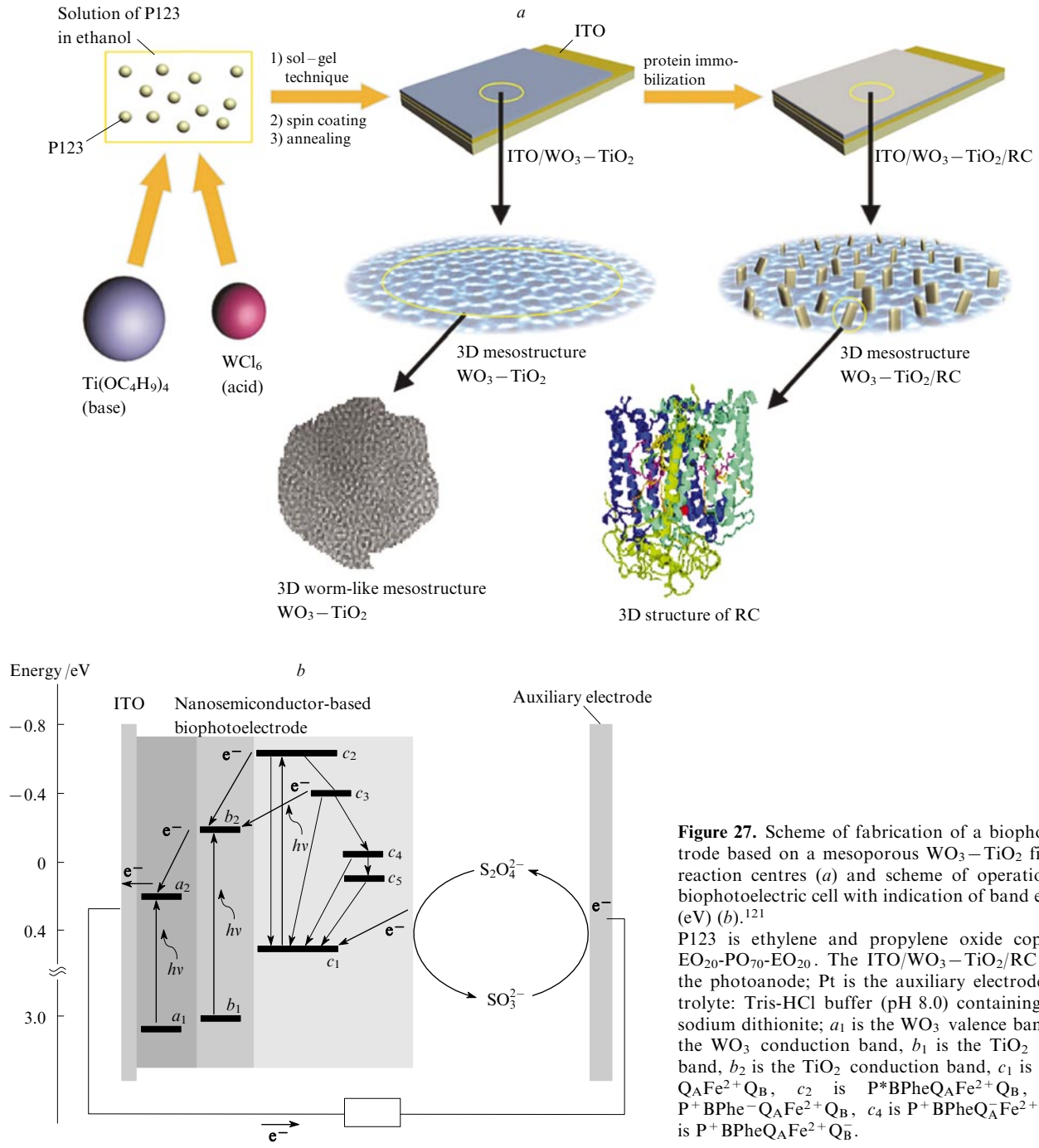


Figure 27. Scheme of fabrication of a biophotoelectrode based on a mesoporous WO_3-TiO_2 film and reaction centres (*a*) and scheme of operation of a biophotoelectric cell with indication of band energies (eV) (*b*).[121]
P123 is ethylene and propylene oxide copolymer EO_{20}-PO_{70}-EO_{20}. The $ITO/WO_3-TiO_2/RC$ film is the photoanode; Pt is the auxiliary electrode. Electrolyte: Tris-HCl buffer (pH 8.0) containing 8 mM sodium dithionite; a_1 is the WO_3 valence band, a_2 is the WO_3 conduction band, b_1 is the TiO_2 valence band, b_2 is the TiO_2 conduction band, c_1 is $PBPheQ_AFe^{2+}Q_B$, c_2 is $P^*BPheQ_AFe^{2+}Q_B$, c_3 is $P^+BPhe^-Q_AFe^{2+}Q_B$, c_4 is $P^+BPheQ_A^-Fe^{2+}Q_B$, c_5 is $P^+BPheQ_AFe^{2+}Q_B^-$.

the nanobiomaterial science.[2–12] These systems based on RC bear an analogy with natural photosynthetic organisms in which light is initially absorbed by antennas (specialized pigment – protein complexes) and, after that, the excitation energy is transferred to the special pairs (P) of the reaction centres in which the light energy is converted to the electrochemical potential energy needed for the vital activity of bacteria. Most studies used simple and well-studied natural structures responsible for the photosynthesis, namely, the RC of purple bacteria, first of all, *Rb. sphaeroides*.

Nabiev *et al.*[2] designed hybrid nanomaterials in which QD collected light energy and transfer it to the RC, thus increasing the efficiency of artificial photosynthesis. For the engineering application of QD in artificial photoconverting devices, they chose QD-530 and QD-570 (*i.e.*, QD having emission maxima at 530 and 570 nm, respectively) able to form stable complexes with RC. It is important to emphasize that most of the known QD absorb light over a broad range of solar spectrum and especially in the UV region where the intrinsic absorption of natural RC is low. Thus, there appears the possibility to considerably extend the spectral limits of the artificial photosynthesis. It follows from the absorption spectrum of the RC that carotenoids (absorption bands at 430–520 nm), bacteriopheophytin (540 nm) and BChl dimer (Q_x transition band at 600 nm) can accept the excitation energy from the QD emitting in the range of 500–600 nm. However, for effective interaction within the manufactured hybrid material QD–RC, the

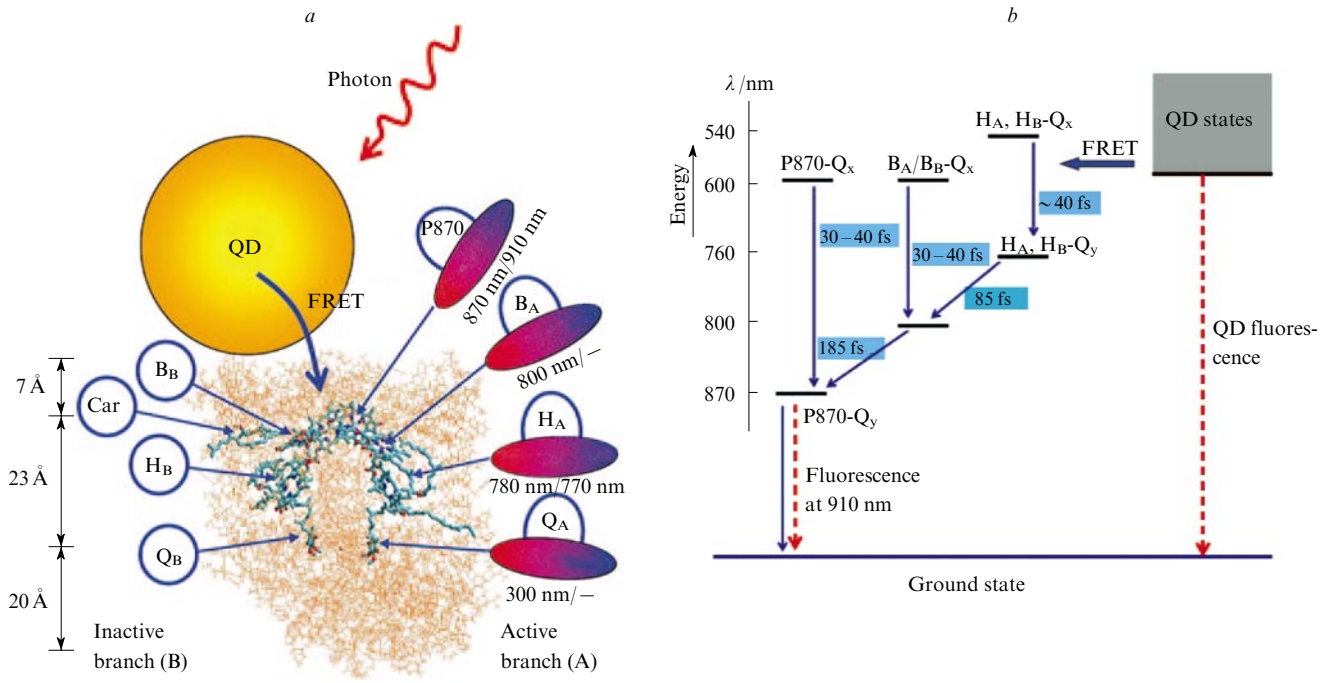


Figure 28. Organization and functional properties of the complex consisting of the reaction centre from *Rb. sphaeroides* and a quantum dot (*a*); and energy level diagram of the RC in the complex with QD on FRET excitation transfer from QD to RC (*b*).[2]
The subscripts designate the active (A) and inactive (B) parts of the cofactor electron transport chains. For the active chain of cofactors, absorption peaks are indicated for the special pair of bacteriochlorophyll (P), bacteriochlorophyll monomer (B), bacteriopheophytin (H) and quinone (Q). Photons are absorbed by QD and RC, the exciton from QD being transferred to RC by FRET. The excitation is rapidly relaxed to the P870-Q_y level.

cited researchers [2] chose QD-530 and QD-570, which complied with the major requirements for nanobiohybrid structures: stability, high fluorescence quantum yield in the visible spectral region and good adhesion to the surface of the RC macromolecule from *Rb. sphaeroides*. Figure 28 shows the arrangement of the QD complex with the purple bacterium RC and the energy level diagram of this complex for the FRET mechanism. The continuous blue arrows designate the non-radiative energy transfer (FRET) between the levels, while dashed red arrows stand for relaxation to the ground state with de-excitation of light quanta. The higher energy levels are schematically shown above; for comparison, the spectral scale corresponding to the absorption of light by each of these levels is given on the left. Apart from the non-radiative resonance energy transfer from the donor to acceptor molecule, fluorescence quenching in the donor–acceptor pair may occur due to the so-called 'inner filter' effect and to re-absorption of the radiation by acceptor molecules. These phenomena may induce fluorescence quenching not related to FRET, which was taken into account [2] by means of appropriate corrections. Thus, critical requirements for the formation of an energetically interacting pair from a QD molecule and a natural pigment–protein photosynthetic complex are both good overlap of the emission and absorption spectra of the donor and the acceptor and their 'tight' positions.[2]

For the QD–RC complex, effective QD fluorescence quenching was found to occur upon QD to RC energy transfer (see Fig. 28). The efficiency of FRET is quantitatively described by the parameter E

$$E = 1 - \frac{\mathrm{PL}_{\mathrm{QD-RC}}^{\mathrm{exciton}}}{\mathrm{PL}_{\mathrm{QD}}^{\mathrm{exciton}}} \qquad (1)$$

where $\mathrm{PL}_{\mathrm{QD-RC}}^{\mathrm{exciton}}$ and $\mathrm{PL}_{\mathrm{QD}}^{\mathrm{exciton}}$ are peak exciton emission intensities for the QD–RC and QD complexes, respectively.

The researchers used the CdTe QD as they are more FRET-efficient owing to the small radius and thin ligand shell. A change in the QD fluorescence intensity with time is shown in Fig. 29 for QD-530 (*a*, *c*) and QD-570 (*b*, *d*). In all cases, fluorescence quenching is observed upon increase in the RC to QD ratio and reaches a maximum when RC : QD = 1 : 1 (Fig. 29 *a*, 30 *a*).

An additional piece of evidence for QD to RC energy transfer is enhancement of the fluorescence of the RC special pair at 910 nm according to the equation

$$A_{910\,\mathrm{nm}}(\lambda_{\mathrm{exc}}) = \frac{\mathrm{PL}_{\mathrm{QD-RC}}^{910\,\mathrm{nm}}}{\mathrm{PL}_{\mathrm{RC}}^{910\,\mathrm{nm}}} = \frac{n_{\mathrm{QD-RC}}}{n_{\mathrm{RC}}} \qquad (2)$$

where λ_{exc} is the excitation wavelength; $\mathrm{PL}_{\mathrm{QD-RC}}$ and $\mathrm{PL}_{\mathrm{RC}}$ are fluorescence peak intensities at 910 nm for the QD–RC conjugate and for RC, respectively; $n_{\mathrm{QD-RC}}$ and n_{RC} are the numbers of electron–hole pairs formed on the special pair in the case of QD–RC and RC, respectively (see Fig. 30 *b*).

The QD-570–RC complex shows an almost threefold enhancement of the fluorescence (for 550 nm excitation wavelength) with respect to the QD-530–RC complex (see Fig. 30 *c*,*d*), which can be attributed to stronger adsorption of QD-570. For appropriate functioning of the system, effective supply of electrons to RC from sodium ascorbate is required. It can be assumed theoretically that

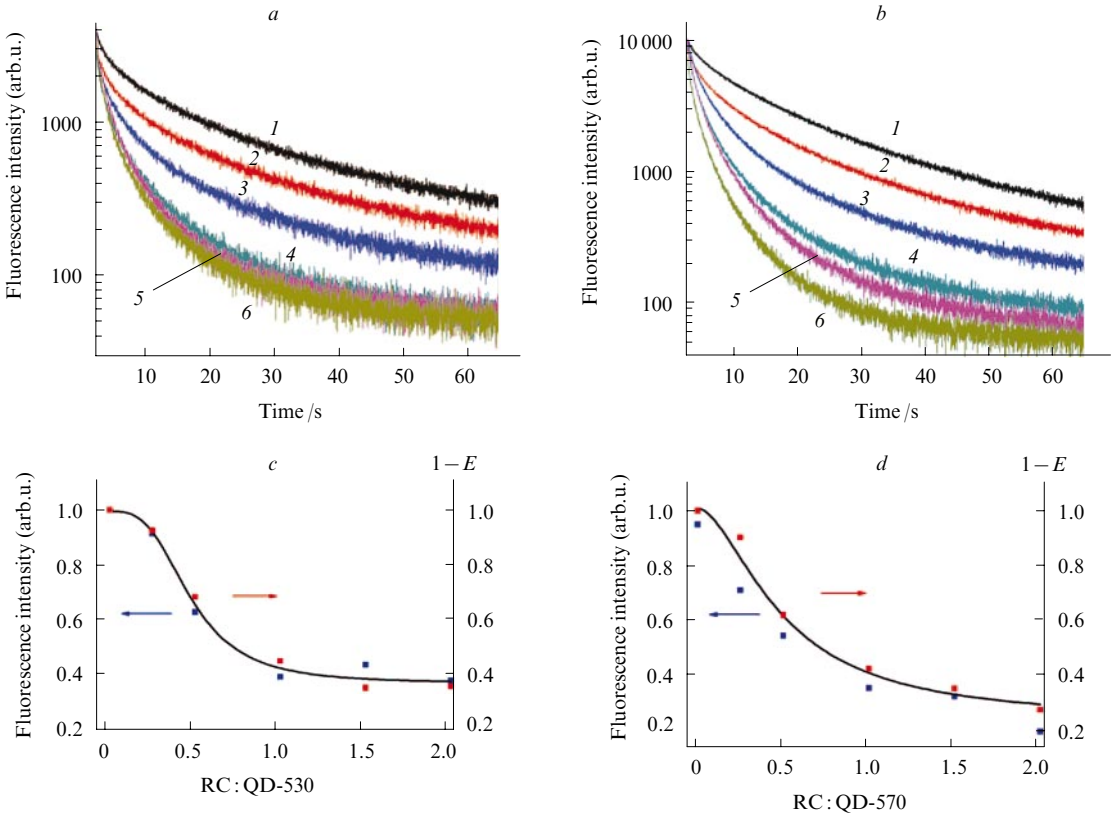


Figure 29. Time-resolved fluorescence of the complexes of CdTe quantum dots with reaction centres: fluorescence decay curves for complexes QD-530 – RC (*a*) and QD-570 – RC (*b*) measured in the spectral range of QD emission at different RC : QD molar ratios and comparison of the normalized integral intensity of the steady-state fluorescence and variation of the fluorescence lifetime at different RC : QD molar ratios (*c*, *d*).[2]
RC : QD = 0 (*1*), 0.25 (*2*), 0.5 (*3*), 1 (*4*), 1.5 (*5*), 2 (*6*); $E = 1-(\tau_{DA}/\tau_D)$ [τ_{DA} is the average fluorescence lifetime of the donor (QD) in the presence of the acceptor (RC); τ_D is the average fluorescence lifetime of the donor (QD)].

the addition of QD would hamper the transfer of these electrons to the special pair; however, kinetic data from the time-resolved fluorescence experiment indicate that the electron transfer to the special pair remains fast in the QD – RC complexes, because the observed reduction time derived from absorption spectra of the complexes remains the same as in individual RC.

Thus, Nabiev *et al.*[2] demonstrated for the first time the possibility of using QD as a light-harvesting antenna for the RC proteins owing to the ability of QD to absorb light much more efficiently than natural light-harvesting protein – pigment complexes and effectively transfer this energy to the RC.

There are almost no more available publications dealing with RC complexes with QD used for photovoltaic cells. Meanwhile, researchers of the Department of Biology of the Moscow State University [123] demonstrated that the electron transport processes in photoconverting RC complexes are essentially related to the structure – dynamic state of the RC. Studies of their dependences on the temperature or on the degree of hydration identified clear-cut correlations between the intramolecular mobility of various regions of photosynthetic apparatuses and changes in the electron transport characteristics of particular units of the photosynthetic electron transfer chain. An achievement of this research group is the inclusion of membrane proteins of photosynthetic RC from purple bacteria and QD into liposomes based on lecithin (phosphatidylcholine) and study of the functional capabilities of these hybrid complexes. Interesting works on immobilization of protein – pigment RC complexes on plasmon particles, porous TiO_2 films and some other are not considered in this review for the lack of space.

Recent joint studies of German and Russian scientists [124–126] were concerned with many other processes in RC and light-harvesting complexes of bacteria and plants. Indeed, it would be of interest to consider some other applications or related systems; however, here we will dwell only on the key publication [126] of the series of works on light-harvesting complexes with QD that can potentially be used in photovoltaic cells. The authors proposed original systems within the framework of general approach of using FRET to overcome the low efficiency of photovoltaic cells based on bacterial RC films related to great path length for electron tunnelling and low density of RC immobilization on the electrode surface. The cited work by Schmitt *et al.*[126] considers a series of functionalized QD based on CdSe/ZnS with fluorescence maxima at 523, 530 and 560 nm (having excess negative charge) and 600 and 640 nm (having excess positive charge) in the presence of one of the following light-harvesting complexes: LH1 from *R. rubrum*, LH2 from *Rb. sphaeroides*, trimeric phycoerythrin (PE) from *Gloeobacter violaceus*, trimeric phytocyanin (PC) from *Spirulina platensis* and trimeric allophytocyanin (APC) from

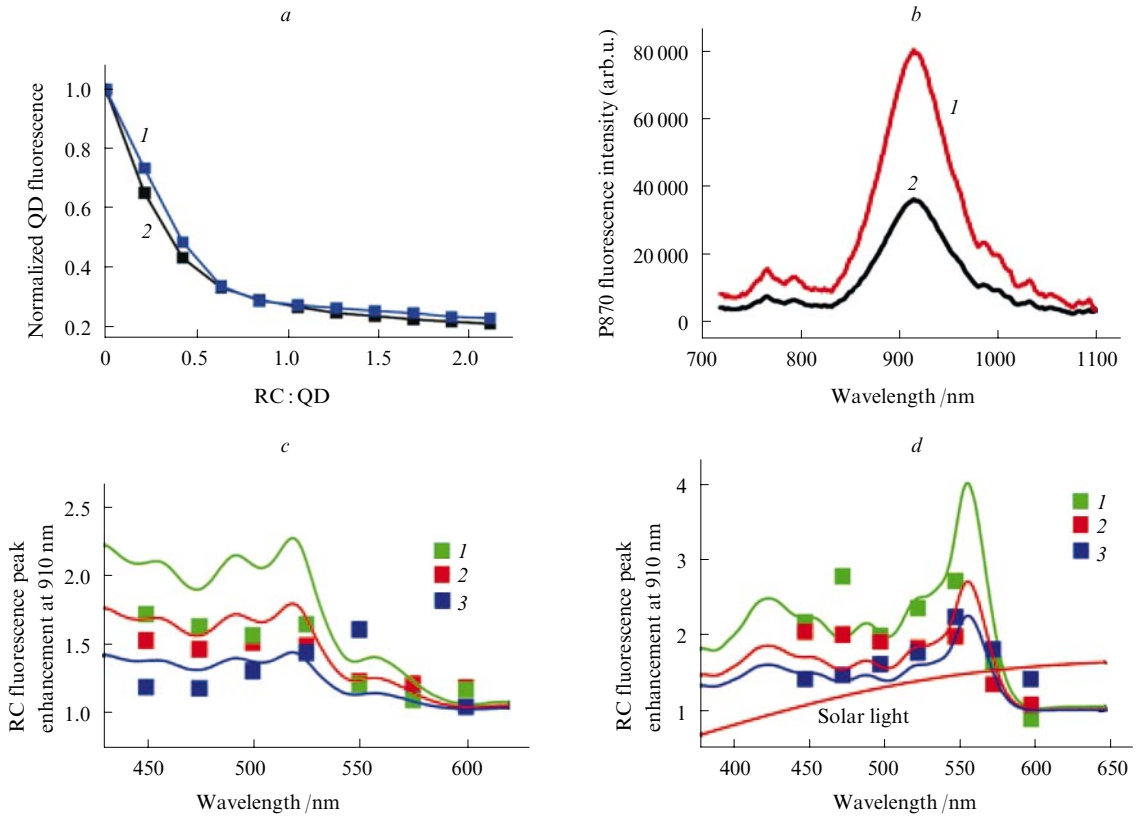


Figure 30. Förster resonance energy transfer and optical amplification in CdTe quantum dot complexes with reaction centres.[2] (*a*) Quenching of photoluminescence of QD-570 (*1*) and QD-530 (*2*) depending on the RC : QD molar ratio. The excitation wavelength is 450 nm; the QD-530 concentration is 0.5 μmol litre^{-1}; the QD-570 concentration is 0.25 μmol litre^{-1}; the volume of the RC solution is 4.8 and 2.4 μl, respectively. The dilution factor, inner filter and reabsorption effects were taken into account; (*b*) increase in the photoluminescence peak at 910 nm related to the photoluminescence of the bacteriochlorophyll special pair (P870) in RC (λ_{exc} = 550 nm, RC : QD-570 = 0.425 : 1); (*c*, *d*) RC photoluminescence enhancement data. Enhancement factors (squares) depending on the excitation wavelength are given for the P870 photoluminescence band at 910 nm for complexes based on CdTe QD-530 (*c*) and QD-570 (*d*); sodium ascorbate (10 mmol litre^{-1}) was added to prevent RC photooxidation. RC : QD = 0.425 : 1 (*1*), 0.85 : 1 (*2*), 1.7 : 1 (*3*). The continuous lines correspond to calculation results.

Arthrospira platensis. Figure 31 schematically shows the structures of some of the above-listed complexes and gives their spectral characteristics.[126] Unfortunately, no results of photoelectric measurements that would confirm their potential applicability for photovoltaic cells were reported for these systems; therefore, the prospects of particularly these systems are still to be proven unlike the data on QD complexes with the RC from purple bacteria, which have been already reported in the publications cited above.[2, 13, 14] Thus, the approaches and methods demonstrated in previous publications[2, 13, 14, 111–122] provide the basis for the design of hybrid nanobiomaterials based on RC proteins, which have a considerable potential for technology.

IV. Planar systems based on the proteins of photosystems I and II

1. Key features of the structure of plant photosystems I and II

This Section deals with photosystems I and II (PSI and PSII) composed of various pigment–protein complexes of intricate composition that are spatially separated in the thylakoid membranes of chloroplasts but are arranged in the common supramolecular biochemical systems with other membrane complexes and are responsible for the light-dependent steps of the plant photosynthesis.[127–132] In the most general case, it is possible to imagine the central parts (cores) of these photosystems as containing several peptides (8 integral and 5 peripheral peptides in the case of PSI) or proteins (two main integral protein subunits in the case of PSII) and chlorophyll dimers with an absorption maximum at 700 (P700) and 680 nm (P680), respectively.[127–129] To increase the efficiency of absorption of solar light and functioning of photosystems, their cores are surrounded by the light-harvesting complex I (LHCI), which contains approximately 95 chlorophyll *a* molecules and 22 β-carotene molecules, and light-harvesting complex II (LHCII), which contains approximately 150 chlorophyll *a* molecules, 100 chlorophyll *b* molecules, 50 carotenoid molecules and 2 pheophytin molecules.[127–129] The formation of two photosystems is stipulated by the need to solve simultaneously several problems of photosynthesis. A major problem for the organisms that perform oxygenic photosynthesis is the difference between the redox potentials of water (E_0 = +0.82 V) and $NADP^+$ (E_0 = −0.32 V). Chlorophyll should have a potential greater than +0.82 V in the ground state in order to oxidize water but the potential in the excited state should be lower than −0.32 V in order to ensure the reduction of $NADP^+$.

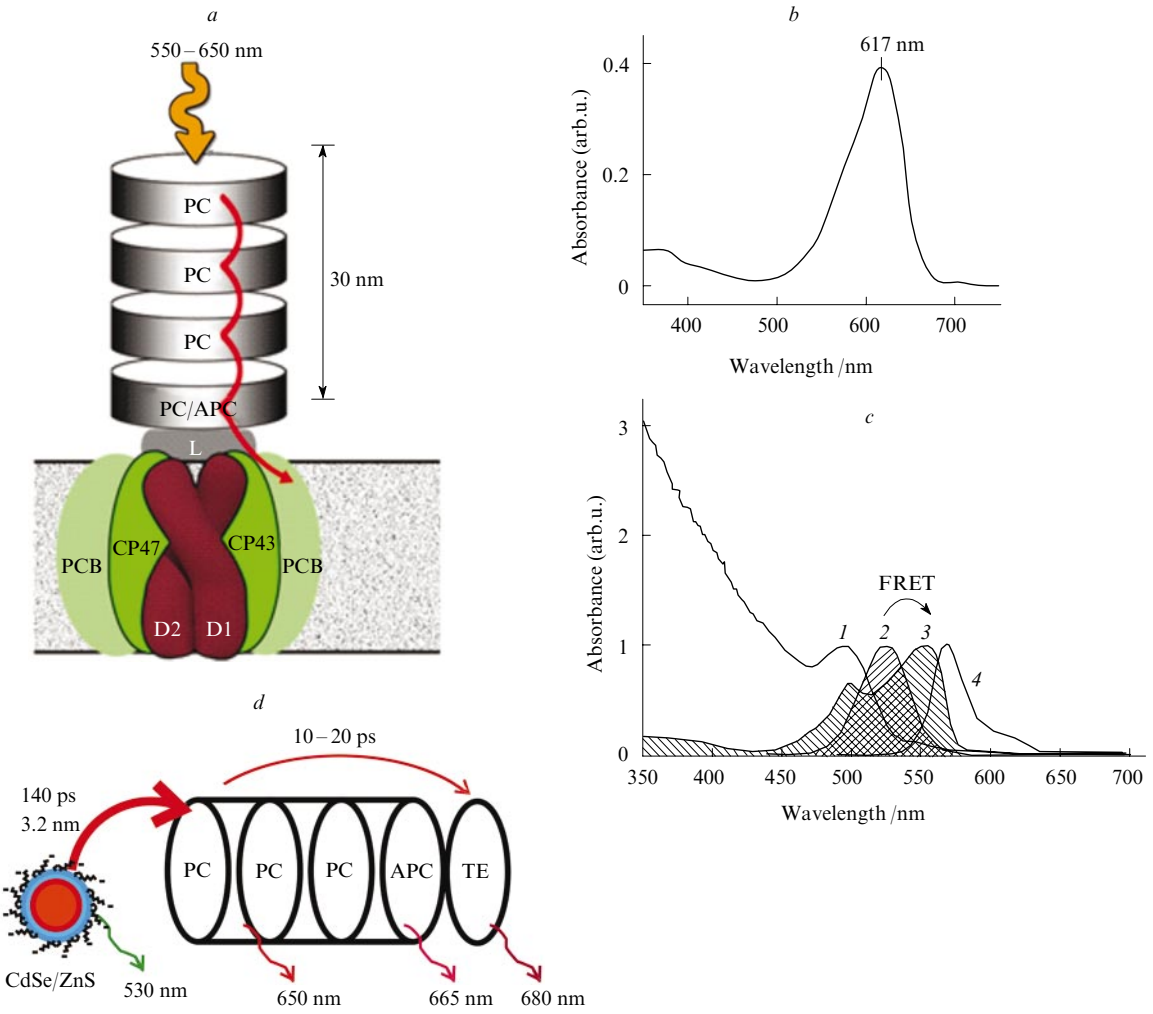


Figure 31. Structural features and spectral characteristics of quantum dots and some light-harvesting complexes.[126]
(*a*) Arrangement of the phycobilin antenna of the cyanobacterium *Acaryochloris marina* and its binding to the main complex of photosystem II; (*b*) absorption spectrum of phycobilin isolated from *A. marina* at room temperature; (*c*) absorption spectra of QD-530 (*1*) and phycoerythrin trimers (*3*); normalized fluorescence spectra of QD-530 (*2*) and phycoerythrin trimers (*4*) at room temperature; (*d*) schematic view of the CdSe/ZnS quantum dots electrostatically linked to the phycobilin rod from *A. marina*. PC is phycocyanine trimer, APC is allophycocyanin trimer, PCB is phycocyanobilin, L is the protein linker, CP47 and CP43 are chlorophyll–protein complexes, D1 and D2 are photosystem proteins, TE is the terminal emitter.

Therefore, only simultaneous functioning of two photosystems with chlorophylls of different types ensures that the process proceeds completely and effectively. In particular, PSI (plastocyanin–ferredoxin–oxidoreductase) performs the cyclic electron transport conjugated with the ATP synthesis to give reduced $NADPH + H^+$, which is needed for the subsequent carbon reduction in chloroplasts (for functioning of the Calvin cycle and conversion of CO_2 to carbohydrates). The pigment–protein complex PSII (H_2O–plastoquinone–oxidoreductase) accomplishes water oxidation to give oxygen (involving so-called 'manganese cluster'[127]) and plastoquinone reduction. Since the structures of these and other components ('cytochrome' b_6f-complex, 'manganese cluster' and so on) of thylakoid membranes and numerous reactions that are involved in photosynthesis have been described in sufficient detail,[127–132] in this review we may proceed straight to consideration of the artificial planar structures based on PSI and PSII.

2. Langmuir–Blodgett and Langmuir–Schaefer monolayers and films based on photosystems I and II and their components

As the key example of the few publications dealing with the Langmuir preparation and investigation of PSI monolayers, it is pertinent to discuss a publication by Qian *et al.*[133] The authors used two cationic polyelectrolytes — PDDA and PBV (polybutylviologen) — in addition to the traditional salts, which was favourable for the formation of a stable pigment–protein complex monolayer at the interface. However, in our opinion, the observed increase in the pressure of the PSI monolayer following an increase in the NaCl concentration does not confirm the specific interaction of PSI with sodium cations (as is stated in the cited publication[133]) because this occurs upon any increase in the ionic strength of the subphase.[17] This is also confirmed by the data of the same authors on PSI monolayers obtained on an aqueous solution of $CaCl_2$.[133] After the LS transfer from salt polyelectrolyte subphases, a 2–3 nm shift of the peak to

longer wavelengths is observed in the spectra of PSI monolayers, while in the case of only a polyelectrolyte subphase, the shift occurs to shorter wavelengths. This was attributed [133] to the influence of adsorbed ions and polyelectrolytes on PSI aggregation after the transfer to solid substrates. As a result of electrochemical measurements of these PSI monolayers transferred to ITO electrodes (a negative shift of the reduction potential of the PSI/PBV LB-film and a positive shift of the oxidation potential) and piezoelectric investigations of PSI monolayers transferred to the surface of a gold-coated quartz crystal, it was concluded that the large PSI complex serves as the electron barrier to electrochemical reactions of PBV. Unfortunately, the preparation conditions of PSI mono- and multilayers were not optimized for subsequent applications.[133]

These drawbacks were largely overcome in the studies [134–139] dealing with the preparation of monolayers of both single PSII components and lipids of thylakoid membranes and light-harvesting complexes of plant PSII. Of principal importance is the discovery of the fact that the parameters of PSII component monolayers depend only slightly on the nature and concentration of a buffer in the aqueous subphase in the concentration range of 1–100 mmol litre^{-1} and that stable PSII monolayers cannot be formed with doubly distilled water. The area per effective reaction centre of photosystem II (PSII RC) depends substantially on many conditions of protein preparation and deposition and is, on average, $\sim$50 nm^2 per pigment–protein complex. The slight increase in the Brewster scattering is fully correlated with pressure build-up upon compression of the PSII RC monolayer to the collapse pressure at 50–55 mN m^{-1} and areas of about 20 nm.^{2} Sodium dodecyl sulfate electrophoresis of samples taken from the surface and from various sites of the subphase in a Langmuir tank demonstrated that the whole PSII RC occurs at the interface as the native complex. Furthermore, the results of numerous experiments demonstrated that the parameters of PSII RC monolayers depend substantially on the pH and temperature of the aqueous subphase. It was found that the LS technique (horizontal lift) is more effective (the transfer coefficient is higher) than the LB technique (vertical lift) for transfer of PSII RC to various solid substrates. The highest transfer coefficient ($95 \pm 5\%$) was detected at a pressure of about 30 mN m^{-1}, which corresponds to the transition pressure between two states of the PSII RC monolayer, *i.e.*, to the onset of formation of the liquid-condensed protein layer. On further pressure increase, the transfer coefficient remained almost invariable, starting to considerably decrease only near the collapse region of the PSII RC monolayer.[134–136]

Mixed PSII RC monolayers with different lipids [phosphatidylcholine (PC), phosphatidylethanolamine (PE), phosphatidylserine (PSer), phosphatidylinositol (PI), phosphatidic acid (PA)] important for modelling of biomembranes were fabricated by both successive deposition of each component to the interface and by using a preliminarily prepared mixture. No considerable differences in the obtained results depending on the preparation method of the mixed monolayers were found. However, not only the quantitative parameters but also the shape of isotherms for the mixed PSII RC–lipid monolayers depend significantly on the nature and concentration of the lipid: up to pressures of 25 mN m^{-1} for PSII RC–PE and PSII RC–PI mixtures and up to pressures of 20 mN m^{-1} for PSII RC–PC and PSII RC–PSer mixtures (1 : 1 molar ratio).[137–139]

The basic results of the above-indicated publications are consistent with the results of US researchers,[140] who clearly demonstrated the presence of two regions in the PSII isotherms, which correspond to the liquid-expanded state (at pressures of up to 15–20 mN m^{-1} and areas of 200 to 50 nm^2) and the liquid-condensed state (at pressures of $>$25–30 mN m^{-1} and areas of 40 to 10 nm^2). Extrapolation of the second region (pressure $>$30 mN m^{-1}) of the surface pressure isotherms gave [140] an area per molecule of about 30–36 nm.^{2} The so large areas per molecule after deposition of PSII are attributable to the presence of a surfactant (β-dodecylmaltoside) in the protein monolayer, which is gradually removed from the monolayer to the aqueous subphase upon monolayer compression and, at high pressures, only the condensed PSII monolayer is left. The surface potential found from the corresponding isotherms for PSII monolayers increases by only 100 mV upon full monolayer compression, which attests to low degree of orientation of PSII at the interface. High quality of the PSII multilayer films transferred at 30 mN m^{-1} to a quartz plate with self-assembled octadecyltrichlorosilane and cadmium stearate layers was demonstrated by absorption spectroscopy and small-angle X-ray scattering and modelling of protein complexes. For example, the bilayer thickness measured by small-angle X-ray scattering was 7.3 nm and, after subtracting the known value for cadmium stearate (2.5 nm), 4.8 nm was left for PSII, which is in good agreement with the PSII thickness in native membranes. In other publications of the same authors,[141–143] the structural and functional integration and the native state of PSII in the monolayers were confirmed by fluorescence spectroscopy and GRS¶ and by measurements of redox potentials.

The photoinduced potential changes in mono- and bilayer lipid films with PSII were estimated [144] in comparison with these values for bacterial RC. On irradiation with a light flash, the increase in the potential was 0.55 mV for PSII and $\sim$7 mV for bacterial RC; in the former case, the potential gradually decreased to 0.40 mV within 10 ms, while in the latter case, it increased to 9 mV within 10 ms. It was shown previously that the charge separation voltage in PSII RC was $\sim$85% of the total electrogenicity, while for bacterial RC this value was only $\sim$70%. This may be attributed to both shorter distances and higher dielectric constants in PSII RC compared to bacterial RC.[144]

Kernen *et al.*[145] comprehensively studied the monolayers of light-harvesting complex II (LHCII), which is the protein–pigment surrounding of the RC in plant PSII (*i.e.*, a sort of antenna for more effective collection of radiation over a broad spectral region and its transfer to PSII). From $\pi - A$ isotherms, the effective size of LHCII was found to be $\sim$14.4 nm^2, which is somewhat larger than the size of the monomer represented as an ellipsoid with 3 and 5 nm axes (*i.e.*, the area of LHCII is $\sim$11.8 nm^2) and is in better agreement with its approximation as an ellipsoid with a $\sim$15.0 nm^2 area. These estimates are arbitrary, the more so, because the really functioning LHCII is a trimer (binding a large number of chlorophyll molecules) [127–132] and often forms even larger protein–pigment aggregates in thylakoid membranes.[81–83] These features were mani-

¶ GRS is the giant Raman scattering.

fested [145] in a study of the LB transfer of LHCII monolayers to glass substrates at a rate of 0.5 cm min^{-1} and at a constant pressure of 15 mN m^{-1}. It was shown that the degree of aggregation depends on the nature and the concentration of lipids in the mixture. Considering that LHCII is assembled to a spherical structure with an inner diameter of 15–25 nm and the outer diameter 30–50 nm, the authors suggest that these complexes contain 50 to 140 LHCII molecules.[145]

A proof for the native structure of PSII proteins and rhodopsins (bacterial and visual) in the monolayers was reported by Pepe *et al.*,[34] who performed detailed comparative study of three types of proteins by polarization modulation infrared diffuse reflectance spectroscopy.

The preparation of PSII RC and membrane fraction (containing both PSII and LHCII) layers on gold electrodes with pre-adsorbed mercaptopropionic acid (MPA) was reported.[146] Gold electrodes (working and reference ones) were deposited onto a ceramic substrate to be used as sensor elements. Electrodes with adsorbed PSII RC layers showed photocurrents of about 1 nA, whereas those with PSII and LHCII layers had photocurrents from 20 to 17 nA (the decrease occurred during 10 s of irradiation at 675 nm). These differences were exlained as being due to the structures of layers of these biosystems, which were manifested in the processing of AFM images. In the case of PSII RC, a continuous film was formed on the electrode consisting of a great number of aggregates of different size (Fig. 32):[146] large aggregates of 22 nm height and 300 nm diameter and small aggregates of 10 nm height and 100 nm diameter (the size of single PSII RC is 6.0 to 9.1 nm height and 20.6×13.1 nm cross-section). Apparently, the continuous and thick PSII RC film precluded charge transfer from the photosystem to the electrode by the quinone derivative. In the case of a less purified membrane fraction (PSII and LHCII), a 8.7–10 nm high monolayer with a cross-section of 25×30 nm having many nano-sized pores accessible for the mediator (quinone) is formed on the electrode surface (see Fig. 32).[146] These structures provide the possibility of detecting various types of herbicides based on the 1.5–2.0-fold decrease in the photocurrent, which makes them suitable as sensor elements.

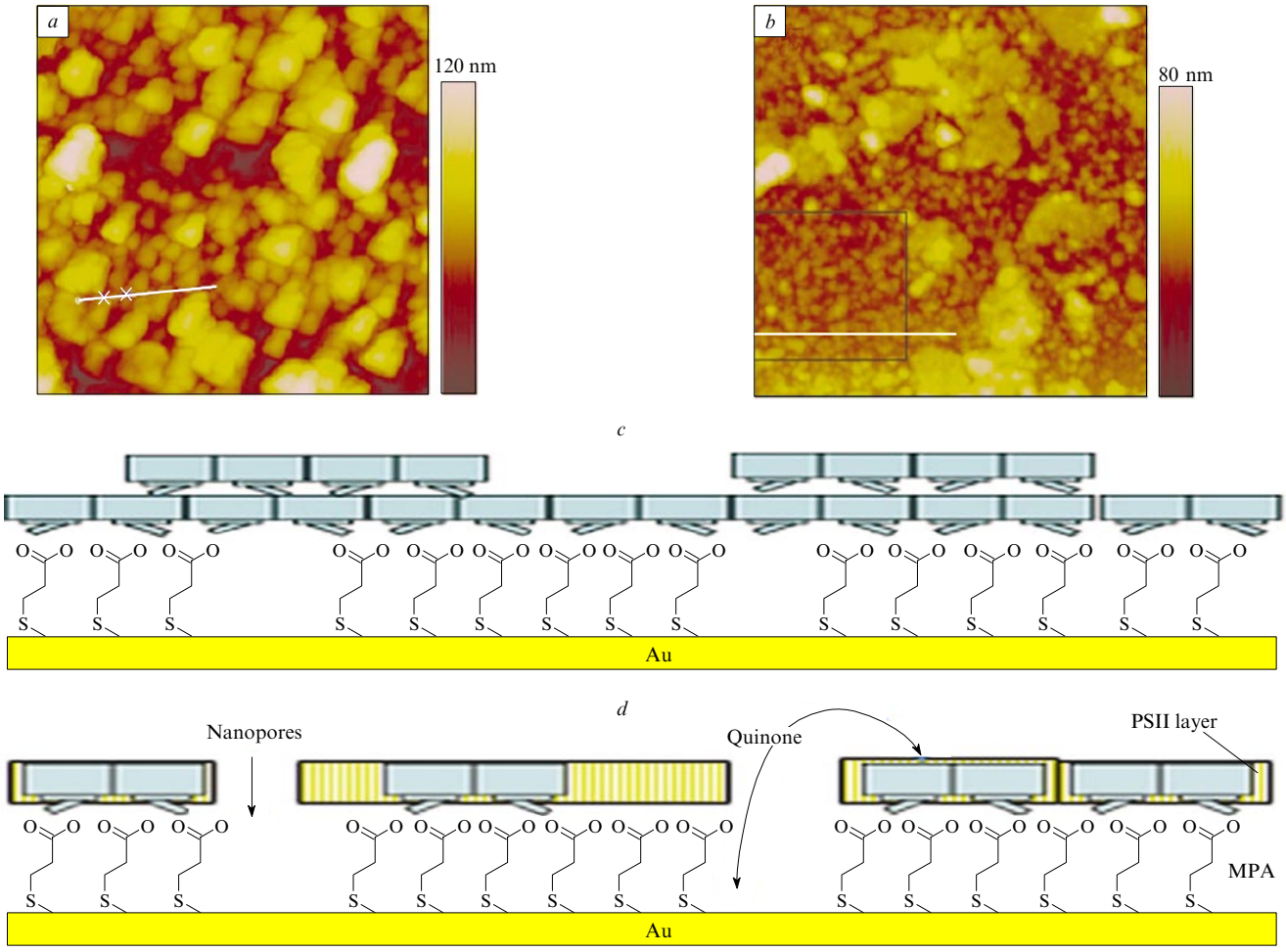


Figure 32. AFM images of PSII particles immobilized on the MPA monolayer (the square side is 2.5 μm).[146]
(*a*) Spinach PSII. The immobilized particles form clusters, thus preventing the quinone access to the electrode surface; (*b*) PSII particles with LHCII: seen are the immobilized particles and the access to the electrode (the root-mean-square roughness in the marked square is 4.16 nm); (*c*, *d*) schematic representation of the corresponding bilayers.

3. Self-assembled and other film systems based on PSI and PSII proteins

An example of an integrated study of self-assembled monolayers of photosystem I is the work by Mukherjee *et al.*,[147] who formed these layers on gold-coated silicon substrates modified with 11-mercaptoundecanol (11-MUD). First, colloidal solutions of PSI as 'dispersed trimers' mixed with two surfactants were synthesized and studied. It was found by dynamic light scattering that out of the two surfactants [*n*-dodecyl-β-D-maltoside (DM) and Triton X-100 (TX-100)], the former stabilizes PSI trimers and prevents them from aggregation over a much broader concentration range than the latter. For DM, the range of concentrations used is from 0.4 to 2.2 CMC (CMC is the critical micelle concentration) [147] (0.18 mmol litre^{-1}), while for TX-100 the same result was achieved only at a ~2 CMC concentration [147] (0.24 mmol litre^{-1}), whereas at lower concentrations, trimers were aggregated and at higher concentrations they were destroyed.

In the authors' opinion,[147] in the case of DM even for concentration of 0.2 CMC, it was possible to select the concentration of PSI trimers (5.4×10^{-4} mmol litre^{-1}) such that the trimers existed in the non-aggregated (individual) state. The trimer to trimer distance at this concentration was only 80–100 nm and the diameter of a trimer surrounded by surfactant molecules was 35–40 nm (without the surfactant, it was < 30 nm). When present at concentration of 2.2 CMC, DM can stabilize the PSI trimers over a broad concentration range (9.1×10^{-6}–2.8×10^{-4} mol litre^{-1}). From solutions in a phosphate buffer (pH 7) in which PSI occurred as individual trimers [c(DM) = 2.2 CMC, c(PSI) = 9.1×10^{-6}–1.4×10^{-3} mol litre^{-1}], deposition during 5 min gave layers on gold-coated silicon substrates modified with 11-MUD. It follows from AFM data that deposition on an Au electrode gave in all cases individual PSI trimers randomly distributed over the substrate surface. The number of trimers depends on the PSI concentration in the solution, *i.e.*, as the concentration of PSI increases, more and more high-quality PSI films can be obtained on the electrode.[147]

In the studies [138, 139] the authors discuss the GRS spectra of PSII RC monolayers transferred to Ag electrodes (1 to 10 layers) by both the LS and LB methods in comparison with the GRS spectra recorded for self-assembled PSII RC films. It was found that upon laser excitation at 406.7 nm (resonance region with the electron transitions in the PSII RC chromophores), clearly seen are the absorption bands of chlorophyll *a* (1693, 1606, 1555, 1495–1224, 980–747 cm^{-1}), which partially overlap with the absorption bands of pheophytin *a* (1693, 1577, 1495, 1224, 1155, 1139, 980–787, 678 cm^{-1}) and cytochrome b_{559} (1372, 1354, 678 cm^{-1}). The GRS spectra also exhibit three absorption bands of carotenoid molecules: at 1525, 1177–1155 and 1006–998 cm^{-1}. These carotenoid absorption bands are more cleat-cut if the excitation wavelength is 488.0 nm, which is in the resonance with the electron transitions in carotenoid molecules. Rather intense GRS spectra were measured even for a single PSII RC monolayer transferred to a silver electrode; furthermore, when the number of monolayers increased to ten, the intensity of the GRS spectrum increased in proportion and the signal to noise ratio improved.[139]

Conversely, the GRS spectra of self-assembled PSII RC layers on Ag electrodes are distinguished by the presence of strong absorption bands of carotenoid molecules, which attests to adsorption of PSII RC on electrodes by the periplasmic side of the membrane near which the carotenoid molecules are located. Upon the LB or LS transfer, the PSII RC monolayers are oriented on the electrode surface by the cytoplasmic side of the membrane near which the chlorophyll *a* molecules are located. The intense GRS spectrum of self-assembled PSII RC layers is apparently related to their polymolecular adsorption.

A study of the protein photochemical activity showed that the intensity of the band for the oxidized form of cyt-559 decreases and the intensity of the reduced form of cytochrome increases following increase in the laser irradiation power (from 0.6 to 20.0 mV).[138] This effect is completely reversible, which attests to full retention of the PSII RC functional activity in the monolayer. This is additionally proven by the presence of only one peak (at 681 nm) typical of the active form of the complex in the fluorescence spectrum of the PSII RC monolayer during fast compression before the transfer to the electrode.[136–138]

In view of the limited size of the review, we will not discuss in detail numerous structural and functional studies of PSI and PSII in micelles, liposomes or on the surface of other nano-sized objects.[148, 149]

4. Hybrid film structures based on PSI and PSII

Film structures with different orientations of PSI and PSII on special electrodes can apparently serve as simplest models of hybrid systems. For example, in the key publication,[150] PSI layers from spinach leaves were obtained (adsorption of PSI for 20 h from the phosphate buffer; PSI concentration 0.1–0.3 mg ml^{-1} with respect to chlorophyll) on special gold electrodes. A specific feature of these Au electrodes is preliminary coating by a self-assembled monolayer of mercaptoethanol or its analogues (the best are 6-mercaptohexan-1-ol and 8-mercaptooctan-1-ol).[151] By cyclic voltammetry, it was shown [150] that 70% of PSI are oriented by the special pair P700 on Au/HS$(CH_2)_2$OH (Fig. 33 *a*), as indicated by the intense peak of P700 at +0.51 V (*vs.* the standard hydrogen electrode).[150]

Since the authors were unable to answer the question about the orientation of the rest 30% of PSI by cyclic voltammetry, they used [150] spectroelectrochemical methods, in particular, EPR, which showed that the rest 30% of PSI point to the opposite direction (two peaks, the anodic peak at −0.28 V and the cathodic peak at −0.45 V give a medium peak at −0.36 V for iron–sulfur complexes in PSI designated by F_A/F_B). Upon irradiation of 0.03 cm^2 of these films (Fig. 34) in the presence of methyl viologen (MV, electron acceptor from F_B) by a 250 W lamp through a red filter, the photocurrent may be 0.1–0.2 nA if the potential applied to the working electrode is about +0.3 V.[150] In the case of a measuring electrode with the same composition but without PSI, no photocurrent was detected (see Fig. 34).[150] These experiments [150] unambiguously attest to retention of the native structure and light-driven functioning of the main bulk of PSI in the nano-biohybrid system, which makes this system promising for the design of photovoltaic devices.

A number of recent publications [152, 153] report detailed consideration of all heterogeneous reactions that take place in the PSI system (Figs 35–37) and are mainly associated

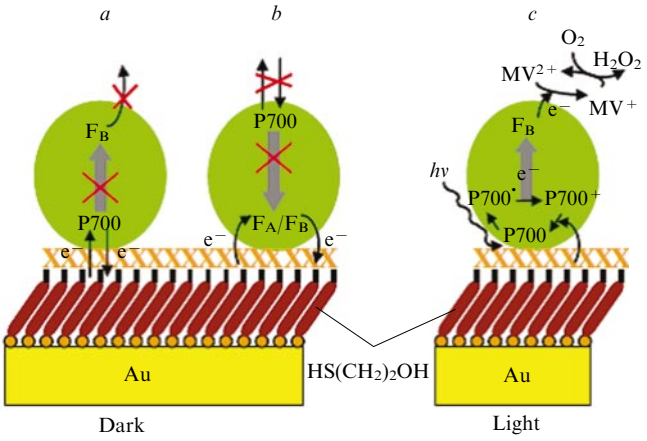


Figure 33. Scheme of the electron transfer in PSII.[150]
Electrochemistry of P700 (*a*) and F_A/F_B (*b*) sites in the dark; active site of the photoelectron transfer in the light in the presence of an electron acceptor (MV^{2+}) (*c*).

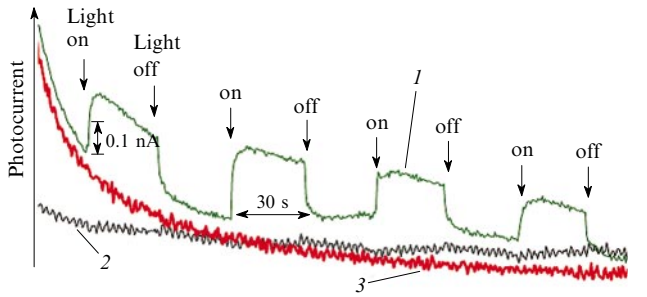


Figure 34. Chronoamperometry of PSI/$HO(CH_2)_6S$/Au electrodes in a phosphate buffer in the presence (*1*) and in the absence (*2*) of methyl viologen; control electrode without PSI but with MV (*3*).[150]
The potential is 0.3 V *versus* the normal hydrogen electrode, illumination with a 250 W lamp through a red filter.

with electron transfer between the working electrode and the redox pair (see Fig. 35):

$$P_{700} + F_B \longrightarrow P_{700}^+ + F_B^-$$

$$P_{700}^+ + \text{Red} \longrightarrow P_{700} + \text{Ox}$$

$$F_B^- + \text{Ox} \longrightarrow F_B + \text{Red}$$

where P_{700} are chlorophyll dimers with an absorption maximum at 700 nm, F_B are iron–sulfur complexes, Ox and Red are the oxidized and reduced states of electrochemical mediators, respectively.

While comparing the recent studies performed by these large groups of US researchers,[150–154] one can evaluate the enormous progress in the efficiency and technological perfection of these systems (see Figs 33–37). For example, the photocurrent parameters of the PSI system in the electrochemical cell varied as follows:

Period	j/nA cm^{-2}	Ref.
2005–2007	3–5	150, 151
beginning of 2008	~100	154
end of 2008	~300	152
2010	~2000	153

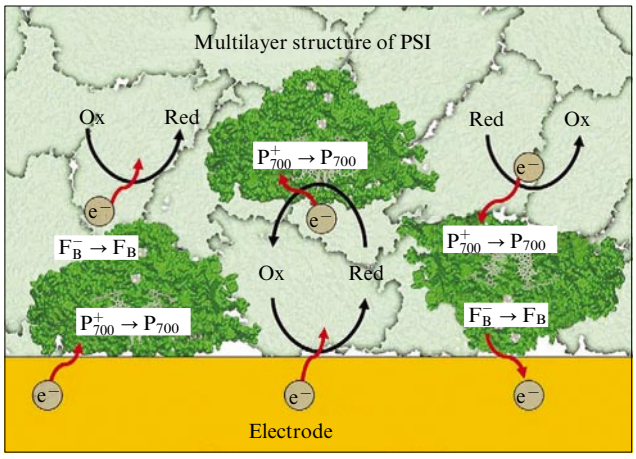


Figure 35. Scheme of the electron transfer between the reaction centres of PSI, electrochemical mediators and the electrode surface.[153]
Reduced and oxidized mediators can react with photogenerated PSI reaction centres P_{700}^+ and F_B^-, respectively, and with the electrode surface. The PSI reaction centres can also transfer electrons directly to the electrode surface; observation of the overall cathodic current indicates that the reduction of P_{700}^+ and oxidized mediators predominate in the reactions at the electrodes. The PSI complexes in the subsequent layers contribute to the photoinduced increase in the cathodic current by providing sites for repeated oxidation of the reduced mediators near the electrode, which efficiently increases the concentration of oxidized substances near the electrode surface and provides more opportunities for heterogeneous reduction processes.

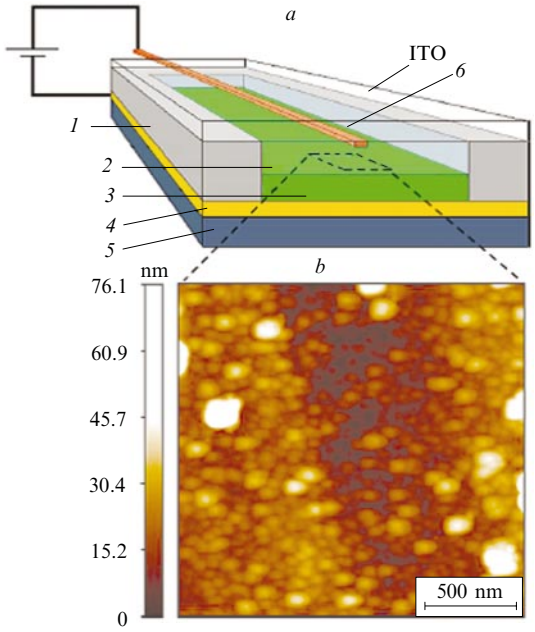


Figure 36. Scheme of PSI-catalyzed photoelectrochemical cell (*a*) and AFM image of the surface of multilayer PSI from the disassembled cell (*b*).[153]
(*1*) Polydimethylsiloxane, (*2*) electrolyte solution, (*3*) PSI multilayer, (*4*) gold electrode, (*5*) silicon substrate, (*6*) copper plate.

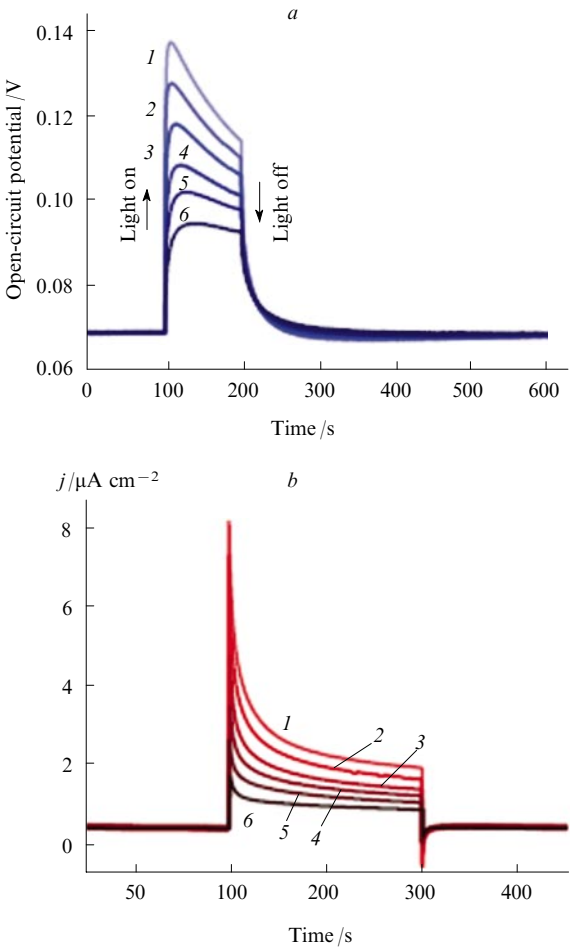


Figure 37. Photoelectric response of a typical PSI-catalyzed photoelectrochemical cell at different light intensities.[153]
(*a*) The open-circuit cell potential increases upon cell irradiation owing to the change in the concentration of electrochemical mediators at the electrode surface; (*b*) photocatalytic effect of PSI multilayers was observed as an increase in the cathodic current upon cell irradiation. The current decays with time due to the consumption of the electrochemical mediators near the electrode surface. Light intensity /mW cm^{-2}: 95 (*1*), 76 (*2*), 41 (*3*), 29 (*4*), 19 (*5*), 13 (*6*).

It is characteristic that the photocurrent and potential values considerably increase (from 1.5 to 2.5 μA cm^{-2} and from 90 to 120 mV) as the exciting light intensity increases (from 13 to 95 mW cm^{-2}) (see Fig. 37). This progress gives grounds for optimistic forecasts, especially in view of the fact that these systems are fairly stable: the average photocurrents at 2–3 μA cm^{-2} were reproduced during 50 days and, after that, they could be restored to the initial level by filling the tank by fresh electrolyte for more 126 days, and retained stability totally for 280 days.[153] It is of interest that the initial photocurrents were at the level of ~4 μA cm^{-2} and even increased to 6–7 μA m^{-2} on the second day, and then decreased and were stabilized on the third day, which was attributed[153] to the ability of PSI in electrolyte solutions (5 mM dichloroindophenol, 100 mM ascorbic acid, 100 mM NaCl in 5 mM phosphate buffer, pH 7.0) to be rearranged on the Au electrode surface to energetically more favourable positions relative to one another as a result of interaction of large numbers of hydrophilic and hydrophobic sites in their molecules.

The next step in the development of hybrid systems was made in the works of researchers from Tel Aviv University,[155,156] who prepared and investigated self-assembled layers of the 'cysteine mutant' Y635C at the PSI subunit PsaB, isolated from cyanobacteria, in comparison with the initial PSI on gold. The authors call these structures 'monolayers' but actually they are described as molecular structures of PSI multilayers. The authors emphasize that a 0.45 V voltage was applied to the lower Au electrode for PSI orientation during film drying. The layers of this mutant are strongly adsorbed on the Au electrode through formation of bonds between the sulfur end of PSI and gold, the resulting systems being both structurally and functionally similar to those composed of the initial (native) PSI, which is in line with the works of other authors.[157–160] It follows from AFM data that the size of PSI somewhat increases in all cases upon deposition of platinum over the vertically oriented layers of PSI by photoreduction of Pt^{4+} ions from solutions giving 2-nanometre 'platinum crystals'.[156] In the authors' opinion,[156] this gives rise to additional bonds between the layers of PSI *via* the formation of sulfide bonds between the sulfur ends of PSI and the 'platinum crystals'; this procedure of successive formation of the PSI/Pt multilayers was repeated several times. The quality control of materials was performed by measuring the contact potential difference (CPD) in these structures by AFM. A decrease in the CPD by about 0.7 V upon the deposition of PSI on the electrode was detected, whereas the deposition of the subsequent Pt layer gives a 0.23 V increase, which is reproduced for each subsequent PSI/Pt layer when measured in the dark. These effects are in good agreement with the data obtained by other methods.[157–160]

Illumination of a film from one Au/PSI/Pt layer with a 40 mW laser diode at 670 nm resulted in an increase in the photopotential by 0.252 V (with respect to dark values) due to the light-dependent charge separation in the system. This value is much smaller than the expected theoretically maximal value for the first layer of PSI, which should have been ~1.0 V due to the energy difference between the primary donor P700 and the final acceptor and also in view of the quantum efficiency (about 1) for PSI.[156] However, one should take into account the real decrease in this theoretical value caused by several effects at the interface. Note the slight but permanent increase in the photopotential by 0.330 V for two PSI/Pt layers and by 0.386 V for three PSI/Pt layers, which is related to the change in the size of the Schottky barrier for the interface between Pt and P700 (PSI). These latest data give hope that more effective nanobiohybrid systems will be designed as elements of photovoltaic cells based on PSI (Fig. 38).

In the next study,[161] the same group of authors obtained SA monolayers of the PSI mutant (D235C/Y634C) containing 2 cysteine residues, which are able to chemically bind to *N*-ε-maleimidocaproic or *N*-ε-maleimidopropionic acid (ECMA or BMPA) adsorbed through the carboxy group on the surface of semiconductor GaAs structures (Fig. 39).

Since this PSI mutant had unique cysteine residues near the special pair P700, the authors[161] were confident that all molecules of these PSI were arranged by P700 site towards the surface of semiconductor GaAs structures. This is directly proven by the significant differences in the surface

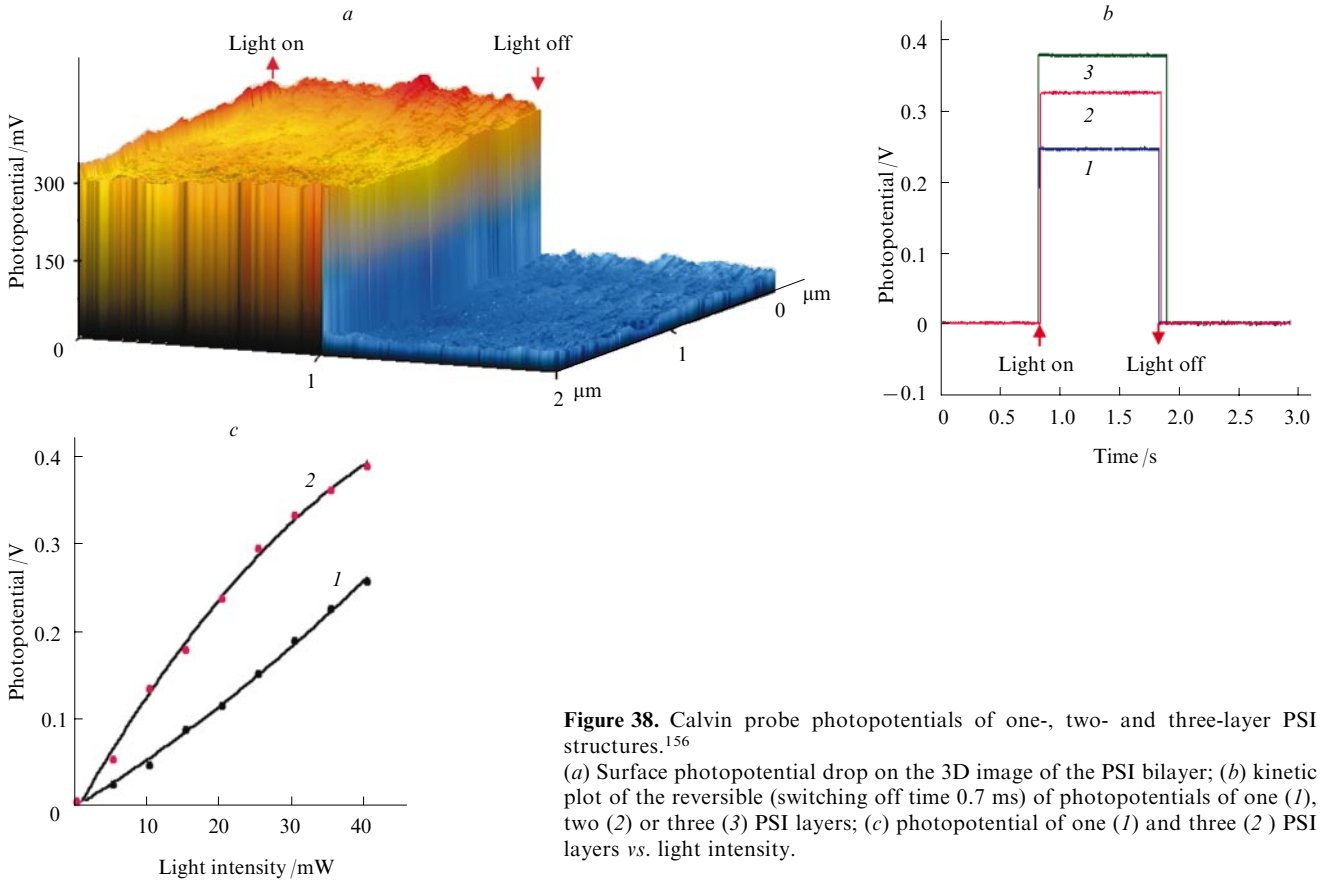


Figure 38. Calvin probe photopotentials of one-, two- and three-layer PSI structures.[156]
(*a*) Surface photopotential drop on the 3D image of the PSI bilayer; (*b*) kinetic plot of the reversible (switching off time 0.7 ms) of photopotentials of one (*1*), two (*2*) or three (*3*) PSI layers; (*c*) photopotential of one (*1*) and three (*2*) PSI layers *vs*. light intensity.

topographies and the contact potentials (determined by AFM) for PSI on semiconductor GaAs structures (of all types) in the dark and on exposure to laser radiation at 632.8 nm with 5 mW cm^{-2} intensity (Fig. 40).[161] The resulting structures and functioning electron contacts present considerable interest both for the study of photo-dependent charge transfer and for the design of elements of bionanoelectronic devices.

One of the most significant studies[162] in modern biotechnology is devoted to the development of a procedure to generate photocurrent from single molecules of PSI. The authors used a special attachment for scanning near-field optical microscope (SNOM) and mutant PSI containing two cysteine residues on the oxidizing side of the pigment–protein complex and one more cysteine residue on the reducing side of the pigment–protein complex (bipolar mutant). For comparison, measurements were carried out for mutant of PSI without the cysteine mutation on the reducing side of the complex (unipolar mutant). In both cases, film thickness of mutant PSI on glass metallized by a gold thin film was ~9 nm, which is similar to the height of native PSI. The average photocurrents obtained in 77 measurements were 9.8 ± 5.1 pA (see Ref. 162) irrespective of the applied bias direction, and the electron turnover time was ~16 nm, *i.e.*, every 16 ns an electron ran across the PSI complex covalently bound between the two electrodes. Rather high dark currents were recorded: ~1.5 nA for a bias voltage of ~1 V. The photocurrent density was ~0.15 mA cm^{-2} upon 0.1 W cm^{-2} illumination at 633 nm. In the authors' opinion, these single PSI blocks

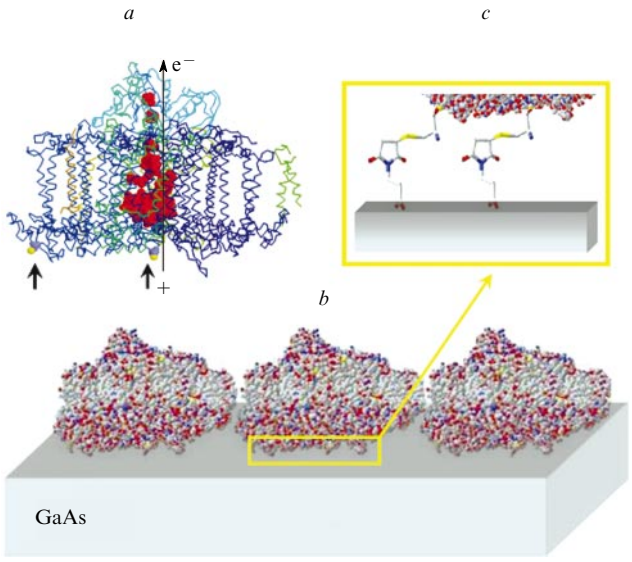


Figure 39. Molecular structure of PSI mutants and their monolayer on a GaAs substrate.[161]
(*a*) Light-induced charge separation (arrow) through the electron transfer chain in the model of PSI with cysteine mutants D235C/Y634C (marked by short allows); (*b*) schematic view of a PSI monolayer on a GaAs substrate; (*c*) binding of PSI molecules to the GaAs surface shown on an enlarged scale.

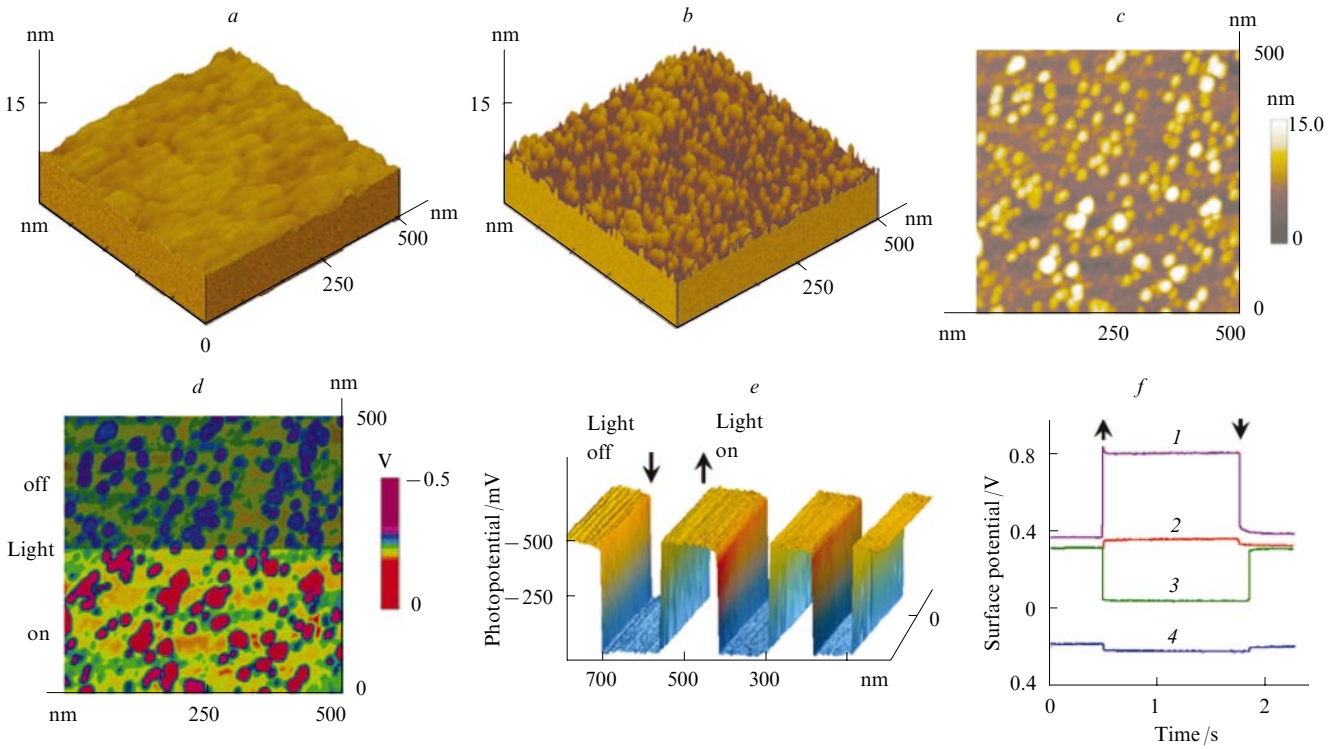


Figure 40. Two- and three-dimensional scanning probe microscopy images of the oriented PSI on the GaAs surface.[161]
3D images of a free (*a*) and PSI monolayer-coated (*b*) GaAs surface; 2D images of the surface (*c*) and the surface potential (*d*) of the same PSI monolayer on the GaAs surface. Image of the light-induced reversible potential of a dense PSI monolayer on GaAs (*e*) (scanning of each image was from the top to the bottom). Time variations of the light-induced surface potential of GaAs with PSI [*n*-type (*1*), *p*-type (*3*)] and without PSI monolayer [*n*-type (*2*) and *p*-type (*4*)] (*f*).

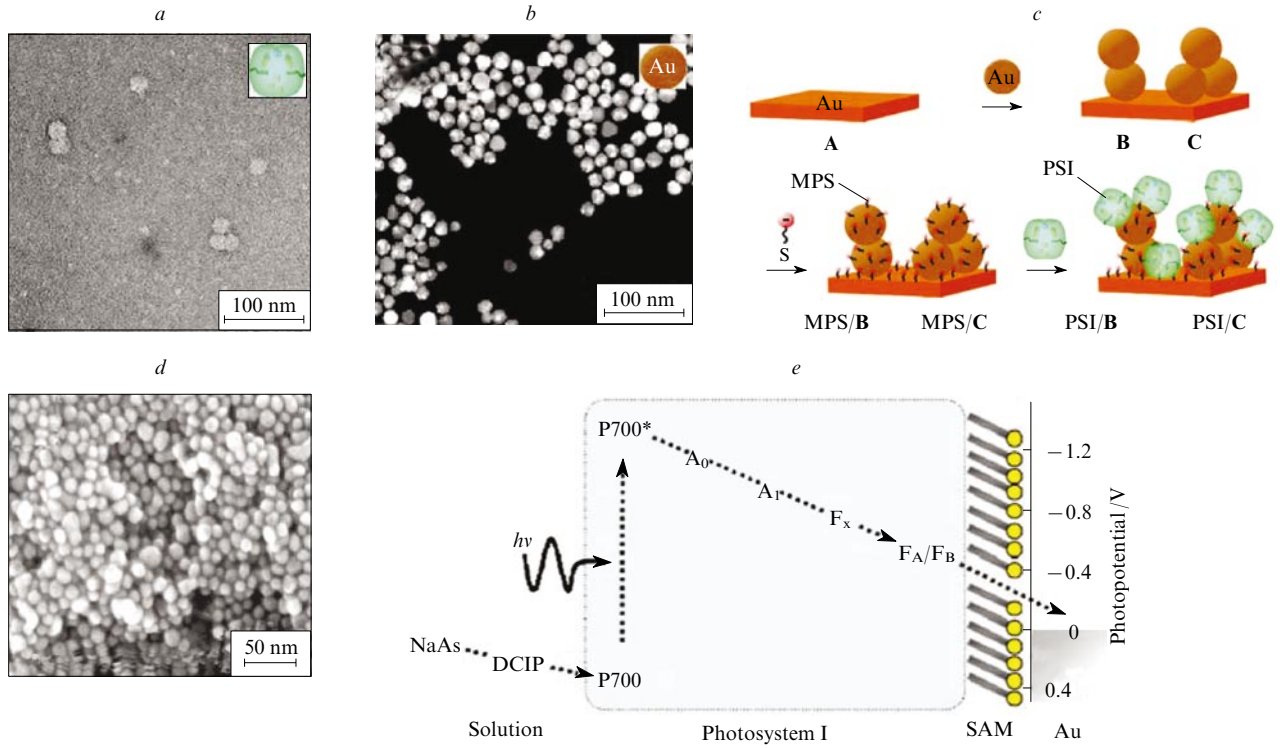


Figure 41. Fabrication of hybrid electrodes containing Au nanoparticles and PSI.[163]
SEM images of PSI (*a*) and gold nanoparticles (*b*), schematic view of the fabrication procedure of PSI/**B** and PSI/**C** hybrid electrodes (*c*), SEM image of a PSI/**C** electrode (*d*), energy diagram of the functional molecules in PSI and electron mediators during generation of photocurrent (*e*). NaAs is sodium L-ascorbate, DCIP is sodium 2,6-dichloroindophenolate hydrate.

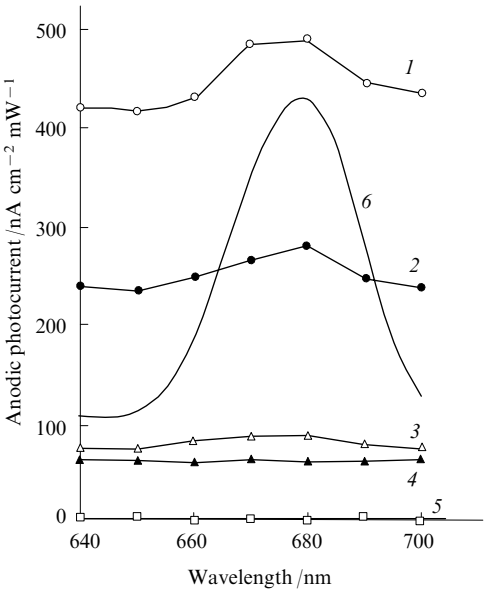


Figure 42. Photocurrent spectra for hybrid electrodes of various types and PSI-free electrodes.[163]
(*1*) PSI/**C**, (*2*) PSI/**B**, (*3*) PSI/**A**, (*4*) MPS/**C**, (*5*) MPS/**A**, (*6*) absorption spectrum of PSI in a MPS–NaOH solution (pH 6.4).

may be integrated and selectively addressed in nano-sized photovoltaic devices while retaining their biomolecular functional properties; they are promising as light-driven, highly efficient single-molecule electron pumps.[162]

Terasaki *et al.*[163] found a new approach to the design of a bionanohybrid electrode, which implies the use of gold nanoparticles for adsorption of PSI. The key element of this approach is deposition of gold nanoparticles (18 nm in diameter) on a planar gold electrode (**A**). This gave structures of two types (**B** and **C** in Fig. 41) depending on the amount of the colloidal gold solution used. This was followed by modification with 3-mercaptopropanesulfonic acid (MPS) by self-assembling and finally modification of this structure by electrostatic adsorption of PSI molecules (see Fig. 41). The surface areas of modified electrodes PSI/**A** , PSI/**B** and PSI/**C** were related as 1 : 12 : 26. Exposure to light at 680 nm [3.3 mW, $E = 0.0$ V *vs.* Ag/AgCl (sat. KCl)] generated a photocurrent, which was 290, 900 and 1600 nA cm^{-2} for structures PSI/**A**, PSI/**B** and PSI/**C**, respectively (Fig. 42).

Although PSI is a rather large pigment–protein complex as compared with known organic dyes that have been found to generate photocurrent,[164–168] Gerster *et al.*[162] were able to fabricate hybrid systems PSI/Au nanoparticles/Au electrode, which produced much higher photocurrents particularly due to PSI compared with the corresponding systems on Au electrodes.[169,170] A similar procedure was used[171] by the same researchers to fabricate the hybrid systems PSII/Au nanoparticles/Au electrode. The surface areas of PSII/**A**, PSII/**B** and PSII/**C** electrodes were related as 1 : 7 : 17. On irradiation at $\lambda = 680$ nm (with a power of 3.3 W) and at applied potential $E = 0.2$ V, the photocurrents were 760 and 2440 nA cm^{-2} for structures PSII/**B** and PSII/**C**, respectively, *i.e.*, they were 6- or 19-fold higher than the value of 130 nA cm^{-2} observed for PSII/**A**. The photocurrents for PSII/**B** or PSII/**C** increase linearly

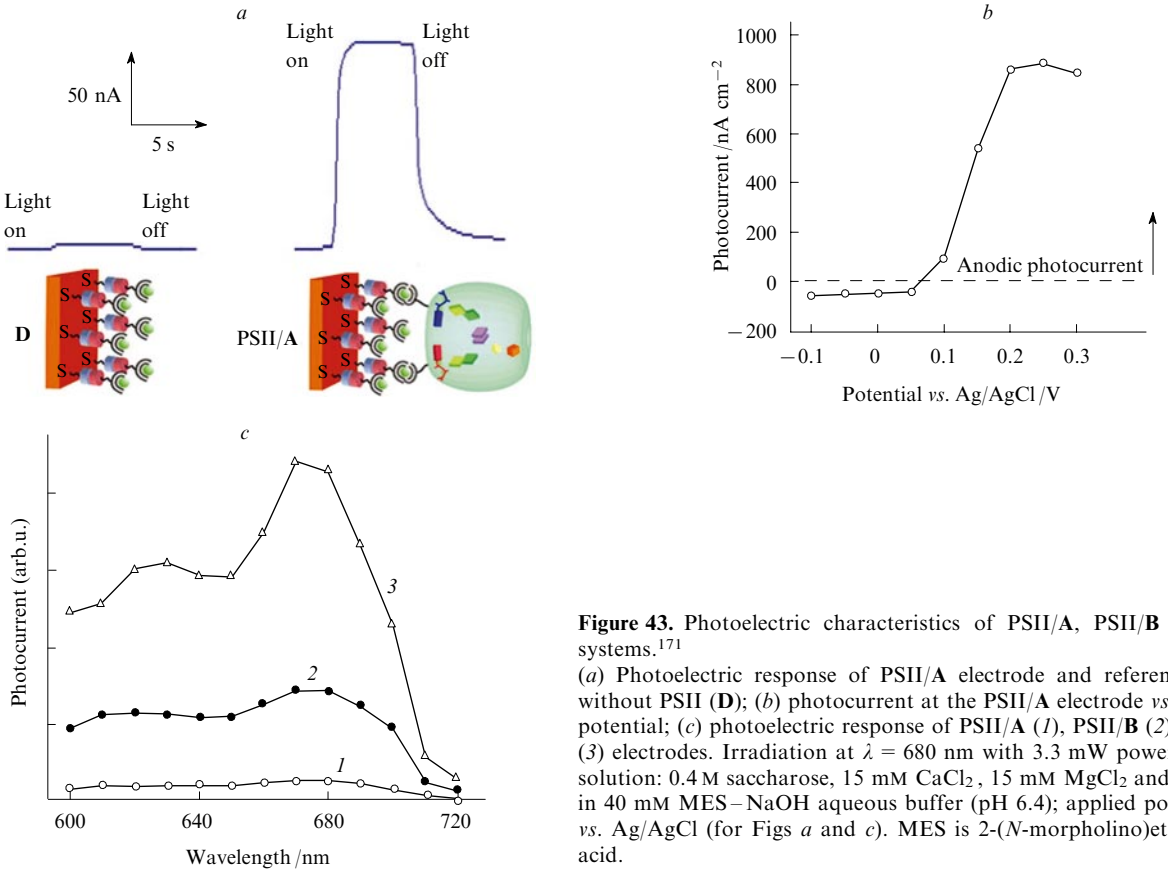


Figure 43. Photoelectric characteristics of PSII/**A**, PSII/**B** and PSII/**C** systems.[171]
(*a*) Photoelectric response of PSII/**A** electrode and reference electrode without PSII (**D**); (*b*) photocurrent at the PSII/**A** electrode *vs.* the applied potential; (*c*) photoelectric response of PSII/**A** (*1*), PSII/**B** (*2*) and PSII/**C** (*3*) electrodes. Irradiation at $\lambda = 680$ nm with 3.3 mW power; electrolyte solution: 0.4 M saccharose, 15 mM $CaCl_2$, 15 mM $MgCl_2$ and 0.1 M NaCl in 40 mM MES–NaOH aqueous buffer (pH 6.4); applied potential 0.2 V *vs.* Ag/AgCl (for Figs *a* and *c*). MES is 2-(*N*-morpholino)ethanesulfonic acid.

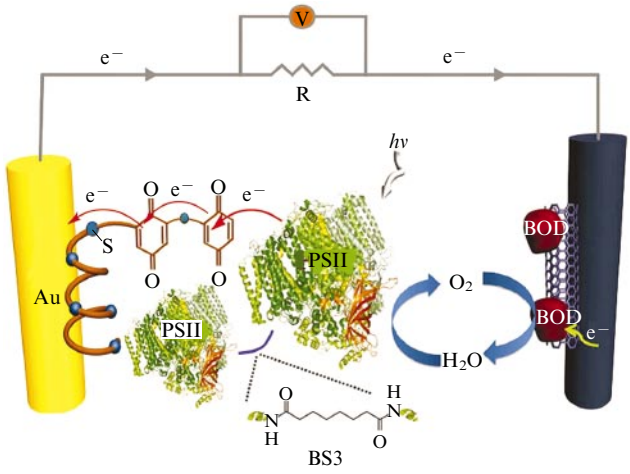


Figure 44. Schematic view of the photoelectrochemical cell poly(mercapto-*p*-benzoquinone)/photosystem II/bilirubin oxidase/carbon nanotubes.[172]

with the increase in the amounts of immobilized PSII and Au nanoparticles (Fig. 43).

Thus, the authors cited above [162, 169–171] believe that the proposed method for enhancement of the photocurrent in hybrid systems based on photosystems I and II by using Au nanoparticles is versatile and suitable for designing elements for photovoltaic cells for practical applications.

Yehezkeli *et al.*[172] devised a hybrid system based on the pigment – protein complex of PSII (Fig. 44). The photoanode was fabricated as follows. First, electropolymerization of mercapto-*p*-benzoquinone on the Au electrode surface was carried out. Then the polymer layer was coated by PSII, which was linked to the quinone units through the Q_B site. Then PSII were cross-linked with one another by bis(sulfosuccinimidyl)suberate (BS3); the surface concentration of PSII was 1.5×10^{-12} mol cm^{-2}. This gave an integrated photoanode able to oxidize water to oxygen upon irradiation.

The cathode of the hybrid photocell was a glass carbon electrode coated by carbon nanotubes that were pre-modified with bilirubin oxidase (BOD). At this electrode, oxygen was reduced to water.

Figure 45 presents the photoelectric characteristics of the hybrid system thus obtained.[172]

It is important that the current generated in the system was almost invariable (300 nA) during 3 h of continuous irradiation and only after that it decreased by 15% during irradiation for the following 10 h.[172] From the known surface concentration of PS and current density, the researchers estimated the electron transfer rate as 518 e s^{-1}. This value is close to the value for PS monolayers and indicates that immobilization of PS almost does not change its activity. An advantage of the system proposed by Yehezkeli *et al.*[172] is that all components are fully integrated on the electrode surface and functioning of the system does not require the addition of any mediators to the electrolyte solution. Generally, this type of hybrid cells represents an alternative approach to the conversion of light energy to electric energy with respect to Grätzel's works [164–166] dealing with cells with a sensitive dye. The system described above was improved by deposition of gold nanoparticles attached through a bis-aniline (BA) spacer to the anode. Gold nanoparticles modified by mercaptoethanesulfonic acid and mercaptoaniline were deposited by electropolyme-

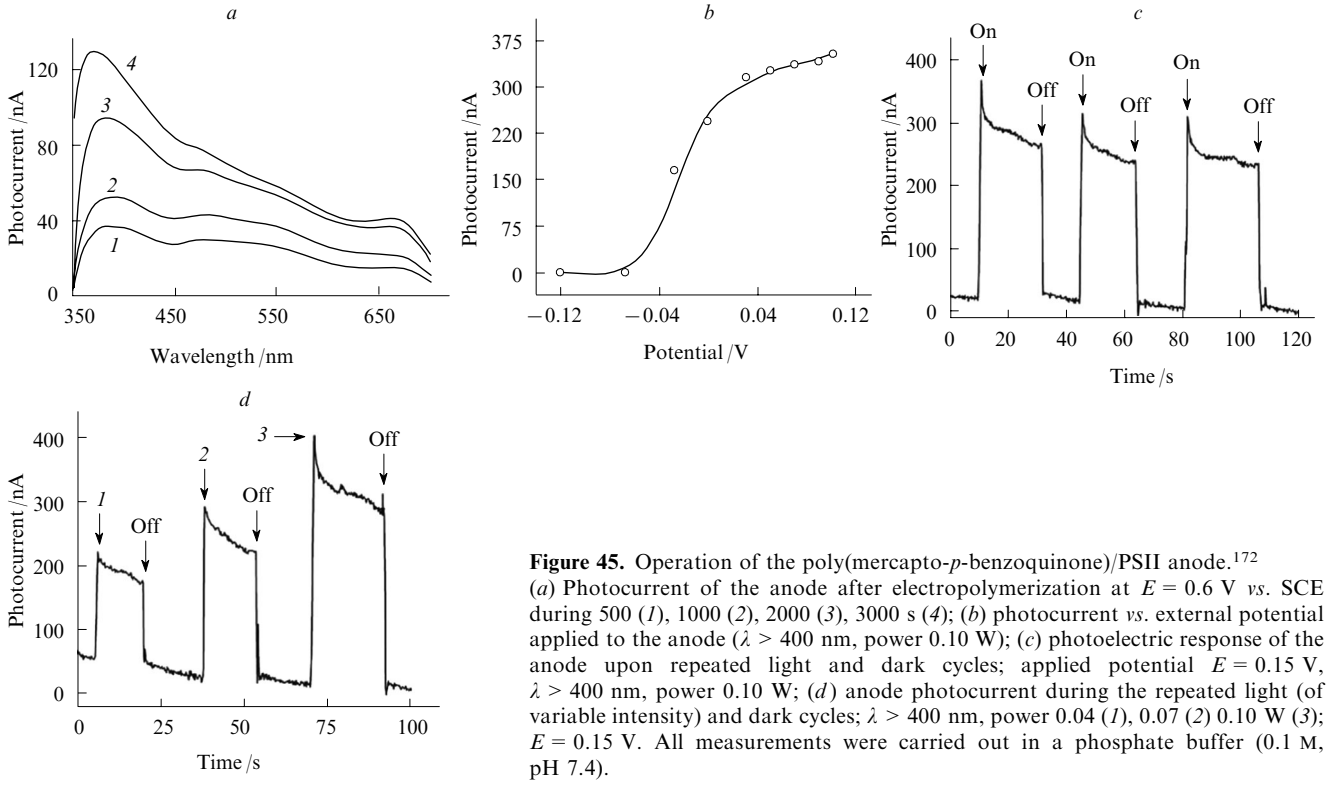


Figure 45. Operation of the poly(mercapto-*p*-benzoquinone)/PSII anode.[172]
(*a*) Photocurrent of the anode after electropolymerization at $E = 0.6$ V *vs.* SCE during 500 (*1*), 1000 (*2*), 2000 (*3*), 3000 s (*4*); (*b*) photocurrent *vs.* external potential applied to the anode ($\lambda > 400$ nm, power 0.10 W); (*c*) photoelectric response of the anode upon repeated light and dark cycles; applied potential $E = 0.15$ V, $\lambda > 400$ nm, power 0.10 W; (*d*) anode photocurrent during the repeated light (of variable intensity) and dark cycles; $\lambda > 400$ nm, power 0.04 (*1*), 0.07 (*2*) 0.10 W (*3*); $E = 0.15$ V. All measurements were carried out in a phosphate buffer (0.1 M, pH 7.4).

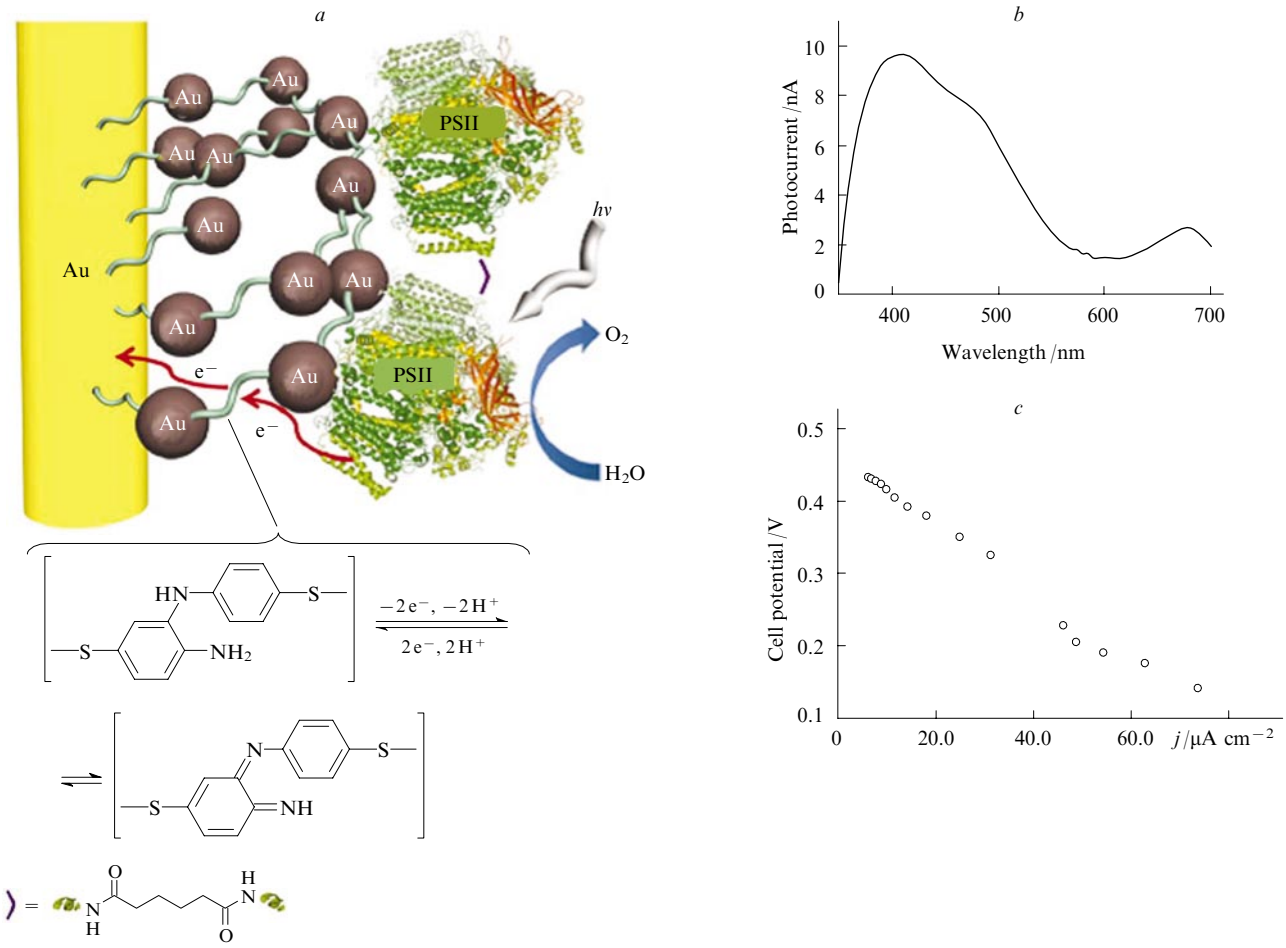


Figure 46. Schematic view of the anode based on the BA spacer–Au-nanoparticles /PSII system (*a*); photocurrent of the anode *vs.* radiation wavelength (*b*) and cell discharge (polarization) curve for the hybrid BA spacer–Au nanoparticles/PSII/bilirubin oxidase/carbon nanotubes.[172]
The measurements were carried out in air using variable external resistors; phosphate buffer (0.1 M, pH 7.4) was used as the electrolyte.

rization to an Au electrode coated by a mercaptoaniline monolayer. Then PSII were deposited on the layer of nanoparticles and cross-linked by BS3 (Fig. 46 *a*). This gave an integrated electrode with a surface concentration of PSII of 8.5×10^{-13} mol cm^{-2}. The photocurrent action spectrum at this anode (see Fig. 46 *b*), the cell discharge polarization curve (see Fig. 46 *c*) and other data confirm the significant advantages of the proposed approach.[172]

The key study devoted to nanobiohybrid systems based on PSII and QD was reported[173] by researchers of the Moscow State University, who inventively modified the idea of Japanese researchers[169] about the possibility to design a hybrid energy photoconverter based on a system of the type 'photosynthetic reaction centre–molecular conductor–macroscopic electrode' for the use in photovoltaics and molecular electronics. It was ascertained by theoretical calculations[173] that the efficiency factor of the photoconverter can be much higher for nanobiohybrid systems based on bacterial and plant RC than for the best today's solar cells.[173, 174] However, there are certain doubts in the practicability of these devices due to the exceptionally low optical density of thin films of photosystems and reaction centre proteins deposited on electrodes. Maksimov *et al.*[173] proposed solving this problem by manufacturing multicomponent energy-converting devices, *i.e.*, nanobiohybrids of PSII and QD, which can both absorb solar energy over a broad range of wavelengths and effectively convert it to the electrochemical potential.

It was shown[173] that QD and core complexes of PSII (PSII CC) form hybrid structures with excitation energy transfer (FRET) from the nanoparticle to the protein–pigment complex, which is fully consistent with the previously studied properties of these components.[2, 175–181] This energy transfer from QD to PS markedly enhances the light-harvesting ability of PSII CC over a broad spectral region, *i.e.*, this brings the efficiency of energy conversion in a nanobiohybrid system closer to the efficiency of operation of natural photosystems. Since these experiments used very low QD PSII CC concentrations (10^{-11}–10^{-8} mol litre^{-1}), the authors reasonably suggested a statistically homogeneous distribution of these molecules in solution. In this case, the average distance between the donor and the acceptor should be several hundreds nanometres, *i.e.*, it should be much greater than the calculated Förster radius (R_0 is ~6 nm according to various data). Therefore, FRET should not theoretically be observed under the above-mentioned conditions in a solution of QD and PSII CC. However, in real experiments,[173] in the optimal concentra-

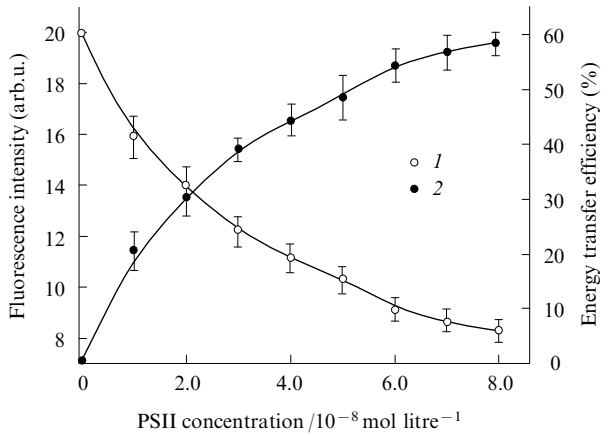


Figure 47. Efficiency of QD-630 fluorescence quenching (*1*) and energy transfer from QD to PSII core complexes (*2*).[173]
Curve *2* was calculated from analysis of intensity variation of QD fluorescence ($E = 1 - F_{da}/F_d$). The excitation wavelength for the binary system is 355 nm. F_d and F_{da} are the relative fluorescence quantum yields of the donor and the donor in the presence of the acceptor, respectively.

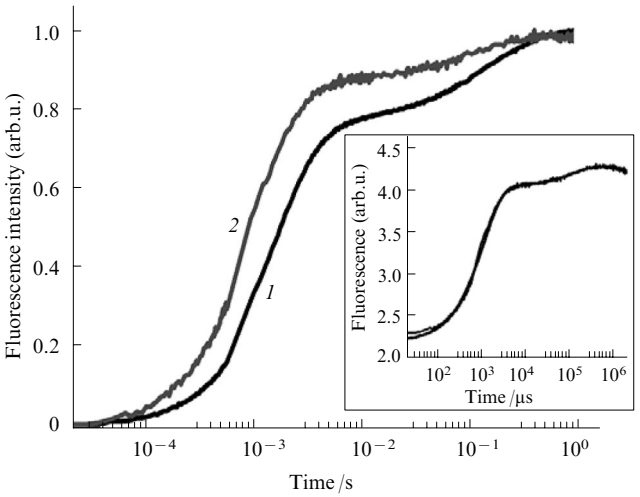


Figure 49. Fluorescence induction curves for the PSII core complexes (*1*) and hybrid systems of the PSII core complexes and QD-630 (*2*).[173]
The excitation photon flux density is 1500 μŒ from a light emitting diode with an emission maximum at 455 nm. The inset shows the results of approximation of the induction curve by the function $X(t) = 1 - [B_1 e^{-t/\tau_1} + B_2 e^{-t/\tau_2}]$.

tion range of QD-630 (donor) and PSII CC (acceptor), quenching of QD-630 fluorescence (Fig. 47, curve *1*) and enhancement of fluorescence of chlorophyll in PSII CC (Fig. 48, curve *4*) were observed.

The authors[173] concluded that even at low concentrations of QD-630 and PSII CC, they still form interacting complexes (hybrid systems) in which effective energy transfer between the components takes place. This explanation is quite reasonable because QD-630 used in the work have negatively charged carboxy groups on the outer surface, while PSII CC proteins have positively charged amino acid residues;[177] hence, donor–acceptor structures are formed in mixed solutions through electrostatic interactions of these groups. It was found[173] that quenching of QD-630 fluorescence reaches 50%–60% at the highest concentrations of the acceptor (see Fig. 47). Since different mechanisms of QD fluorescence quenching are possible in this system,[178] an additional piece of evidence for the FRET mechanism is the increase in the fluorescence intensity of the energy acceptor — PSII CC (see Fig. 48). Calculations showed that for a QD-630–PSII CC mixture, the fluorescence enhancement factor reached 0.65 at a PSII CC concentration of about 10^{-8} mol litre^{-1}. Yet another approach to determine the fluorescence enhancement factor for the PSII core complexes is to compare the rates of formation of products of the photochemical reaction. Processing of the fluorescence induction curves (Fig. 49) by the procedure developed by the authors demonstrated that the addition of QD-630 results in an increase in the rate of PSII CC fluorescence enhancement; this procedure was used to estimate both the change in the effective excitation cross-section for PSII CC fluorescence upon the addition of QD-630 (by a factor of 1.6) and the corresponding fluorescence enhancement factors for the acceptor (0.55–0.60). These values determined by the fluorescence induction method are in good agreement with the estimates obtained in the same work by steady-state fluorimetry.[173] In conclusion, the authors[173] state that the QD they used are virtually not inferior to natural light-harvesting complexes in the efficiency of fluorescence enhancement of the acceptor (PSII CC).

In our opinion, switching from mixtures to chemically cross-linked QD-630–PSII CC (as new nanobiohybrid systems) is a promising trend of the development of this area, which will undoubtedly lead to the design of new materials for photovoltaics and molecular electronics.

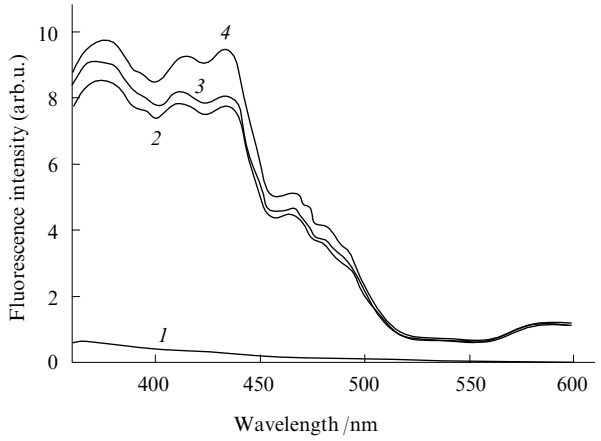


Figure 48. Fluorescence excitation spectra of QD-630 (*1*), PSII core complexes (*2*) and QD-630–PSII hybrid complexes (*4*). Given for comparison, the sum of the excitation spectra of solutions of quantum dots and PSII core complexes (*3*).[173]
The fluorescence was measured at 685 nm.

V. Conclusion

The design, the structural and functional investigations and applications of supramolecular film systems and hybrid nanomaterials based on membrane proteins and semiconductor (or metallic) nanocrystals constitute a rapidly developing line of research which combines the ideas and approaches of many subdivisions of chemistry with the advanced methods of nanobiotechnology. This review gives an account of characteristic features of film systems and hybrid nanobiomaterials based on vitally important photosensitive membrane proteins (retinal-containing proteins, reaction centres from photosynthetic bacteria and plants). In natural photosynthetic organisms, light is initially absorbed by the pigment–protein complexes (antennas) and then the excitation energy is transferred to specialized RC in which the light energy is converted to chemical energy of molecular bonds needed for the vital activity of the body. The photosynthetic pigment–protein complexes of plants, algae and various sorts of bacteria ensure the conversion of the electromagnetic energy of solar light to the electrochemical potential energy. The simplest and the best studied natural photosynthetic objects are the RC of purple bacteria.

Despite the fact that the artificial membrane systems based on bacteriorhodopsin and bacterial RC are already ready to use in some scientific and technological applications, the design of competitive materials requires invoking new (first of all, nanobiotechnological) approaches. The recently proposed methods for the fabrication of hybrid nanobiomaterials make it possible to use complexes of biomembranes (proteins) with colloidal metal or metal oxide nanoparticles or quantum dots, which can absorb large amounts of light energy and transfer it to biological systems in the desired spectral range to enhance the operation efficiency of these systems in the required direction. As an example, it is interesting to note the design of a nanobiohybrid system based on bioengineered PSI stabilized by special ZnO-binding peptide and arranged on ITO substrates with semiconductor TiO_2 and ZnO layers.[182] It is important to emphasize the unique parameters achieved on exposure of this nanobiohybrid system to light simulating the standard solar spectrum: open-circuit photopotential of ~ 0.5 V, fill factor of $\sim 71\%$, electrical power of ~ 81 μW cm^{-2}, and current density of ~ 362 μA cm^{-2} (*i.e.*, $\sim 362\,000$ nA cm^{-2}). The last-mentioned value is most significant and several orders of magnitude (from 4 to 10^4)[182] higher than the best values attained previously for the hybrid systems based on bacterial RC and PSI. According to Mershin *et al.*[182] such film systems can become promising biophotovoltaic cells for practical applications.

The key issue in the fabrication of these supramolecular systems and materials for practical applications in various fields is the preparation of ultrathin oriented films at the interface. Comparative analysis of the literature devoted to the fabrication methods and properties of such supramolecular film systems provides the conclusion that the main parameters of these systems depend on the method of preparation being improved in the sequence: layer-by-layer assembly and self-assembly, Langmuir–Blodgett and Langmuir–Schaefer methods, electrophoretic deposition and sedimentation. The fabrication of high-quality oriented films using advanced technologies is a key to success of the future design of the devices based on hybrid materials.

The example of nanobiohybrid system[182] discussed above was obtained by self-assembly of native or bioengineered PSI (with ZnO-binding peptide) on semiconductor TiO_2 and ZnO layers located on ITO electrodes, and as regards the parameters,[182] this system is promising for biophotovoltaics. The review demonstrated the pronounced technological potential of hybrid nanobiomaterials based on photosensitive membrane proteins and the possibilities of fabrication of materials with unique photovoltaic properties for practical applications.

It should be emphasized that further optimization of hybrid materials should involve the development of highly oriented hybrid films with enhanced light-capture and energy transfer characteristics (photoelectric and optical properties). In these films, the 'inner filter' effect should be reduced and the efficiency increase should be achieved by means of higher 'nano to bio' ratio in the material. In addition, hybrid materials can be optimized using QD or metal nanoparticles with strong absorption or by fabricating hybrid materials comprising biological systems and nanowires or nanorods, the absorbance of which is usually much higher than that of spherical nanoparticles of the same diameter. The biotechnological approaches, such as directed mutagenesis, allow one to tune some parameters of biological functions (quite a few examples are given in the review). The controlled binding of functionalized nanomaterials to specified molecular groups of wild-type or mutant light-sensitive proteins and subsequent fabrication of highly oriented homogeneous films gives rise to materials with markedly enhanced biological functions useful for industrial applications. The hybrid nanoelements operating in the FRET mode would ensure 'nanoresolution' for the applications in biomolecular electronics, optical switching and photovoltaics due to advantages of their size, efficiency of light- and electro-controlled functions, structure reliability, stability and low production cost. In general, we expect that approaches and methods described in this review would serve for the design of more efficient film systems and hybrid nanobiomaterials.

The authors are grateful to V Ushakov for the help in the preparation of the manuscript. The review was prepared with the financial support of the RF Ministry of Higher Education and Science (Project No. 11.G34.31.0050) and the European Commission within the Seventh Framework Programme for Research and Development (FP7) (Grant NMP-2009-4,0-3-246479 NAMDIATREAM).

References

1. C E Lubner, R Grimme, D A Bryant, J H Golbeck *Biochemistry* **49** 404 (2010)
2. I Nabiev, A Rakovich, A Sukhanova, E Lukashev, V Zagidullin, V Pachenko, Y P Rakovich, J F Donegan, A B Rubin, A O Govorov *Angew. Chem., Int. Ed.* **49** 7217 (2010)
3. M A Green, K Emery, Y Hishikawa, W Warta *Prog. Photovolt.: Res. Appl.* **18** 346 (2010)
4. N Hampp, D Oesterhelt, in *Nanobiotechnology* (Eds Ch Niemeye, Ch Mirkin) (Weinheim: Wiley-VCH, 2004) p. 146

5. F T Hong *Prog. Surf. Sci.* **62** 1 (1999)
6. N N Vsevolodov *Biomolecular Electronics: An Introduction via Photosensitive Proteins* (Boston: Birkhiuser, 1998)
7. S Yu Zaitsev *Supramolekulyarnye Nanorazmernye Sistemy na Granitse Razdela Faz. Kontseptsii i Perspektivy dlya Bionanotekhnologii* (Supramolecular Nano-sized Systems at the Interface. Conceps and Prospects of Bionanotechnology) (Moscow: LENAND, 2010)
8. S Yu Zaitsev *Ros. Nanotekhnol.* **4** (7 – 8) 44 (2009) [a]
9. J Boucher, E Trudel, M Méthot, P Desmeules, C Salesse *Colloids Surf., B* **58** 73 (2007)
10. H Lavoie, J Gallant, M Grandbois, D Blaudez, B Desbat, F Boucher, C Salesse *Mater. Sci. Eng., C* **10** 147 (1999)
11. R B Vasiliev, D N Dirin, A M Gaskov *Russ. Chem. Rev.* **80** 1139 (2011)
12. I L Medintz, H T Uyeda, E R Goldman, H Mattoussi *Nat. Mater.* **4** 435 (2005)
13. I Nabiev, A Sukhanova, M Artemyev, V Oleinikov, in *Colloidal Nanoparticles in Biotechnology* (Ed. A Elais-sari) (Hoboken: Wiley, 2008) p. 133
14. V A Oleinikov, A V Sukhanova, I R Nabiev *Ros. Nanotekhnol.* **2** (1 – 2) 160 (2007) [a]
15. P B Kocherginskaya, A V Romanova, I A Prokhorenko, D M Itkis, V A Korshun, E A Goodilin, Yu D Tretyakov *Russ. Chem. Rev.* **80** 1209 (2011)
16. G G Roberts *Langmuir-Blodgett Films* (New York, London: Plenum, 1990)
17. S Yu Zaitsev *Supramolekulyarnye Sistemy na Granitse Razdela faz kak Modeli Biomembran i Nanomaterialy* (Supramolecular Systems on Interface as Model of Biomembranes and Nanomaterials) (Donetsk, Moscow: Nord-komp'yuter, 2006)
18. A Ulman *An Introduction to Ultrathin Organic Films from Langmuir-Blodgett to Self-Assembly* (Boston: Academic Press, 1991)
19. S Yu Zaitsev, D O Solovyeva, I Nabiev *Adv. Colloid Interface Sci.* **183 – 184** 14 (2012)
20. Y Lvov, H Möhwald *Protein Architecture: Interfacial Molecular Assembly and Immobilization Biotechnology* (New York: Marcel Dekker, 2000)
21. H Ai, Y Lvov, in *Bottom-Up Nanofabrication: Supramolecules, Self-Assemblies, and Organized Films* (Ed. K Ariga) (New York: American Scientific Publ., 2009) p. 217
22. K Ariga, Y Lvov In *Biopolymers at Interfaces* (Ed. M Malmsten) (New York: Marcel Dekker, 2003) p. 367
23. M A Ostrovsky, T B Feldman *Russ. Chem. Rev.* **81** 1071 (2012)
24. D Oesterhelt *Curr. Opin. Struct. Biol.* **8** 489 (1998)
25. U Haupts, J Tittor, D Oesterhelt *Ann. Rev. Biophys. Biomol. Struct.* **28** 367 (1999)
26. Y Jin, T Honig, I Ron, N Friedman, M Sheves, D Cahen *Chem. Soc. Rev.* **37** 2422 (2008)
27. K J Wise, N B Gillespie, J A Stuart, M P Krebs, R R Birge *Trends Biotechnol.* **20** 387 (2002)
28. R R Birge *Annu. Rev. Phys. Chem.* **41** 683 (1990)
29. R Henderson, J M Baldwin, T A Ceska, F Zemlin, E Beckmann, K H Downing *J. Mol. Biol.* **213** 899 (1990)
30. S Subramaniam, R Henderson *Nature (London)* **406** 653 (2000)
31. T Furuno, H Sasabe *J. Colloid Interface Sci.* **147** 225 (1991)
32. H H Weetall, L A Samuelson *Thin Solid Films* **312** 306 (1998)
33. M Méthot, P Desmeules, D Vaknin, F Boucher, C Salesse *Langmuir* **20** 934 (2004)
34. I M Pepe, M K Ram, S Paddeu, C Nicolini *Thin Solid Films* **327 – 329** 118 (1998)
35. S Yu Zaitsev, V P Zubov, D Möbius *Biochim. Biophys. Acta: Biomembranes* **1148** 191 (1993)
36. S Yu Zaitsev, Yu Maak, V P Zubov *Biol. Membr.* **11** 525 (1994) [b]
37. T Miyasaka, K Koyama *Thin Solid Films* **210 – 211** 146 (1992)
38. C Ganea, J Tittor, E Bamberg, D Oesterhelt *Biochim. Biophys. Acta: Biomembranes* **1368** 84 (1998)
39. J Tittor, U Schweiger, D Oesterhelt, E Bamberg *Biophys. J.* **67** 1682 (1994)
40. C Horn, C Steinem *Biophys. J.* **89** 1046 (2005)
41. A Dolfi, F T Buoninsegni, M R Moncelli, R Guidelli *Bioelectrochemistry* **56** 151 (2002)
42. A Dolfi, F Tadini-Buoninsegni, M R Moncelli, R Guidelli *Langmuir* **18** 6345 (2002)
43. C Nicolini, V Erokhin, S Paddeu, C Paternolli, M K Ram *Biosens. Bioelectron.* **14** 427 (1999)
44. K Seifert, K Fendler, E Bamberg *Biophys. J.* **64** 384 (1993)
45. W Roemer, C Steinem *Biophys. J.* **86** 955 (2004)
46. R A Brizzolara *BioSystems* **35** 137 (1995)
47. J Chu, X Li, J Zhang, J Tang *Biochem. Biophys. Res. Commun.* **305** 116 (2003)
48. J A He, L Samuelson, L Li, J Kumar, S K Tripathy *Langmuir* **14** 1674 (1998)
49. J A He, L Samuelson, L Li, J Kumar, S K Tripathy *J. Phys. Chem. B* **102** 7067 (1998)
50. H H Weetall *Appl. Biochem. Biotechnol.* **49** 241 (1994)
51. H-G Choi, J Min, W H Lee, J-W Choi *Colloids Surf., B* **23** 327 (2002)
52. R Li, X Cui, W Hu, Z Lu, C M Li *J. Colloid Interface Sci.* **344** 150 (2010)
53. J A Stuart, D L Marcy, R R Birge, in *Bioelectronic Applications of Photochromic Pigments (NATO Sci. Ser. I)* Vol. 335 (Eds A Dér L Keszthelyi) (Amsterdam: IOS Press, 2001) p 16
54. R Tdth-Boconvdi, A Dér, L Keszthelyi *Bioelectrochemistry* **81** 17 (2011)
55. H Takei, A Lewis, Z Chen, I Nebenzahl *Appl. Opt.* **30** 500 (1991)
56. G E Adamov, A G Devyatkov, L N Gnatyuk, I S Goldobin, E P Grebennikov *J. Photochem. Photobiol., A: Chem.* **196** 254 (2008)
57. S Yu Zaitsev, N M Kozhevnikov, Yu O Barmenkov, M Yu Lipovskaya *Photochem. Photobiol.* **55** 851 (1992)
58. Z Chen, A Lewis, H Takei, I Nebenzahl *Appl. Opt.* **30** 5188 (1991)
59. A G Manoj, K S Narayan *Biosens. Bioelectron.* **19** 1067 (2004)
60. A G Manoj, K S Narayan *Appl. Phys. Lett.* **83** 3614 (2003)
61. A Rakovich, A Sukhanova, E Lukashev, V Oleinikov, M Artemyev, N Gaponik, N Bouchonville, M Molinari, M Troyon, Y P Rakovich, J F Donegan, I Nabiev *Nano Lett.* **10** 2640 (2010)
62. M Hardzei, M Artemyev, M Molinari, M Troyon, A Sukhanova, I Nabiev *ChemPhysChem.* **13** 330 (2012)
63. N Bouchonville, M Molinari, A Sukhanova, M Artemyev, V A Oleinikov, M Troyon, I Nabiev *Appl. Phys. Lett.* **98** 013703 (2011)
64. A R Clapp, I L Medintz, H Mattoussi *ChemPhysChem.* **7** 47 (2006)
65. R Li, Ch M Li, H Bao, Q Bao, V S Lee *Appl. Phys. Lett.* **91** 223901 (2007)

66. M H Griep, K A Walczak, E M Winder, D R Lueking, C F Friedrich *Biosens. Bioelectron.* **25** 1493 (2010)
67. Appl. US 2009/0142852 (2009)
68. M H Griep, E M Winder, D R Lueking, G A Garrett, S P Karna, C R Friedrich *Mol. Biol. Int.* Article ID 910707 (2012)
69. M H Griep, E M Winder, D R Lueking, C R Friedrich, C Mallick, S P Karna *J. Nanosci. Nanotechnol.* **10** 6029 (2010)
70. V Thavasi, T Lazarova, S Filipek, M Kolinski, E Querol, A Kumar, S Ramakrishna, E Padros, V Renugopalakrishnan *J. Nanosci. Nanotechnol.* **9** 1679 (2009)
71. L-K Chu, C-W Yen, M A El-Sayed *J. Phys. Chem. C* **114** 15358 (2010)
72. C -W Yen, S C Hayden, E C Dreaden, P Szymanski, M A El-Sayed *Nano Lett.* **11** 3821 (2011)
73. C-W Yen, L-K Chu, M A El-Sayed *J. Am. Chem. Soc.* **132** 7250 (2010)
74. A Biesso, W Qian, X Huang, M A El-Sayed *J. Am. Chem. Soc.* **131** 2442 (2009)
75. A Biesso, W Qian, M A El-Sayed *J. Am. Chem. Soc.* **130** 3258 (2008)
76. A V Patil, T Premaruban, O Berthoumieu, A Watts, J J Davis *J. Phys. Chem. B* **116** 683 (2012)
77. Y Lu, J Xu, B Liu, J Kong *Biosens. Bioelectron.* **22** 1173 (2007)
78. H Axelrod, O Miyashita, M Okamura, in *The Purple Phototrophic Bacteria (Advances in Photosynthesis and Respiration)* Vol. 28 (Eds C N Hunter, F Daldal, M C Thurnauer, J T Beatty) (Dordrecht: Springer, 2009) p. 323
79. M Y Okamura, G Feher *Annu. Rev. Biochem.* **61** 861 (1992)
80. C R Lancaster, H Michel, B Honig, M R Gunner *Biophys. J.* **70** 2469 (1996)
81. V A Shuvalov *Preobrazovanie Solnechnoi Energii v Pervichnom Akte Razdeleniya Zaryadov v Reaktsionnykh Tsentrakh Fotosinteza* (Conversion of Solar Energy in the Initial Event of Charge Separation in Reaction Centres of Photosynthesis) (Moscow: Nauka, 2000)
82. M M Leonova, T Yu Fufina, L G Vasil'eva, V A Shuvalov *Usp. Biol. Khim.* **51** 193 (2011) [c]
83. W W Parson, A Warshel, in *The Purple Phototrophic Bacteria (Advances in Photosynthesis and Respiration)* Vol. 28 (Eds C N Hunter, F Daldal, M C Thurnauer, J T Beatty) (Dordrecht: Springer, 2009) p. 337
84. E V Kitzing, H Kuhn *J. Phys. Chem.* **94** 1699 (1990)
85. L-N Liu, X-L Chen, Y-Z Zhang, B C Zhou *Biochim. Biophys. Acta: Bioenergetics* **1708** 133 (2005)
86. G Alegria, P L Dutton *Biochim. Biophys. Acta: Bioenergetics* **1057** 239 (1991)
87. G Alegria, P L Dutton *Biochim. Biophys. Acta: Bioenergetics* **1057** 258 (1991)
88. Yu M L'vov, V V Erokhin, S Yu Zaitsev *Biol. Memb.* **7** 917 (1990) [c]
89. N A Kalabina, S Yu Zaitsev, M A Kutuzov, A S Zolotarev, V P Lukashev, A A Kononenko, N G Abdulaev, V P Zubov *Biol. Memb.* **7** 1086 (1990) [b]
90. S Yu Zaitsev, N A Kalabina, V P Zubov, E P Lukashev, A A Kononenko, R A Uphaus *Thin Solid Films* **210** – **211** 723 (1992)
91. N A Kalabina, S Yu Zaitsev, V P Zubov *Biol. Memb.* **11** 324 (1994) [b]
92. S Yu Zaitsev, Yu M Lvov *Thin Solid Films* **254** 257 (1995)
93. N A Kalabina, E P Lukashev, S Yu Zaitsev, A A Kononenko, N Kh Seifulina, V P Zubov *Biol. Memb.* **13** 410 (1996) [b]
94. E P Lukashev, N A Kalabina, S Yu Zaitsev, A A Kononenko, N Kh Seifulina, V P Zubov *Biol. Memb.* **13** 497 (1996) [b]
95. N A Kalabina, S Yu Zaitsev, V P Zubov, E P Lukashev, A A Kononenko *Biochim. Biophys. Acta: Biomembranes* **1284** 138 (1996)
96. M Loesche, C Erdelen, E Rump, H Ringsdorf, K Kjaer, D Vaknin *Thin Solid Films* **242** 112 (1994)
97. D Moebius, H Moehwald *Adv. Mater.* **3** 19 (1991)
98. P Facci, V Erokhin, C Nicolini *Thin Solid Films* **243** 403 (1994)
99. V Erokhin, P Facci, L Gobbi, S Dante, F Rustichelli, C Nicolini *Thin Solid Films* **327** – **329** 503 (1998)
100. Y Yasuda, Y Hirata, H Sugino, M Kumei, M Hara, J Miyake, M Fujihira *Thin Solid Films* **210** 733 (1992)
101. Y Yasuda, H Sugino, H Toyotama, Y Hirata, M Hara, J Miyake *Bioelectrochem. Bioenerg.* **34** 135 (1994)
102. Y Yasuda, H Toyotama, M Hara, J Miyake *Thin Solid Films* **327** 800 (1998)
103. E Y Katz, A Y Shkuropatov, V A Shuvalov *Bioelectrochem. Bioenerg.* **23** 239 (1990)
104. A A Solov'ev, E Y Katz, V A Shuvalov *Bioelectrochem. Bioenerg.* **26** 29 (1991)
105. E Y Katz, A A Solov'ev *Anal. Chim. Acta* **266** 97 (1992)
106. E Katz *J. Electoanal. Chem.* **365** 157 (1994)
107. A Mahmoudzadeh, R Saer, D Jun, S M Mirvakili, A Takshi, B Iranpour, E Ouellet, E T Lagally, J D W Madden, J T Beatty *Smart Mater. Struct.* **20** 094019 (2011)
108. A Takshi, J D Madden, J T Beatty *Electrochim. Acta* **54** 3806 (2009)
109. A Takshi, J D Madden, A Mahmoudzadeh, R Beatty *J. Energ.* **3** 1721 (2010)
110. R Das, P J Kiley, M Segal, J Norville, A A Yu, L Wang, S A Trammel, L E Reddick, R Kumar, F Stellacci, N Lebedev, J Schnur, B D Bruce, S Zhang, M Baldo *Nano Lett.* **4** 1079 (2004)
111. S A Trammell, L Wang, J M Zullo, R Shashidhar, N Lebedev *Biosens. Bioelectron.* **19** 1649 (2004)
112. S A Trammell, A Spano, R Price, N Lebedev *Biosens. Bioelectron.* **21** 1023 (2006)
113. N Lebedev, S A Trammell, A Spano, E Lukashev, I Griva, J Schnur *J. Am. Chem. Soc.* **128** 12044 (2006)
114. S A Trammell, I Griva, A Spano, S Tsoi, L M Tender, J Schnur, N Lebedev *J. Phys. Chem. C* **111** 17122 (2007)
115. S A Trammell, N Lebedev *J. Electroanal. Chem.* **632** 127 (2009)
116. C Nakamura, M Hasegawa, N Nakamura, J Miyake *Biosens. Bioelectron.* **18** 599 (2003)
117. C Nakamura, M Hasegawa, Y Yasuda, J Miyake *Appl. Biochem. Biotechnol.* **84** 401 (2000)
118. J Q Zhao, B H Liu, Y L Zhou, C H Xu, J L Kong *Electrochim. Acta* **47** 2013 (2002)
119. J Zhao, N Ma, B Liu, Y Zhou, C Xu, J Kong *J. Photochem. Photobiol., A: Chem.* **152** 53 (2002)
120. J Q Zhao, Y L Zhou, B H Liu, C H Xu, J L Kong *Biosens. Bioelectron.* **17** 711 (2002)
121. Y Lu, M Yuan, Y Liu, B Tu, C Xu, B Liu, D Zhao, J Kong *Langmuir* **21** 4071 (2005)
122. Y Lu, J Xu, Y Liu, B Liu, C Xu, D Zhao, J Kong *Chem. Commun.* 785 (2006)
123. E P Lukashev, V A Nadtochenko, E P Permenova, O M Sarkisov, A B Rubin *Dokl. Akad Nauk* **415** 696 (2007) [d]
124. V Z Paschenko, V V Gorokhov, B N Korvatovskiy, E A Bocharov, P P Knox, O M Sarkisov, C Theiss, H J Eichler, G Renger, A B Rubin *Biochim. Biophys. Acta: Bioenergetics* **1817** 1399 (2012)

125. I N Stadnichuk, M F Yanyushin, E G Maksimov, E P Lukashev, S K Zharmukhamedov, I V Elanskaya, V Z Paschenko *Biochim. Biophys. Acta: Bioenergetics* **1817** 1436 (2012)
126. F-J Schmitt, E G Maksimov, P Hätti, J Weißenborn, V Jeyasangar, A P Razjivin, V Z Paschenko, T Friedrich, G Renger *Biochim. Biophys. Acta: Bioenergetics* **1817** 1461 (2012)
127. N D Alekhina, Yu V Balnokin, V F Gavrilenko *Fiziologiya Rastenii* (Physiology of Plants) (Moscow: Akademiya, 2007)
128. B Alberts, D Bray, J Lewis, M Raff, K Roberts, J D Watson *Molecular Biology of the Cell* (New York, London: Garland Publ., 1994)
129. A B Rubin *Biofizika* (Biophysics) (Moscow: Moscow State University, Nauka, 2004)
130. P H Raven, R F Evert, S E Eichhorn *Biology of Plants* (New York: Freeman, 2005)
131. L Taiz, E Zeiger *Plant Physiology* (Sunderland, MA: Sinauer Associates, 2006)
132. *Photosynthesis (McGraw-Hill Encyclopedia of Science Technology)* Vol. 13 (New York: McGraw-Hill, 2007)
133. D-J Qian, T Wakayama, C Nakamura, S-O Wenk, J Miyake *Biohydrogen III: Renewable Energy System by Biological Solar Energy Conversion* (Amsterdam: Elsevier, 2004)
134. S Yu Zaitsev *Biol. Memb.* **13** 50 (1996) [b]
135. S Yu Zaitsev, T A Volchenkova, N A Kalabina, C Schaefer, V P Zubov *Macromol. Symp.* **136** 119 (1998)
136. S Yu Zaitsev, N A Kalabina, B Herrmann, C Schaefer, V P Zubov *Mater. Sci. Eng., C* **8–9** 519 (1999)
137. T A Volchenkova, N A Kalabina, S Shefer, V P Zubov, S Yu Zaitsev *Biol. Memb.* **17** 464 (2000) [b]
138. T I Ksenevich, A A Beloglazov, P I Nikitin, N A Kalabina, S Yu Zaitsev *Appl. Surf. Sci.* **92** 426 (1996)
139. N A Kalabina, S Yu Zaitsev, V P Zubov, E P Lukashev, A A Kononenko *Macromol. Symp.* **106** 193 (1996)
140. R A Uphaus, J Y Fangt, R Pisorel, G Chumanov, J Y Wang, T M Cotton, M Seibe *Photochem. Photobiol.* **65** 673 (1997)
141. R Picorel, G Chumanov, T M Cotton *J. Phys. Chem.* **98** 6017 (1994)
142. G Chumanov, R Picorel, S Toon, M Seibert, T M Cotton *Photochem. Photobiol.* **58** 757 (1993)
143. C E Martin, M Higley, W-Z Wang *Plant Physiol.* **87** 303 (1988)
144. F Höök, P Brzezinski *Biophys. J.* **66** 2066 (1994)
145. P Kernen, W I Gruszecki, M Matula, P Wagner *Biochim. Biophys. Acta: Biomembranes* **1373** 289 (1998)
146. V Bhalla, V Zazubovich *Anal. Chim. Acta* **707** 184 (2011)
147. D Mukherjee, M May, B Khomami *J. Colloid Interface Sci.* **358** 477 (2011)
148. Z Yang, X Su, F Wu, Y Gong, T Kuang *J. Photochem. Photobiol., B: Biol.* **78** 125 (2005)
149. O Yehezkeli, R Tel-Vered, D Michaeli, I Willner, R Nechushtai *Photosynth. Res.* (2013): doi 10.1007/s11120-03-9796-3 (published on line)
150. M Ciobanu, H A Kincaid, V Lo, A D Dukes, G K Jennings, D E Cliffel *J. Electroanal. Chem.* **599** 72 (2007)
151. M Ciobanu, H A Kincaid, G K Jennings, D E Cliffel *Langmuir* **21** 692 (2005)
152. P N Ciesielski, A M Scott, C J Faulkner, B J Berron, D E Cliffel, G K Jennings *ACS Nano* **2** 2465 (2008)
153. P N Ciesielski, F M Hijazi, A M Scott, C J Faulkner, L Beard, K Emmett, S J Rosenthal, D Cliffel, G K Jennings *Bioresource Technol.* **101** 3047 (2010)
154. C J Faulkner, S Lees, P N Ciesielski, D Cliffel, G K Jennings *Langmuir* **24** 8409 (2008)
155. L Frolov, Y Rosenwaks, C Carmeli, I Carmeli *Adv. Mater.* **17** 2434 (2005)
156. L Frolov, O Wilner, C Carmeli, I Carmeli *Adv. Mater.* **20** 263 (2008)
157. K Brettel, W Leibl *Biochim. Biophys. Acta: Bioenergetics* **1507** 100 (2001)
158. K Brettel *Biochim. Biophys. Acta: Bioenergetics* **1318** 322 (1997)
159. I Lee, J W Lee, R J Warmack, D P Allison, E Greenbaum *Proc. Natl. Acad. Sci. USA* **92** 1965 (1995)
160. S Yu Zaitsev, D O Solov'eva *Osnovy Biomeditsinskikh Nanotekhnologii* (Fundamentals of Biomedical Nanotechnologies) (Moscow: Moscow State Academy for Veterinary Medicine and Biotechnology, 2012)
161. L Frolov, Y Rosenwaks, S Richter, C Carmeli, I Carmeli *J. Phys. Chem. C* **112** 13426 (2008)
162. D Gerster, J Reichert, H Bi, J V Barth, S M Kaniber, A W Holleitner, I Visoly-Fisher, S Sergani, I Carmeli *Nat. Nanotechnol.* **7** 673 (2012)
163. N Terasaki, N Yamamoto, T Hiraga, I Sato, Y Inoue, S Yamada *Thin Solid Films* **499** 153 (2006)
164. M Grätzel *Nature (London)* **414** 338 (2001)
165. M Grätzel *J. Photochem. Photobiol., C* **4** 145 (2003)
166. M Grätzel *Electrochemistry* **79** 760 (2011)
167. M Hambourger, P A Liddell, D Gust, A L Moore, T A Moore *Photochem. Photobiol. Sci.* **6** 431 (2007)
168. R E Blankenship, D M Tiede, J Barber, G W Brudvig, G Fleming, M Ghirardi, M R Gunner, W Junge, D M Kramer, A Melis, T A Moore, C C Moser, D G Nocera, A J Nozik, D R Ort, W W Parson, R C Prince, R T Sayre *Science* **332** 805 (2011)
169. N Terasaki, N Yamamoto, T Hiraga, Y Yamanoi, T Yonezawa, H Nishihara, T Ohmori, M Sakai, M Fujii, A Tohri, M Iwai, Y Inoue, S Yoneyama, M Minakata, I Enami *Angew. Chem., Int. Ed.* **48** 1585 (2009)
170. N Terasaki, N Yamamoto, K Tamada, M Hattori, T Hiraga, A Tohri, I Sato, M Iwai, S Taguchi, I Enami, Y Inoue, Y Yamanoi, T Yonezawa, K Mizuno, M Murata, H Nishihara, S Yoneyama, M Minakata, T Ohmori, M Sakai, M Fujii *Biochim. Biophys. Acta: Bioenergetics* **1767** 653 (2007)
171. N Terasaki, M Iwai, N Yamamoto, T Hiraga, S Yamada, Y Inoue *Thin Solid Films* **516** 2553 (2008)
172. O Yehezkeli, R Tel-Vered, J Wasserman, A Trifonov, D Michaeli, R Nechushtai, I Willner *Nat. Commun.* **3** Art. No 742 (2012)
173. E G Maksimov, V N Kurashov, M D Mamedov, V Z Pashchenko *Biokhimiya* **77** 767 (2012) [e]
174. A A Kononenko, E P Lukashev *Adv. Biosens.* **3** 191 (1995)
175. *Artificial Photosynthesis* (Eds A Collins, C Critchley) (Weinheim: Wiley-VCH, 2005)
176. E G Maksimov, T S Gostev, F I Kuz'minov, N N Sluchanko, I N Stadnichuk, V Z Pashchenko, A B Rubin *Ros. Nanotekhnol.* **5** (5) 107 (2010) [a]
177. F-J Schmitt, E G Maksimov, H Suedmeyer, V Jeyasangar, C Theiss, V Z Paschenko, H J Eichler, G Renger *Photon Nanostruct.: Fundam. Appl.* **9** 190 (2010)
178. Y Umena, K Kawakami, J-R Shen, N Kamiya *Nature (London)* **473** 55 (2011)
179. J R Lakowicz *Principles of Fluorescence Spectroscopy* (2nd Ed.) (Dordrecht: Kluwer Academic, Plenum, 1999)

180. B J Strasser, R J Strasser, in *Photosynthesis: from Light to Biosphere* (Ed. P Mathis) (Dordrecht: Kluwer Academic, 1995) p. 977
181. E G Maksimov, F I Kuzminov, I V Konyuhov, I V Elanskaya, V Z Paschenko *J. Photochem. Photobiol., B* **104** 285 (2011)
182. A Mershin, K Matsumoto, L Kaiser, D Yu, M Vaughn, Md K Nazeeruddin, B D Bruce, M Graetzel, S Zhang *Sci. Rep. (Nature)* **2** Art. No 234 (2012)

[a] — *Nanotechnol. Russ. (Engl. Transl.)*
[b] — *Biochemistry (Moscow), Ser. A: Membr. Cell Biol. (Engl. Transl.)*
[c] — *Biochemistry (Moscow) Special Issue Biol. Chem. Rev. (Engl. Transl.)*
[d] — *Dokl. Biochem. Biophys. (Engl. Transl.)*
[e] — *Biochemistry (Moscow) (Engl. Transl.)*